Determining Femoral Component Goodness-of-Fit using Computer Segmentation and Numerical Simulation

By

Etienne P. van Schalkwyk

Thesis presented at the Stellenbosch University in partial fulfilment of the requirements for the degree of

Master of Science in Mechanical Engineering

Department of Mechanical Engineering
Stellenbosch University
Private Bag X1, 7602 Matieland, South Africa

Supervisor: Prof. C. Scheffer

March 2010

Determining Femoral Component Goodness-of-Fit using Computer Segmentation and Numerical Simulation

by

Etienne P. van Schalkwyk

March 2010

Declaration

I, the undersigned, hereby declare that the work contained in this thesis is my own original work and that I have not previously in its entirety or in part submitted it at any university for a degree.

Signature: .....
E. P. van Schalkwyk

Date: March 2010

Abstract

Determining Femoral Component Goodness-of-Fit using Computer Segmentation and Numerical Simulation

E. P. van Schalkwyk

Department of Mechanical Engineering

Stellenbosch University

Private Bag X1, 7602 Matieland, South Africa

Thesis: MScEng (Mech)

March 2010

The χ^2 goodness-of-fit (GOF) test was used to determine which standard femoral component would achieve the best geometrical fit for a specific patient. This was done by creating 3D models from computerized tomography scan data through computer segmentation using Materialise MIMICS. The second step was to measure the morphological dimensions of the distal femur whereof twelve were selected and compared to the dimensions of two commercial femoral prosthesis designs. Thirdly, cadaveric femurs were scanned with a 3D desktop scanner to create a database with the dimensions of healthy knees. The 3D model database of the cadaveric femurs included cartilage layer. A cartilage thickness was added to the CT knee dimensions using a self-organizing map (SOM) calculation based on the healthy knee database. The developed method calculated alignment angles with higher accuracy than presently used and determined preoperatively which size to implant. Kinematic simulations of total knee arthroplasty (TKA) knees were compared to normal knee simulations created in LifeMOD. The articulating surface was the only variable changed between the two simulations and the kinematics of different sizes were evaluated. A method was created to scale the femoral component using the standard available sizes. The completed project will be used as foundation for customization of TKA prostheses.

Uittreksel

Bepaling van Femorale Komponent Passing deur Rekenaar Segmentasie en Numeriese Simulasie

E. P. van Schalkwyk

Departement Meganiese Ingenieurswese

Universiteit van Stellenbosch

Privaat Sak X1, 7602 Matieland, Suid Afrika

Tesis: MScIng (Meg)

Maart 2010

Die χ^2 graad van passing toets metode was gebruik om te bereken watter standaard femorale komponent 'n patiënt die beste geometries pas. Dit was gedoen deur eerstens 3D modelle gemaak vanaf CT skandeer data deur rekenaar segmentasie met Materialise MIMICS. Daarna was morfologiese dimensies gemeet vanaf die distale femur, waarvan twaalf gekies en vergelyk was teen two kommersiële femorale prostesis ontwerpe. Laastens was kadawer femurs geskandeer met 'n 3D skandeerder om 'n databasis van gesonde knieë te maak. Die 3D modelle van die kadawer bene het die kraakbeen laag bevat. Die kraakbeen dikte was by die CT knie dimensies gevoeg d.m.v. SOM en die gesonde knie databasis. Die nuwe metode bereken die belynings hoeke met hoër akkuraatheid as wat huidiglik gebruik word en bereken voor die operasie watter grote om te gebruik. Kinematiese simulasies van knie prostesis was vergelyk met 'n normale knie simulasies gemaak in LifeMOD. Die artikulêre oppervlakte was die enigste veranderlike tussen die twee simulasies en kinematika van verskillende grotes was ondersoek. 'n Metode was geskep om die standaard femorale komponent se skaal te verander vir 'n beter passing.

Acknowledgements

I would like to express my sincere thanks to the following people and organizations who have contributed to this project and help make it possible:

- To my promoter, Prof. Cornie Scheffer. Thank you for your valuable inputs and advice. Thank you for granting me the freedom to use my own ideas and for guidance in completing my project.

- Thanks to Dr. Spike Erasmus, Dr. Edwin Dillon and Dr. Richard de Villiers for their wisdom and knowledge throughout the project.

- Great thanks to Linda for keeping me on track, and always picking me up when I needed support, and for always believing in me.

- My mom and dad for all the love and support and allowing me to fulfil my dreams.

- Thank you to Linda's parents for everything that they did for me, it's greatly appreciated.

- To all my fellow students at BERG, thanks for the support and assistance.

- Annelize Coetzee, Gerna Neethling and Annelie Brangança for their help with all the necessary CT scans.

- And lastly, the Lord for granting me these wonderful abilities and opportunities

Dedications

To
Pieter George
Pretorius

Contents

List of Figures

List of Tables

Nomenclature

Variables

χ^2	Chi squared goodness-of-fit parameter
k	Number of dimensions used to calculate the goodness-of-fit parameter
$\overline{E}$	Vector containing morphological dimensions of distal femur
$\overline{Z}$	Vector containing dimensions of prosthesis sizes

Abbreviations

2D	Two Dimensional
3D	Three Dimensional
ACL	Anterior Cruciate Ligament
ADAMS	Automatic Dynamic Analysis of Mechanical Systems
AP	Anterior/Posterior
AP_{BOX}	Anterior/Posterior Box
AMA	Anatomical/Mechanical Angle
ASCII	American Standard Code for Information Interchange
ASTM	American Society of Testing and Materials
BMU	Best Matching Unit
CAD	Computer Aided Design
CAM	Computer Aided Manufacturing
CAS	Computer Aided Surgery
CARE	Combined Applications of Reduce Exposure
CNC	Computer Numerical Control
CT	Computerized Tomography
DICOM	Digital Imaging and Communications in Medicine
Dof	degrees of freedom
FE	Flexion-Extension
GeBOD	Generator of Body Data
GGOF	Geometric Goodness-of-Fit
GOF	Goodness-of-Fit
HU	Hounsfield
KGOF	Kinematic Goodness-of-Fit
LCL	Lateral Collateral Ligament
LCR	Lateral Condyle Radius
LPFL	Lateral Patellofemoral Ligament
MCL	Medial Collateral Ligament
MCR	Medial Condyle Radius

MIMICS	Materialise's Interactive Medical Image Control System
ML	Medial/Lateral
MLT	MultiStripe Laser Triangulation
MPFL	Medial Patellofemoral Ligament
MRI	Magnetic Resonance Imaging
NaN	Not a Number
PCL	Posterior Cruciate Ligament
PLR	Posterior Lateral Radius
PMR	Posterior Medial Radius
PMTA	Proximal Medial Tibial Angle
PRP	Posterior Retaining Prosthesis
PSP	Posterior Sacrificing Prosthesis
PTMA	Proximal Tibial Medial Angle
RPC	Resected Posterior Condyle
SD	Sulcus Depth
SL	Sulcus Length
SOM	Self-Organizing Map
STL	Stereo Lithography (file format)
TA	Trochlear Angle
TKA	Total Knee Arthroplasty
TKR	Total Knee Replacement
TR	Trochlear Radius
TT/TG	Tibial Tubercle/ Trochlear Groove

Chapter 1

1 Introduction

1.1 Background

Total knee replacement is a surgical procedure performed when severe degeneration of the knee joint is present [1]. Knee replacement surgery is a routine procedure performed on over 400 000 people worldwide each year [2]. Total knee replacement has become one of the most common orthopaedic procedures performed on older persons. In the past 20 years, the rates of knee replacement procedures have increased approximately eightfold [3]. Over 90% of people who have had a total knee replacement experience an improvement in knee pain and function [4]. The average joint replacement patient is around 65-70 years old; however people of all ages have received knee implants. Studies have consistently shown knee implants are functioning well in 90-95% of patients between 10 and 15 years after surgery [5].

1.2 Motivation

In total knee arthroplasty (TKA) prostheses are used to replace a damaged knee joint. Surgeons use X-rays of the lower limbs, focused on the knee, to determine the alignment, rotation and to a lesser extent the required prosthesis size for a patient. Parameters such as age, weight, ethnicity, gender and lifestyle determines the shape of the femur. The final decision on the best size for the particular patient can only be done during surgery, when the surgeon compares the actual knee to standard size samples. Typically the femoral knee prostheses are commercially available in typically six standard sizes [6]. The prearranged size range of commercial prostheses cannot be altered to fit a specific individual's morphological bone structure. Although most designs allow inter-changability between femoral and tibial components [7], they still cannot deliver uniquely customized features to fit an individual. Prosthesis designs and surgical techniques must account for a possible mismatch between the medial-lateral and the anterior-posterior dimensions [8]. Over- and under sizing of the femoral component can cause numerous problems [9]. Medial-lateral overhang can result in capsule impingement, while anterior-posterior mismatch can result in notching of the anterior femur, over-stuffing of the patellofemoral joint or a mismatch between flexion and extension gaps [10]. Although computer navigation has improved the accuracy and alignment of a TKA procedure, correct placement and sizing of components should be improved [11]. Proper implant sizing will avoid complications and improve the patient outcomes. Surgeons rely on manufacturers to provide appropriately-sized implants. Early designs of the total knee prosthesis were limited in the number of sizes available. The evolution of the design and kinematics in total knee replacement led to improved sizing options in an attempt to more closely duplicate a patient's anatomy.

1.3 Objectives

The first objective of the study is to gain experience in knee joint anatomy, physiology and replacement surgery. This will aid in understanding the shape and function of the distal femur, as well as the different aspects of a total knee replacement.

The second and main objective is to preoperatively determine the accurate implant size using more morphological dimensions of the patients. Computer segmentation will be used on the CT scan data to create 3D models of the bone structures. Following this, a method of measuring the dimensions of the 3D distal femur is created. A process will be generated which adds the cartilage layer thickness to the measured dimensions. Through 3D scanning of the components the dimensions of the prostheses are acquired. A template can then be created to measure all the required dimensions on the 3D models of the prosthesis sizes.

Based on the data collected, the final objective is to create numerical simulations of a normal and replacement knee using the 3D models. The results of the simulations are evaluated according to similar simulations performed in other studies. These results lead to the following research question: would a perfect replica of the distal femur recreate normal femoral kinematics.

An additional objective is to write a program to implement the χ^2 goodness-of-fit (GOF) method which compares the femur and prosthesis dimensions. This program would therefore determine preoperatively which size prosthesis to implant. The method should be evaluated through various tests and case studies.

The last objective is to stipulate different methods to customize the dimensions of the prosthesis according to the dimensions of the patient.

Specific objectives for this project can hence be summarized as:

- Study literature of knee and total knee replacement surgery
- Calculate dimensions of femur and prosthesis with computer segmentation
- Create numerical simulations of 'normal' and replaced knee
- Perform GOF method using the dimensions acquired
- Develop different methods of customization

1.4 Project Outline

In Chapter 2 the knee anatomy, physiology of the knee joint, the types of implantation and alignment methods are described. Related studies done on morphological measurements and orthopaedic surgeries performed with customized components will be discussed.

Using the material of Chapter 2, Chapter 3 explains the segmentation and morphological measurement procedures and how the 3D femur models are created. Measurements are performed on the distal femur using programs such as MIMICS and Matlab. The measuring techniques are evaluated and tested individually. A method was developed to add cartilage layer thickness to the dimensions collected from the CT scans. Healthy cadaveric femurs were dissected and scanned with a 3D scanner to acquire the models. Self-organizing maps (SOMs) was applied with the healthy knee

database to incorporate the cartilage thickness. The dimensions of femoral components were obtained through 3D scanning of test prostheses and measured in MIMICS.

The models used in the numerical simulation of a knee joint given in Chapter 4 were the 3D models used in Chapter 3. This includes the creating of the normal and replaced knee simulations as well as the results of these simulations.

The dimensions determined (Chapter 3) and the simulations created in Chapter 4 are used for the overall GOF calculation (Chapter 5). GOF is determined by the geometric and kinematic GOF parameters. The geometric is calculated using the morphological dimensions calculated (Chapter 3) and the kinematic is determined with the results obtained from the kinematic simulations in Chapter 4. This GOF method is evaluated with simple volumetric tests and a case study is performed on physical models.

After the GOF method has been completed, Chapter 6 derives new principles for prosthesis customization. Two methods are given to change the dimensions of the femoral component for a better fit to a specific individual. The first method scales the standard femoral component, while the second method uses SOM to customize the components.

Conclusions and recommendations are presented in Chapter 7. All the research questions are answered and recommendations for further work are given.

Chapter 2

2 Literature Review

A literature review was done for better understanding of the anatomy, physiology of the knee joint as well as the surgical procedure of a total knee replacement.

2.1 Anatomy of the Knee

2.1.1 Bone Structure

The knee is a hinge joint made up of three bones held firmly together by ligaments. These bones are the femur (upper leg bone), the tibia (shin bone) and the patella (knee cap). The tibial plateau and two condyles on the distal end of the femur make contact (Figure 1).

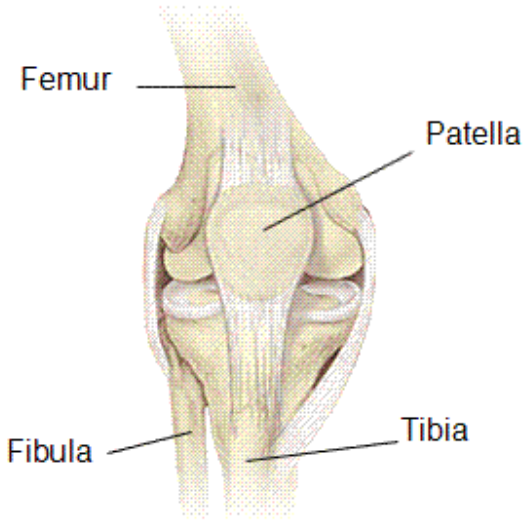

Figure 1: Knee Bones [12]

The anatomy of the knee is important for the design of the total knee replacement prosthesis. The orientation, shape and kinematics of the knee depend on the morphological shape of the distal femur.

2.1.2 Ligaments

There are four major ligaments in the knee joint: two cruciate and two collateral ligaments. The two cruciate ligaments are located inside the joint between the femur

and the tibia, while the collateral ligaments are found on either side of the knee [13-16] (Figure 2).

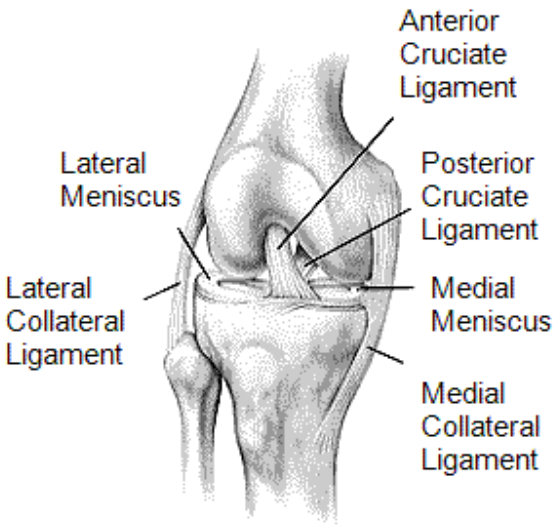

Figure 2: Ligaments of knee joint [13]

2.1.3 Morphological Landmarks

Morphological landmarks are specific points that exist on the bone surface. These landmarks are attachment regions of different ligaments which are clearly visible [21]. These points are used to identify different parameters required for the alignment of the femoral component. The three most important landmarks are the medial sulcus and prominence and the lateral prominence. These landmarks are the femoral attachment points of the collateral ligaments (Figure 3). Only the two prominences were clearly visible on 2D CT scans.

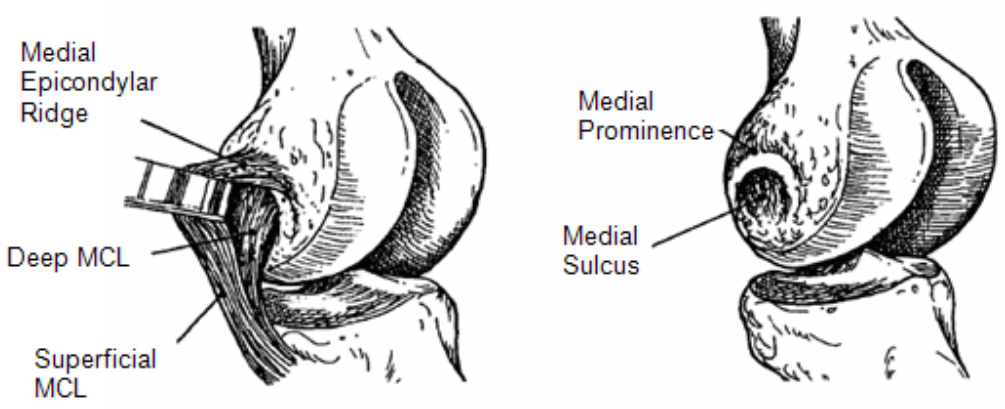

Figure 3: Ligament attachment points [21]

2.1.4 Axes

There are a number of axes in the leg and knee joint which are important to the total knee replacement procedure. Only a few of the axes play an important role in knee alignment during operation and were therefore relevant to the project. These include the mechanical axis of the leg, the anatomical axis of the femur and tibia as well as the flexion-extension (FE) axis of the knee joint.

2.1.5 Mechanical Axis

The mechanical axis of the knee passes from the centre of the hip to the centre of the ankle (Figure 4) [22, 23]. In a TKA, the distal cut is made perpendicular to the mechanical axis of the femur. It is the deviation of the mechanical axis to the anatomical axis that is important with standard TKA (i.e. Intramedullary guides). If using computer aided surgery (CAS), the mechanical axis is used.

Figure 4: Mechanical axis of the knee [24]

The tibio-femoral joint line of the knee is not perpendicular to the mechanical axis (3° varus deviation). The anatomical axis of the femur and tibia runs down the centre of the bone shafts and intersect each other at the knee joint centre.

2.1.6 Condylar Axes

There exist two transepicondylar axes: the clinical and surgical epicondylar axis. The clinical axis is a line connecting the prominence of the medial epicondyle (m_p) with the lateral epicondylar prominence (l_p). The surgical axis is a line connecting the sulcus of the medial epicondyle (m_s) with the lateral epicondylar prominence (Figure 5) [25].

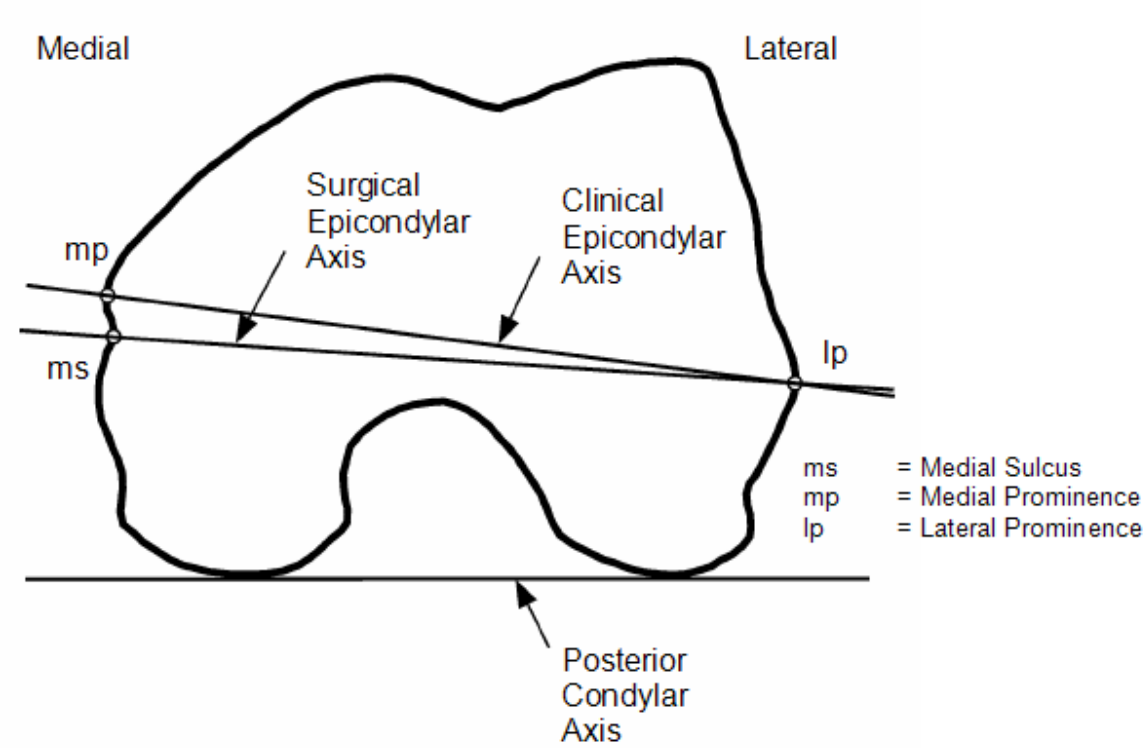

Figure 5: Anatomical landmarks and reference axes in the distal femur [26]

Conventional understanding of the knee kinematics suggested that the knee has no fixed flexion-extension (FE) axis. This was based on observations in the sagittal plane, which showed that the instantaneous centre of rotation moved within the posterior femoral condyle during the flexion cycle [27-28]. Locations of the functional flexion-extension axis were investigated in reference to the anatomical landmarks and reference axis in the distal femur. The flexion-extension axis of each flexion angle crossed at the medial side of the tibia, showing a medial pivoting motion. In the axial view of the tibia plateau the FE axis is projected during knee flexion from 0° to 90° (Figure 6). In the frontal view superior-inferior translation was minimal [29].

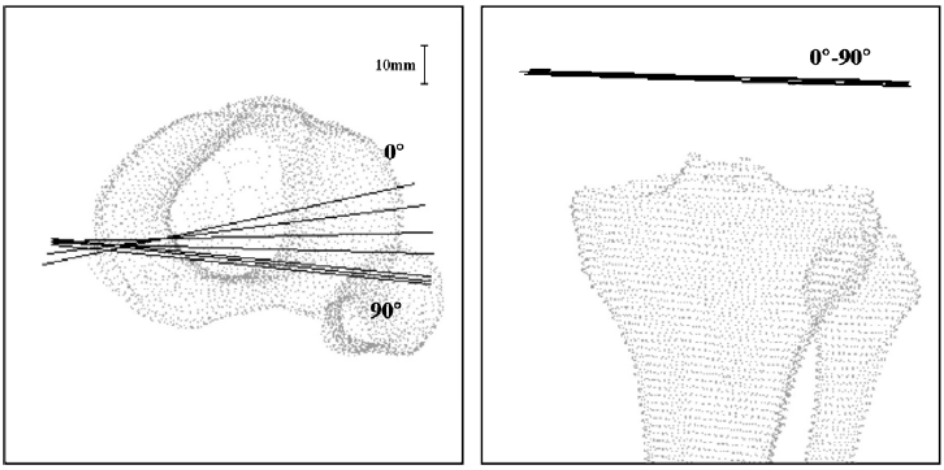

Figure 6: Movement of flexion-extension axis during knee flexion from 0° to 90° [26]

It has been proposed that the knee flexion and extension can be better described as a rotation around a fixed functional FE axis in the posterior femoral condyles. In total knee arthroplasty, the femoral component is generally set in slight external rotation relative to the posterior condylar axis. Many studies have shown that the transepicondylar axis is a useful reference axis for rotational alignment of the distal femur, especially for the positioning of the femoral component in total knee arthroplasty. Although this representation of the fixed axis is limited within the range of 0° to 90° of flexion, the results of the present are used for the positioning of the prosthesis in total knee arthroplasty [30]. This is because the flexion gap and ligament balance of the knee joint during total knee arthroplasty are usually evaluated within this range.

2.2 Kinematics of the Knee

The basic mechanism of movement between the femur and the tibia is a combination of rolling, gliding and spinning during flexion and extension [31]. The basic kinematic principle of motion in the knee joint can be represented by a mechanism called the crossed four-bar linkage (Figure 7) [32].

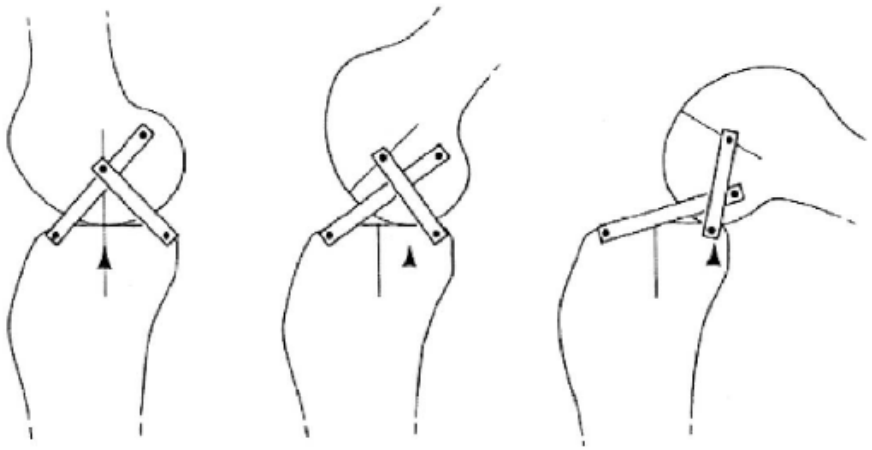

Figure 7: Four-bar linkage [32]

This is only a schematic representation because the cruciate ligaments are not rigid bars and can stretch under load. Although the cruciate ligaments play an important role in the motion of the knee joint, the shape of the distal femur is largely responsible for the movement. The distal articulating surface of the femur could be described as being composed of three circular surfaces [28, 33-34]:

1. An anterior circle representing the floor of the patellar groove.
2. A posterior circle representing the posterior femoral condyles.
3. A middle circle with a larger radius representing the distal femoral condyles.

The lateral and medial condyles of the distal femur are asymmetric in a number of morphological features [35]. The lateral condyle is flattened distally and has a larger radius than the medial condyle. The medial condyle can be viewed as a sphere and is somewhat constrained to a ball-in-socket joint. Minimal anterior/posterior translation occurs on the medial side of the femur. The posterior medial and lateral condyles are circular in shape and have an almost equal radius [36] (Figure 8).

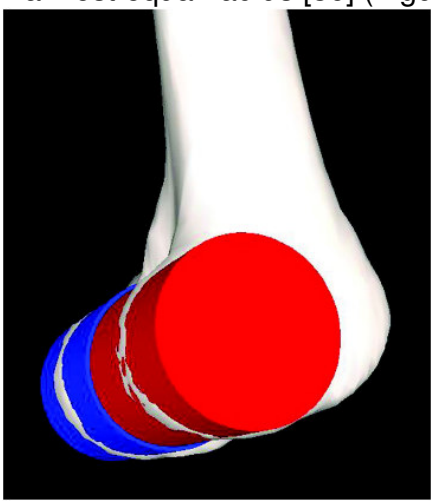

Figure 8: Circular posterior condyles [36]

2.2.1 Tibial Plateau

There exists a difference between the medial and lateral side of the tibial plateau. The medial plateau is slightly concave, whereas the lateral is convex [38]. The tibial plateau only affects the kinematics of the knee and not the dimensions of the distal femur. [37]

2.2.2 Patella

The trochlear groove in which the patella moves is relevant to the dimensions of the distal femur. The forces of the quadriceps muscles are guided around the distal end of the femur with a sesamoid bone called the patella [39]. The tracking of the patellofemoral joint is an important anatomical consideration of a total knee arthroplasty [40]. The patellar groove position of the femoral component should be equal to the healthy knee. There are a few factors of the trochlear groove and patella which should be accounted for when designing a knee prosthesis. These factors include the trochlear radius, depth of groove, the wedge angle and the angle between the groove and the anatomical axis.

2.3 Total Knee Arthroplasty

2.3.1 Diseases

These are a few of the most common diseases of knee joints requiring a replacement procedure [41].

- Osteoarthritis
- Rheumatoid arthritis
- Post-traumatic arthritis
- Avascular necrosis
- Malalignment – leads to osteo-arthritis

Many of the knees investigated in this thesis were affected by one of these diseases. Therefore it was important to understand the changes of the morphological structure and cartilage layer of the bones.

2.3.2 Alignment

The ultimate goal of TKR is to produce a well-aligned joint with good ligament balance [42]. Exact implant alignment is crucial to the normal functioning of the knee after the replacement procedure [43]. Failure to achieve normal limb alignment is one of the common errors in TKA and may lead to premature failure of the implant system [44]. Inaccurate location of the transepicondylar axis presents a high variability of femoral rotational alignment [45]. Normal knee alignment will be examined in the coronal and sagittal plane only for the femoral component.

2.3.3 Coronal Alignment

Perfect coronal alignment would have the femoral and tibial long axis in line with each other, to insure that the ground reaction force pass through the centre of the knee [24]. At present the prosthesis is aligned by resecting the joint surfaces of the tibia and femur to place the tibio-femoral joint line perpendicular to the mechanical axis. In a normal knee joint, the line is not perpendicular to the mechanical axis as mentioned previously (2.1.5). Cutting the tibia perpendicular to its mechanical axis usually removes more bone laterally than medially as a consequence of the sloped joint line [46].

2.3.4 Sagittal Alignment

Alignment of the prosthesis in the sagittal plane is of great importance to ensure correct functioning. There are three major factors that are important in the sagittal plane: the tibial slope, position of the FE axis and the path of the patella during motion [47]. These factors are corrected by the external rotation of the femoral component, through alignment parallel to the surgical epicondylar axis. This is done for the following reasons. First, external rotation is necessary to compensate for the angular discrepancy resulting from the proximal tibia being cut perpendicular to the tibial shaft axis. Secondly, setting the femoral component parallel to the transepicondylar axis corresponds to the FE axis and produces an appropriate ligament balance in flexion and extension. Thirdly, this improves patellar tracking and brings it closer to normal conditions.

2.3.5 Preoperative Planning

Prior to surgery, the required cutting angles and prosthesis size are determined. The aim of the preoperative planning is to determine the height of the horizontal tibia cut to fit the tibial component. Thereafter the size of the femoral component is chosen. The possible risk of overcorrection of the mechanical axis can be evaluated. Preoperative planning can only provide indicative information concerning size and two-dimensional positioning. The final decision as to which prosthesis size is suited for the individual and its positioning can only be determined during surgery.
In addition, CT scans can be made of the unhealthy knee for the planning procedure. X-rays are required from anterior and posterior as well as a sagittal view while in extension and 90° flexion. The X-rays are then compared to templates in catalogues to choose the closest fit.

2.3.6 Implantation

There are two different methods used when implanting the femoral component on the distal femur. The selected size can differ depending on the type of method used [48]. In both these methods the distal cut is done before the other cuts. It is made perpendicular to the mechanical axis resecting the same thickness as that of the prosthesis [49]. As presently mentioned, due to the 3° tibia varus, more bone is usually removed on the lateral side. The first method is called *flexion spaced-balancing* (Anterior referencing) [50]. In this method the anterior cut is made, followed by the posterior cut. The anterior cut is made the same thickness as the anterior thickness of the implanted prosthesis. The required prosthesis distance is then measured from the anterior cut to make the posterior cut. Therefore the posterior cut is the variable dimension to ensure the correct flexion space. The second method is called the *size-matched resection* (Posterior referencing) [51]. In this method the posterior cut is first made to the thickness of the posterior part of the prosthesis. The anterior cut is then made to the correct prosthesis internal dimension. Thus the thickness of the anterior cut is changed according to the size of the selected prosthesis [52]. The surgeon in this study used a posterior referencing technique for all the procedures.

During the preoperative planning the appropriate rotational alignment of the femoral component can be determined. Most prosthesis designs suggest a standard 3° of external rotation of the prosthesis, or have a built in 3° of external rotation in the prosthesis and the bone is cut parallel to the PCA. The medial and lateral prominences are used to determine the clinical epicondylar axis from the 2D sagittal CT scans [25]. Because the femoral component should be aligned with the surgical epicondylar axis, an average value is subtracted from the clinical epicondylar axis angle [53]. This is done because the medial sulcus is difficult to accurately pin point on the 2D scans. The posterior cut is then made parallel with the calculated angle, the same thickness as the artificial replacement [54]. The anterior cut is made according to the Anterior-Posterior Box (AP_{BOX}) size of the selected prosthesis (Figure 9).

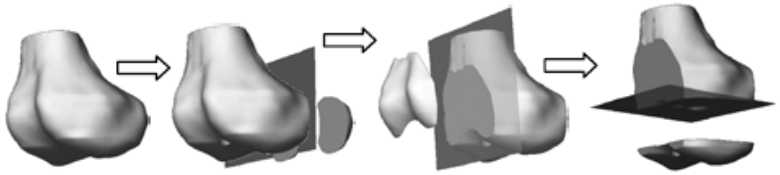

Figure 9: Surgical simulation [52]

After all the components have been implanted in the correct positions, the prosthesis is evaluated geometrically by the surgeon for any incorrect fits. The kinematics are evaluated by evaluating the ligament balance in flexion and extension and the range of motion. Existing prostheses designs and surgical techniques do not restore the function of the knee to normal as recorded by gait analysis or other functional analysis [40].

2.3.7 Prosthesis Design

Overall there exits only two types of TKA femoral component designs. In both cases the anterior cruciate ligament is sacrificed, while the posterior ligament is either retained or sacrificed during the procedure. The posterior retaining design replaces the ACL function by the shape of the components. The PCL sacrificing designs use different shapes to replace the function of the ACL and PCL. Large numbers of different prosthesis designs are available from different companies which can be divided into one of these two groups. Thus companies could produce the same type of prosthesis, but the overall shape of the prostheses is different.
All designs have a limited size range which can be manipulated to fit a specific individual. These manipulations are not of the physical shape of the prosthesis, but using different combinations of the femoral and tibial component sizes. Thus there is interchangability between the component sizes, which allows for a small amount of manipulation.

2.4 Imaging

Two types of medical scanners were available for use in the project: computerized tomography (CT) and magnetic resonance imaging (MRI). Illustration of the hard bone materials as well as the cartilage layer of the articulating surfaces is required. Each one had to be investigated to determine what can be performed by the scanner and the uses of each type of scanner with relation to this study and the software application.

2.4.1 CT scanner

A computerized tomography (CT) scanner is a special kind of X-ray machine. Instead of sending out a single X-ray through your body as with ordinary X-rays, several beams are sent simultaneously from different angles. The beams are detected after passing through the body and their strengths are measured. A computer uses this information to determine the relative density of the examined tissues. Each set of measurements made by the scanner is a cross-section through the body.

2.4.2 MRI scanner

A magnetic resonance imaging (MRI) scanner is a radiology technique that uses magnetic waves, radio waves and a computer to produce images of bodily structures. Magnetic resonance has been applied successfully to medical imaging of the body because of its high water content. The hydrogen atoms in water and fat make up approximately 60% of the total body weight [55]. The MRI scanner is a tube surrounded by a giant circular magnet. The magnet creates a strong magnetic field through the body which aligns the protons of hydrogen atoms. The protons are then exposed to a beam of radio waves which cause the various protons of the body to spin. A faint signal is then produced that is detected by the receiver portion of the MRI scanner. The receiver information is processed by the computer and an image is then produced.

2.4.3 Evaluation

The MRI scanner is in practice mainly used for screening of soft tissue with bones and used to analyze knee kinematics [18]. On a CT scan only the high density bone structures are displayed clearly and it is mostly used to accurately visualize the bone [56]. The CT scanner is good for bone visualisation and the MRI has good soft tissue definition (e.g. Cartilage) Therefore, in this study of measuring the morphological anatomy of the knee, the CT scanner is preferred.

2.5 Morphological Measurements

2.5.1 Different measurements

Two sets of measurements are required: the morphological dimensions which define the shape of the distal femur as well as the measurements required to align the femoral knee component during surgery. Manufactures of knee prostheses use the morphological dimensions to design a knee prosthesis range. Data can be collected from a large number of specimens to obtain knee dimensions. Specific sizes are then developed to fit the average morphological dimensions of the data. The calculated size range normally includes six sizes ranging from small to large. This requires a good method for acquisition of the dimensions. The second set of measurements is performed before surgery to accomplish accurate alignment. The different methods of acquiring these measurements were studied to reproduce similar measurements. Presently, not all the required measurements can be directly measured and some are determined using approximated values.

2.5.2 Previous Studies

Dry Bone

Dry femur bones are sometimes used to measure the morphological dimensions [10]. The method can only be used to accumulate more morphological dimensions for a database. Alignment measurements cannot be performed using this method. The measurements are done by hand using different measuring tools. Although this method is accurate, no cartilage layer is present on the dry bones.

Jigs

Dry bones are placed in constructed jigs to measure specific dimensions. This technique is mostly used to measure specific axes of the femur. Dry bones are used and though the measurements are accurate, only a few measurements can be made using a jig. It is commonly used to measure the transepicondylar axis [57] and the femoral anteversion of the femur head [58] (Figure 10).

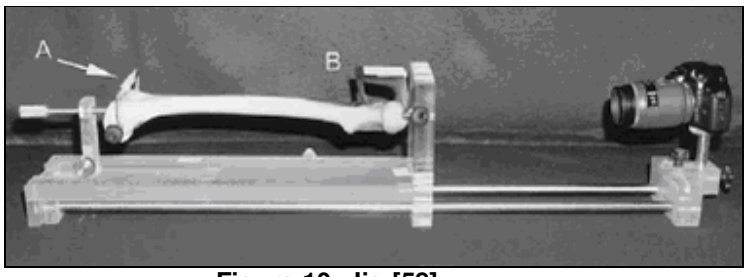

Figure 10: Jig [58]

Surgery

Measurements collected during surgery are used to measure how well the prosthesis fits the resected bone [59]. During surgery, when the bone cuts have been completed, dimensions of the resected area and bone cuts are recorded [9] (Figure 11). These measured dimensions are then compared to the prosthesis dimensions to determine how well the prosthesis fits [60]. This is a very good procedure to measure the dimensions of the resected distal femur, but the measurements are very dependent on the alignment of the components [46]. Only a limited numbers of anatomical landmarks are accessible and axes cannot be measured [61].

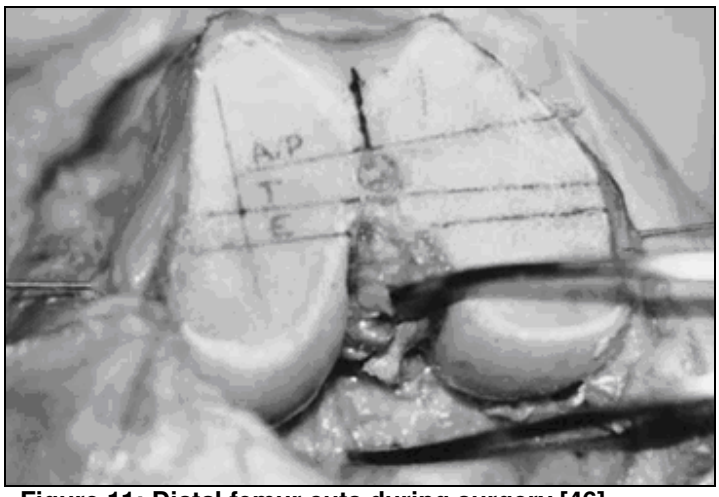

Figure 11: Distal femur cuts during surgery [46]

2D CT

This method can be used to measure the SEA and CEA during preoperative planning. As previously mentioned, the capabilities of this method are limited to two dimensions. The CT scanner is equipped with different software tools for measuring distances and angles. It is commonly used to measure the rotational orientation of the femoral component, anatomical/mechanical axis deviation angle and the intercondylar notch

width [62]. An example of the anatomical axis is displayed in the figure below [63] (Figure 12).

Figure 12: Anatomical axis of femur in 2D CT [63]

3D Models

This method uses the 2D scan data to create 3D models through computer segmentation. The models can then be viewed from any angle to determine the morphological dimensions (Figure 13). The method is depended on the type of scan (CT or MRI) and the quality of the scan data. Geometric dimensions of angles [64-65] can easily be measured using this method.

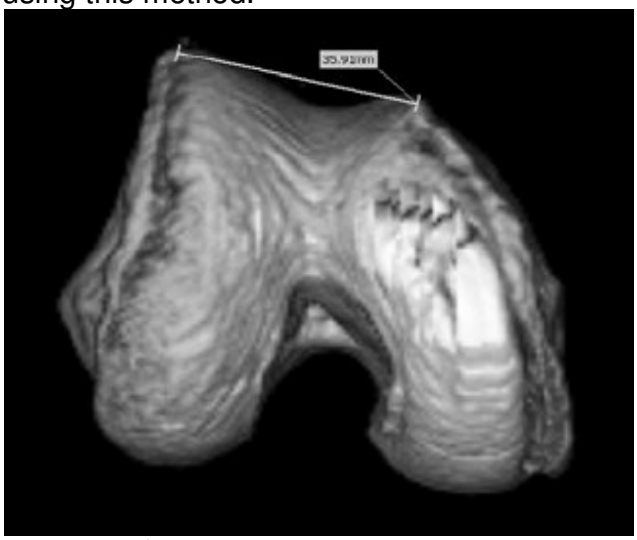

Figure 13: Computer segmented femur [66]

2.6 Simulation Models

Simulation models are created to determine certain kinematic properties of the knee. These simulations recreate normal knee kinematics and motion. Cadaveric models are limited in their range of motion and are generally expensive. These are used to test the performance of a knee replacement, simulating orthopaedic surgical procedures and investigating the loading mechanisms of the joint [67]. The type of simulation depends upon the result which is required. Normally knee simulators are used to determine the wear of a new prosthesis design. First, the knee is simulated where after the results are validated with a physical model. Simulations are mostly used to determine the wear of a prosthesis design [68] or to calculate the contact stress in a certain part of the prosthesis [69] (Figure 14).

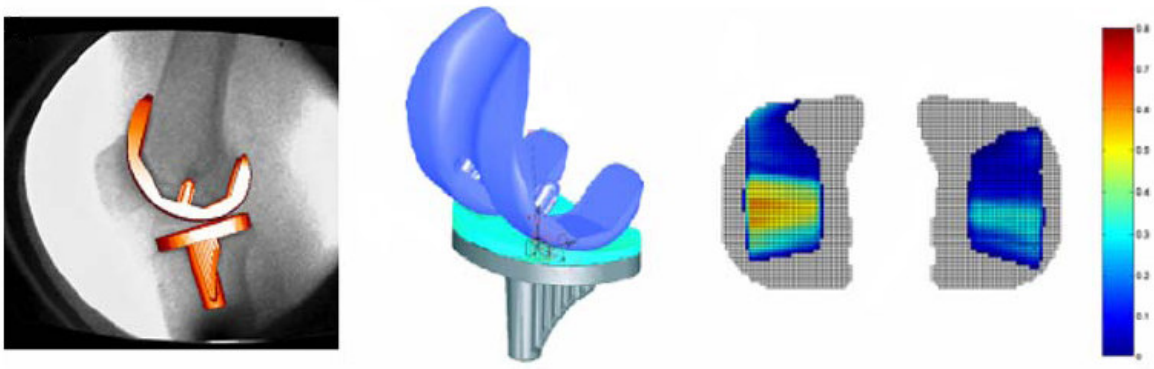

Figure 14: Wear calculation simulation results [68]

2.7 Customization

As previously mentioned a standard size range is used to fit an entire population. In the majority of knee replacement cases, the standard design endoprosthesis is used [70]. In some cases the anatomical features are abnormal and would favour the application of an anatomic custom design implant [71]. Customizations of the hip prosthetic implants are common, due to the available manufacturing processes and complexity of the parts. The custom hip design can be manufactured with numerically controlled machine tools while the complex knee design has to be cast or laser sintered. Casting is only effective through mass production, which is not viable for single part production. The laser sintering would be perfect, however the technology of sintering implants is still under development. Seedhom [72] and OtisMed [73] illustrated a concept of a custom fit total knee replacement. Standard components were implanted with customized jigs created from 3D CT scan models. Harrysson *et al*. [74] created custom femoral components from 3D models using MIMICS. CAD models of the bone profile were evaluated with finite element methods (FEA).

2.8 Custom Hip Design

The design and manufacturing of a custom hip prosthesis in a computerized system requires a multistage design and manufacturing process. A hip joint endoprosthesis is characterized by its stem and neck. The stem has to exactly fit into the marrow cavity

[75] and the neck requires the correct ante version angle [76]. This results in a stable structure with reduced risk of loosening. The anatomical forms of the patient bones are identified from CT scans. 3D reconstruction is applied to the images of the femur to select only those regions where cortical bone is present.

The design and manufacturing of the customized implants are based on CT scans. The data is used to create a three-dimensional reconstruction of the femoral canal. Several design criteria have been established and are implemented in the computer aided design (CAD) and the computer aided manufacturing (CAM) of the implant. The CT scanner transverse images are obtained from the hip joint and the upper femur. The images are analyzed using special software developed for the hip application. It generates contours to describe the implant design. The combination of all these contours forms the basis for the three-dimensional computer model of the implant (Figure 15). The 3D computer model of the implant forms the basis for the manufacturing of the implant. The implant is processed in a 5-axis CNC machine. The implant is manufactured in titanium alloy according to the ASTM standard for using this alloy in implants. An individual implant requires an individual rasp for broaching the medullar canal of the femur. This rasp has to have the same geometry of the implant to provide the right seat for the implant. The rasp is processed in approved steel and provided with sharp teeth for effective broaching. The prosthesis is then cleaned, packed and sterilized using gamma irradiation. The broaches are glass blasted, cleaned and checked before being sent to the hospital. Despite the more thorough broaching that is required with a customized broach, this procedure usually takes no longer than conventional hip surgery using non-cemented femoral components.

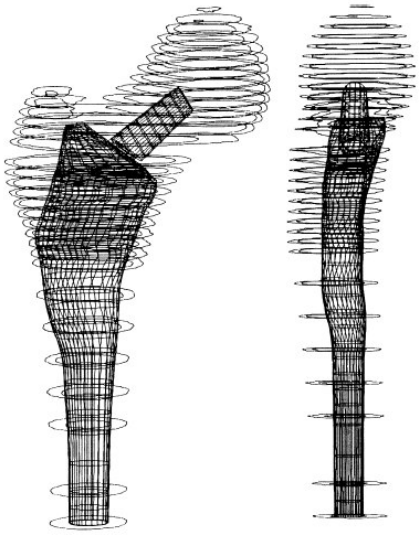

Figure 15: Hip implant in femur [71]

Chapter 3

3 Morphological Measurements

The morphological measurements describe the overall dimensions of the distal femur. These dimensions were measured during the operation and compared to dimensions of the template to select the size. These dimensions include the medial lateral (ML) and anterior posterior (AP) dimensions. The main aim of this study was to determine how well available prosthesis sizes replicate the dimensions of the femur. Therefore the measuring procedure during surgery had to be replicated. The 3D models of the bones were used to measure the required dimensions. Patients, undergoing a total knee replacement, were scanned to create the 3D models through computer segmentation of the CT data.

3.1 Segmentation Procedure

3.1.1 Scanning of Patients

The patients were scanned with a Siemens SOMATOM Emotion 16-slice CT scanner [77]. Patients were placed on the scanning bed with the patella positioned anterior and the feet held together. The leg window was selected with a topogram length of 1024 mm. The scans were performed with a 5 mm slice thickness and a 0.0° gantry tilt for 15 seconds. The patient was then removed from the scanning table. The images were reconstructed with a 1 mm slice thickness. A filter was applied to the data for improved reconstruction of the 3D models. The CARE (Combined Applications to Reduce Exposure) Dose4D setting was enabled to automatically adjust the emitted X-ray dose according to the cross-sectional area of the individual.

3.1.2 Procedure

The CT scan data are essentially 3D information displayed in 2D. The third dimension is related to the colour of the pixels (voxels) in Hounsfield (HU) domain [78]. Segmentation algorithms were used to identify certain voxel intensity linked to the bone in the CT scan data [79]. Thus in each slice a surface was extracted of which the voxel colour intensity fell in a specific threshold interval. These algorithms were applied to all the slices of the scan data and then stacked upon each other to create a 3D model.

3.1.3 Importing Data

The data exported from the CT scanner was in DICOM file format. A single file contained a number of different types of scans. These different scans could be separated according to their gantry tilt, pixel size and location of centre. Thus each scan was of the same image viewed with different settings. Each type of scan consisted

of a large number of slices. The selected type was imported and converted in the Materialise MIMICS workspace.

When importing the images, different types of image compressions were available. The three image compressions were CT, MR and Lossless. CT compression was used for the removal of background noise from CT-images. All voxels with a grayvalue between 0 and 200 were set to zero. MR compression was used for the removal of noise from the MR-images. In this case all voxels with a grayvalue between 0 and 10 were set to zero. Voxels were unchanged with the Lossless compression.

3.1.4 Segmentation Technique

The software automatically creates two additional views, apart from the original transverse view (Figure 16). These could be used to further enhance the capabilities of the CT scan for the preoperative planning measurements before surgery. These views consisted of varying pixel intensities, with the light being hard material and low intensity for softer material.

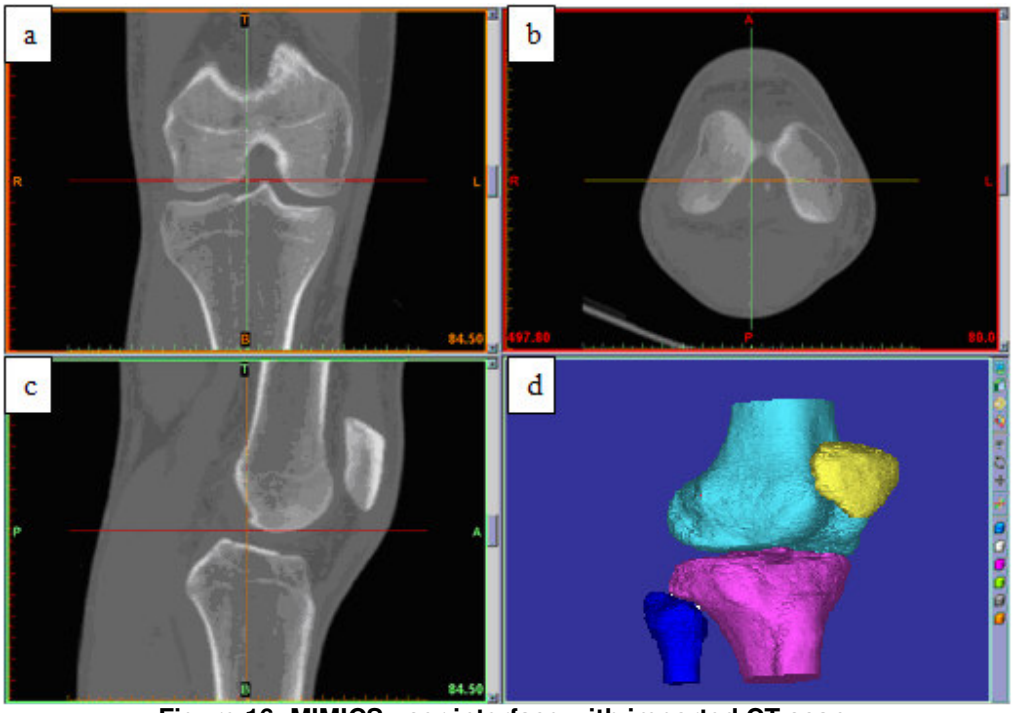

Figure 16: MIMICS user interface with imported CT scan:
a) front view b) top view c) side view d) 3D view

After the mentioned views have been created, a pixel intensity threshold was selected which represents the cortical bone structures. All the pixels that fell outside the interval were ignored. The pixels that were in the interval were added to a mask. MIMICS used different masks to separate different items. In the older versions of MIMICS, the threshold interval limits was selected manually. The newer versions contained certain preset threshold intervals that could be selected, depending on the type of tissue that was investigated. Therefore the 3D models were created automatically and were independent of the user's judgment. The *BoneCT* threshold interval was selected,

creating a mask which represents the bone structures in all images. This mask included the femur, tibia, patella, hip and fibula. The different bones were then separated with method called region growing. A single voxel was selected and all other voxels connected to the first were removed from the original mask and added to a new mask. This option can be applied to a single plane or through the entire image. When this procedure has been completed, a mask was created for each specific bone. Although the bones were separate in the specific masks, perfect 3D models could not be created. The threshold interval only selected the hard bone pixels (displayed white) and added it to the masks. The porous, soft bone and bone marrow fell in a lower threshold than the hard bone structures. This problem could not be eliminated during the threshold procedure by lowering the threshold limit to accommodate for the other bone types. This decreased the accuracy of the selected structures and parts of the surrounding soft tissues would be included in the mask. Thus the masks had to be edited by hand to only select the required voxels to complete the 3D models of the bones.
There are two regions of the masks that required manual editing before a completed 3D model was created. The first was when the hard bone pixels were selected in the threshold interval, a cavity was formed in the mask due to the softer bone marrow. This was corrected by using functions of the MIMICS software. Polylines were created around the outer edges of selected voxel regions (Figure 17). All unselected voxels found inside a polyline region was added to the mask with the cavity fill tool.

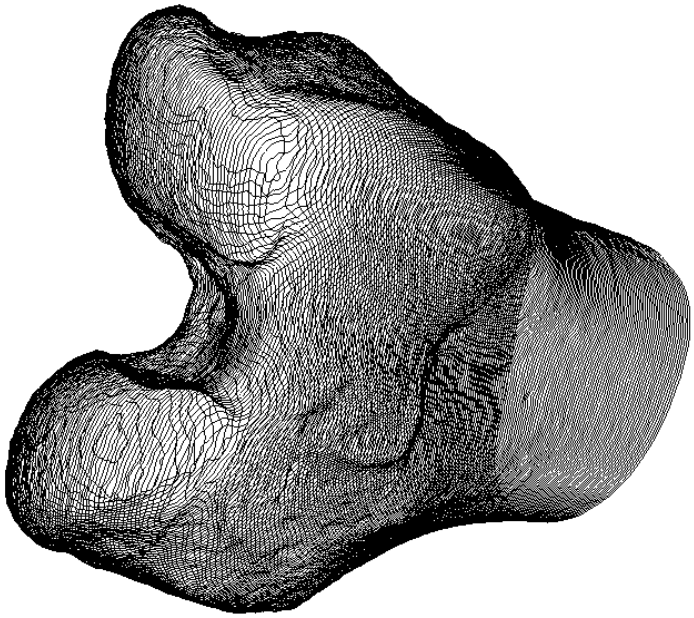

Figure 17: Polylines created around the outer edges of distal femur

The second region was the three contact areas between the femur and tibia, hip and femur as well as the femur and patella. The two different filters were investigated and are presented in Appendix B and the B10 filter was applied to the CT scan data

3.1.5 Post-processing

Post-processing was performed on the 3D models to remove any imperfections. The models were smoothed and any free particles were removed. Most of the measured patients had large numbers of osteophites growing from the distal femur (Figure 18).

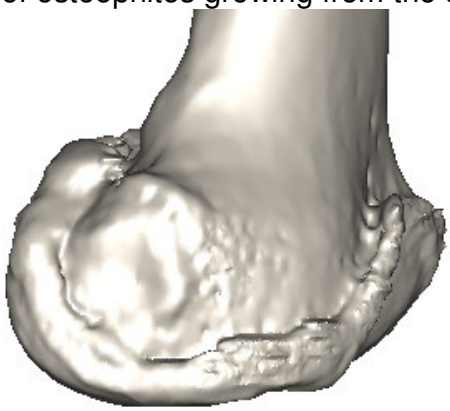

Figure 18: 3D model of distal femur with osteophites

Thus any osteophites that could be removed were cut off from the models. When the post processing procedure was completed, the models were finished and ready for measurement.

3.2 Morphological Measurements

The dimensions measured had to be comparable to dimensions of the prosthesis and vice versa. The bone resections made during surgery for component placement were easily compared to the prosthesis. Although certain measurements were required to perform these bone resections. Thus other measurements had to be incorporated into the analysis to determine the fit of the component. The measured dimensions of the unhealthy knees are given in Appendix A.

3.2.1 Mimics Analysis

The knees of 35 patients (mean age 65 yrs) who required a total knee replacement (TKR) were scanned and imported into MIMICS. The MIMICS software consists of a base platform with different add-on modules to enhance the functionality of the software in a specific area. The *Simulation* and *STL+* modules were added to the platform for this study. The *Simulation* module is used to simulate different surgical procedures, while the *STL+* module allows for STL file format importing and exporting. Included in the simulation module is a model measuring tool called Anthropometric Analysis

3.2.2 Anthropometric Analysis

Anthropometric Analysis uses templates to measure specific user defined dimensions. These templates consist of points and planes which can be used to calculate allocated measurements. Pre-set templates were available or new templates could be created for specific problem.

The required template was selected from the list and the points were placed on the specific landmarks. The planes and measurements were created automatically after all

the dependant points were placed. The point coordinates and measurements were exported to a text file with the export function.

3.2.3 Template Setup

A template was created in the anthropometric analysis to measure the required dimensions of the femur. Different settings could be selected to create parallel or perpendicular planes. The measurements included point-to-point or point-to-plane distance measurements and the angular difference between two planes could also be measured. The points required for the study was divided into three groups. The first group of points were necessary to measure other dependant parameters. These included reference markers too measure certain dimensions from. The second group of points were to calculate the parameters required for the goodness-of-fit equation, such as the AP and ML dimensions. The last group of points was to gain specific data of the femur, which was not used for the GOF calculation. Femoral version and TT/TG were the most important measurements from this group. The femoral version was a angle measurement between the posterior epicondylar axis plane and a plane through the proximal femur neck. The TT/TG is a distance measurement between the trochlear groove plane and the tibial tubercle point viewed in the transverse plane. The knee analysis template consisted of 63 points, 29 planes and 37 measurements (Figure 19).

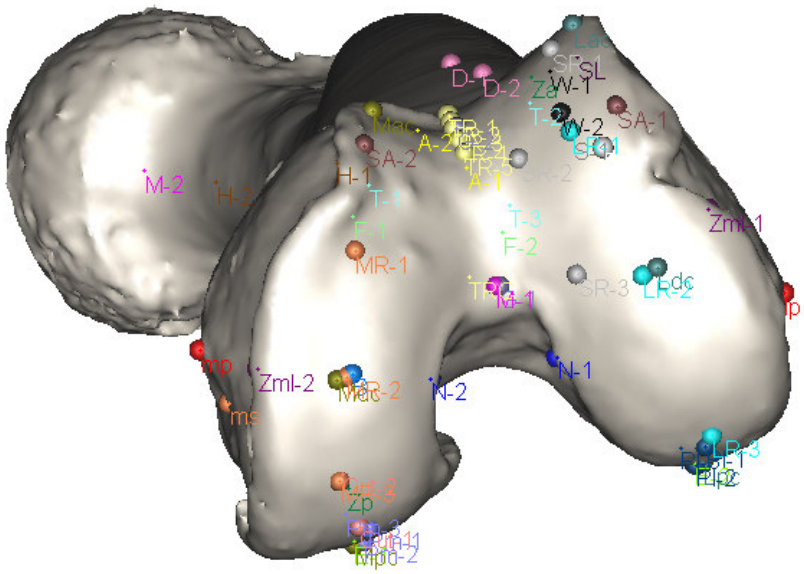

Figure 19: Full femur with all the required template points

The most important parameters of the knee analysis will be explained in the following paragraphs. The full template analysis and point placement is given in Appendix B.

3.2.4 Reference cuts

The MIMICS measurements were compared to the measurements made on the 2D CT scans. Therefore reference planes had to be generated on the models to perform the rest of the measurements. Three planes were made on the 3D models as a reference to

the 2D scans. The reference planes were the transverse plane, sagittal plane and frontal plane. The transverse plane was set parallel to the CT slices. The frontal plane was created parallel to the bed on which the patient was scanned and the sagittal plane was made perpendicular to the previous two planes. The position of these planes were not important and could be placed anywhere on the femur.

3.2.5 Anatomical Axis

The anatomical axis of the femur is the line down the centre of the femoral shaft. The anatomical axis was measured by making two cuts perpendicular through the shaft of the femur. The accuracy of the cutting angle was not important and therefore the cutting line was drawn by hand. The first cut was made 100 mm proximal to the condyles and the second cut was 100 mm proximal to the first cut (Figure 20). The centre point of each cut was identified on the end of the cut out. These two points were connected to form the anatomical axis.

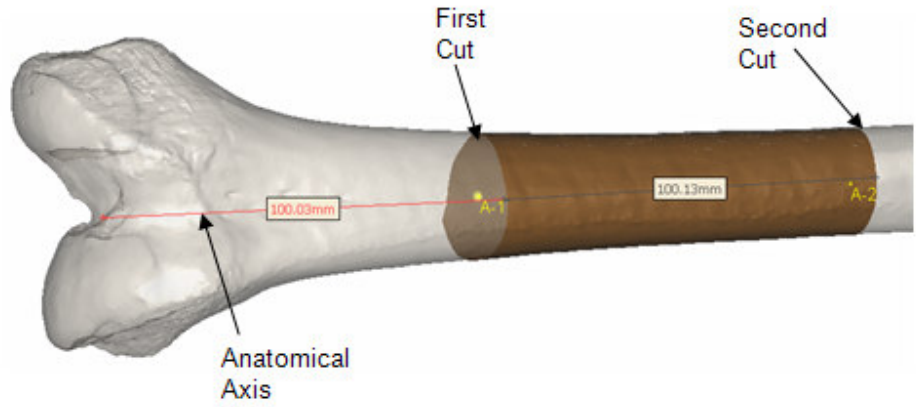

Figure 20: Anatomical axis cuts through femur shaft

The mechanical axis was also created and used with the anatomical axis to determine the vulgus angle or anatomical/mechanical angle (AMA). The mechanical axis was created by placing one point on the epicondylar arch and the second point at the hip centre of the proximal femur (Figure 21). The hip centre was allocated by viewing the model from different angles until it was acceptable.

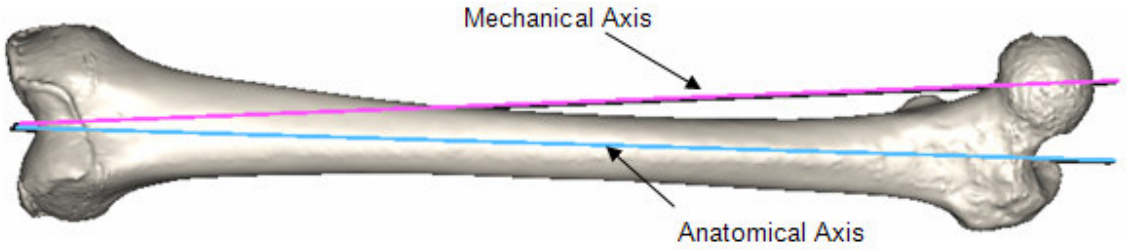

Figure 21: Mechanical and Anatomical Axis

3.2.6 Epicondylar Axes

The angle between the surgical epicondylar axis and the posterior epicondylar axis was measured to determine the rotational alignment of femoral component. Three points

were added to the template and was placed on the three specific landmarks. These points were connected with planes set perpendicular to the transverse plane. The posterior epicondylar axis was created by placing two points on the most posterior point of each distal condyle. This plane was also set perpendicular to the transverse plane (Figure 22). An angle measurement was created between each plane and the posterior epicondylar axis.

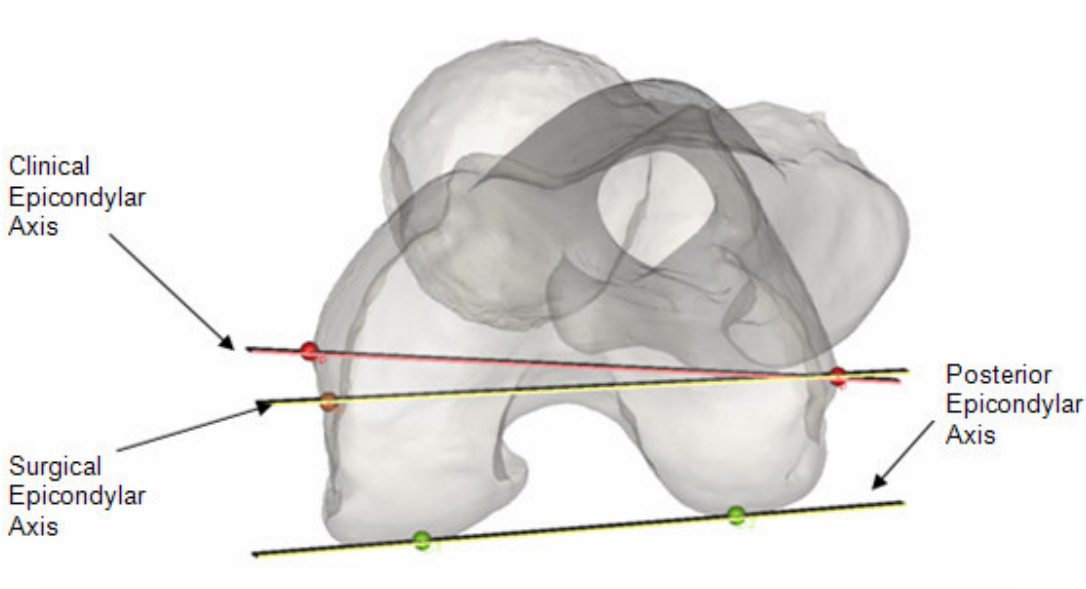

Figure 22: Epicondylar axes viewed from the bottom

3.2.7 Cuts

The resections of the distal femur had to be created to simulate the component implantation. The posterior, distal and anterior cuts were included in the analysis template. The distal cut was represented by a plane which was set perpendicular to the mechanical axis. The posterior cut was made parallel to the surgical epicondylar axis and perpendicular to the distal cut. The anterior was also parallel to the surgical epicondylar axis and not perpendicular to the distal cut (Figure 23).

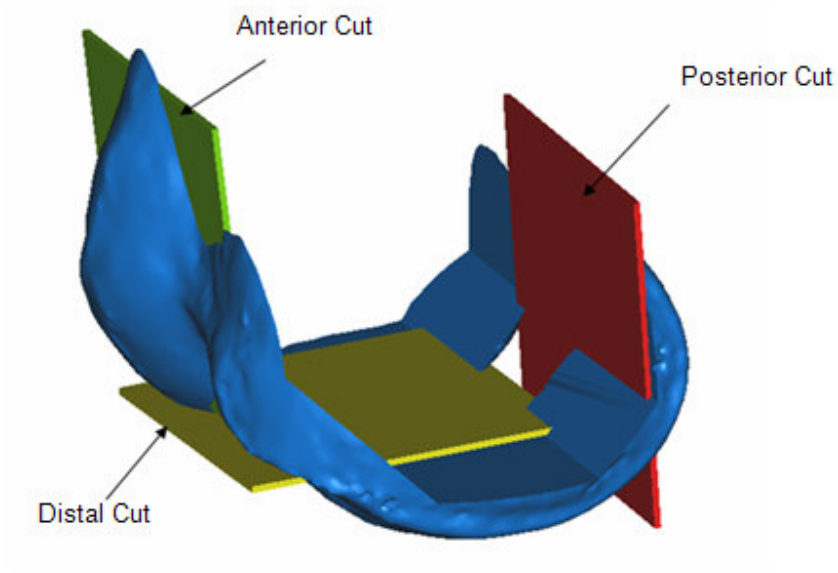

Figure 23: Cutting planes

3.2.8 Trochlear Depth

Throughout the trochlear groove length there was a variation in the depth. Therefore it was decided to measure the depth at only one specific point for all models. The trochlear depth was measured 60° from the most distal point in the trochlear groove. This was the point in the groove where the patella was in full contact during flexion from full extension. The depth was measured with a point to plane measurement. Two points were placed on the highest medial and lateral position on either side of the point inside the groove. A plane was created perpendicular to the depth measurement direction (Figure 24).

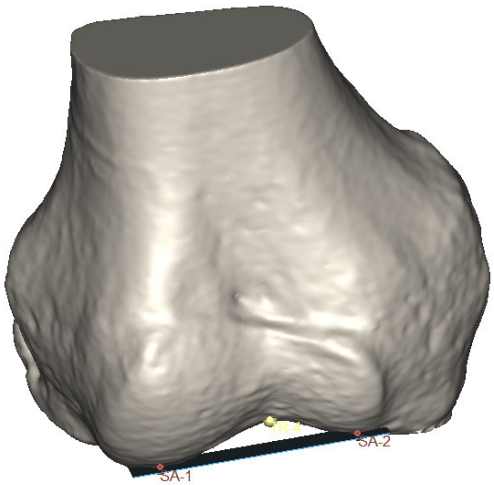

Figure 24: Trochlear depth measurement in MIMICS

3.2.9 Trochlear Angle

The trochlear angle is the angle with which the trochlear groove deviates from the natural anatomical axis. The angle can be measured in MIMICS with a plane representing the trochlear groove. This meant that the trochlear angle would only be calculated using two points and assumes that the trochlear was in a straight line. A different method was used which allocated more points to symbolize the trochlear groove. Four points were placed, respectively at -10°, 0°, 15° and 30° in the trochlear groove with 90° representing the most distal point of the anatomical axis (Figure 25). Planes set perpendicular to the trochlear groove were created at each angle. The planes were viewed from the side to select the lowest point of the groove found in the plane.

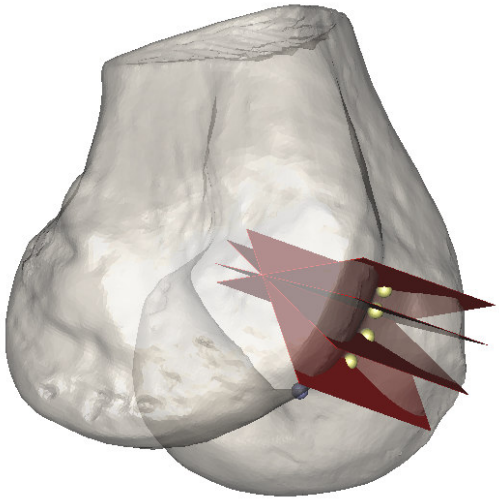

Figure 25: Trochlear planes

The angle was calculated with a Matlab program using the exported measurements from MIMICS. The distance from the anatomical axis and proximal distance to the 90° point was measured for each of the four points. The four points were placed on a 2D graph with the anatomical axis on the x-axis and a plane through the 90° point on the y-axis. A regression line was drawn through the four points and the angle measured from the x-axis to the regression line. The trochlear angle measured in MIMICS was also displayed on the graph (Figure 26).

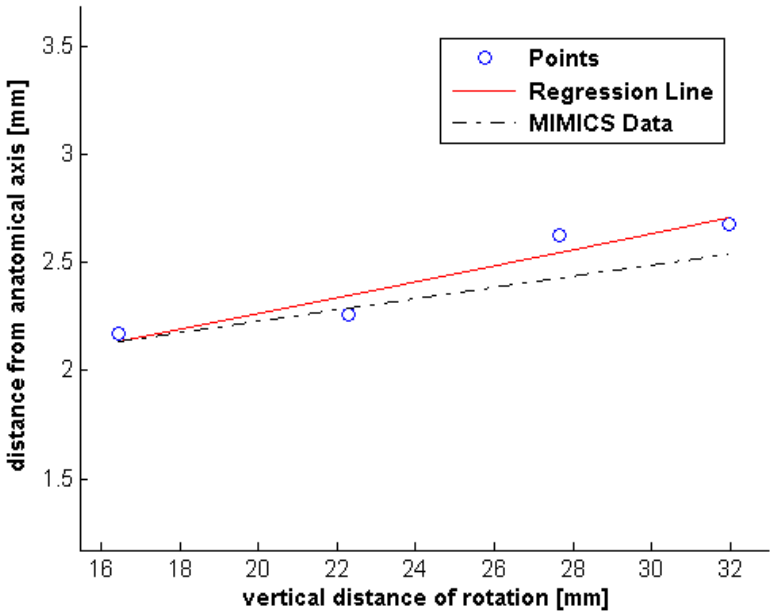

Figure 26: Trochlear angle calculation method results

A clear difference was visible between the two methods of measuring the trochlear groove angle.

3.2.10 Radius Measurement

The anthropometric analysis could not be used to calculate the radius of a specific curvature. The principle that any three points, not in a straight line, creates a circle was used (Figure 27). The centre of the circle was calculated by connecting the points P1 to P2 and P2 to P3. Perpendicular lines were created at the centre points of the connecting lines. The intersection point of the two lines gave the position of the circle centre. The distance from each point to the centre was constant and equal to the radius of the circle.

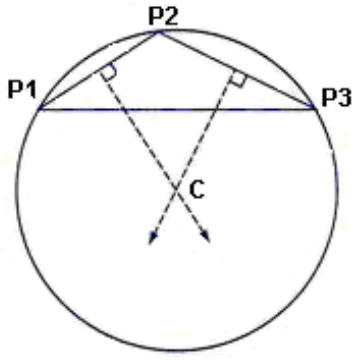

Figure 27: Simple centre calculation principle

The point was only placed in MIMICS and the coordinates of the three points were

exported to a text file. Firstly the text file was imported into Matlab and the points displayed on a 3D graph. A plane was created through the three points and all calculations were done in the created plane. Vectors were utilized to determine the connecting lines between points 1-2 and 2-3 (Figure 28). The cross product of the two connecting lines was applied to calculate the vector normal to the plane. The midpoints of each connecting line was calculated and displayed on the graph. Using the cross product of the connecting lines and the plane normal vector, vectors were computed on the plane at the connecting line midpoints. The intersection point of these two vectors delivered the circle centre point. The intersection point was calculated by creating a plane perpendicular to the original plane at the midpoint of the connecting line between points 1 and 2. The centre point was calculated where the other vector intersected the calculated plane. The radius was measured from each point to the centre point.

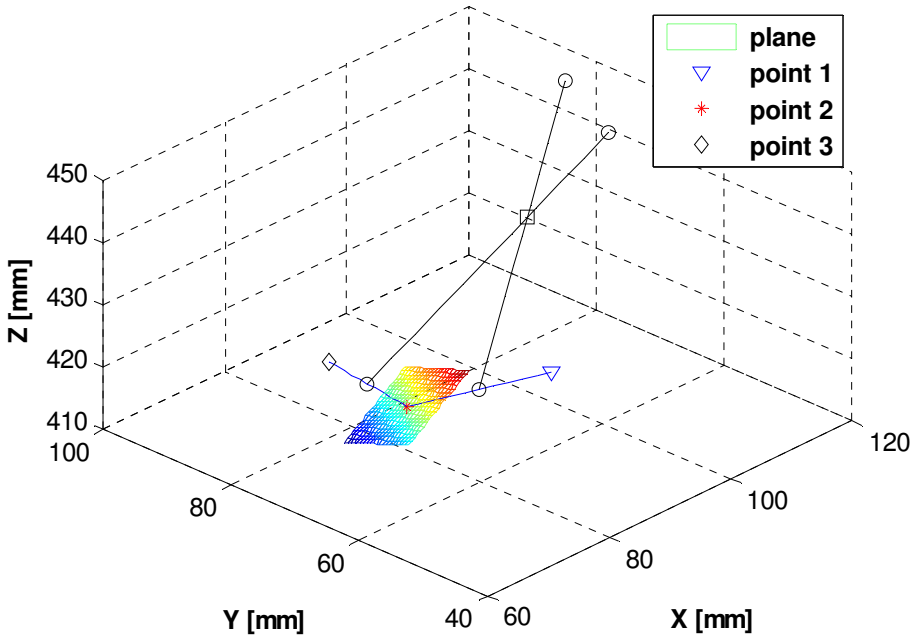

Figure 28: Centre calculation method in 3D using Matlab

This radius calculation method was used to calculate the five main radii of the distal femur:

- Medial and lateral condyle radii
- Medial and lateral posterior condyle radii
- Trochlear groove radius

The positions of the points were very important for accurate measurement. Only the trochlear groove points had specified angles at which each point had to be placed. The four other radii measurements were produced by first placing the second point and then indicating the positions of the first and third. On the distal condyles, the second point was placed on the most distal face and the most posterior face was used for the

posterior condyles (Figure 29). This ensured that the radius measuring procedure was done in an equivalent manner for each knee.

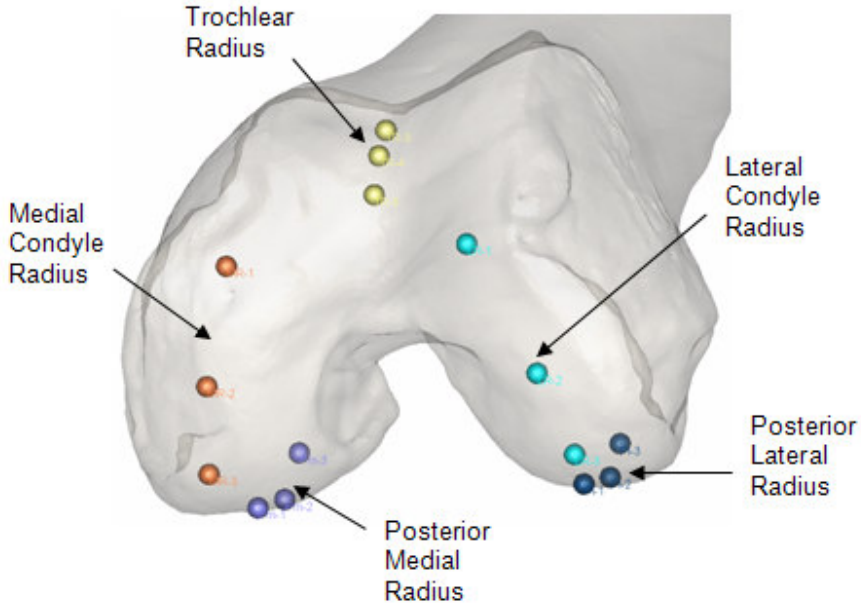

Figure 29: Five radii measurement positions on distal femur

3.3 Cartilage Estimation

CT scans were utilized to measure the morphological dimensions of the femur. Only the hard bane materials were detectable in the scans and no cartilage layer was observed. Measurements performed during surgery were made from the cartilage layer surface. Thus, the results of the two measuring methods were incomparable. Although the cartilage thickness was worn down in many of the patients used in the database, it could not be excluded and had to be integrated in the 3D CT scan measurements.

3D models of the cartilage layer were created through MRI scans of the knees. The models could then be added to the CT model in MIMICS. However, ideal 3D models could not be created due to soft tissues surrounding the cartilage layer perimeter that had to be removed through manual segmentation (Figure 30). This was frequently found at the trochlear groove, which had the patella cartilage and fat pad in the vicinity. The cartilage model could not be placed accurately on the bone structure, because three reference points were required on both models.

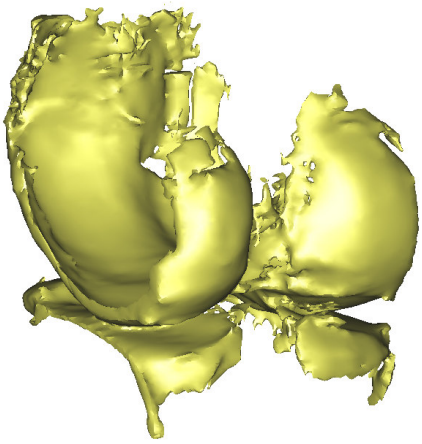

Figure 30: 3D model of cartilage using MRI scanner

Cadaveric distal femurs were dissected to examine the cartilage layer thickness. A CT as well as a 3D scan was performed on all the femurs and the two obtained shells were overlaid. The CT scan included the bony structure, while the 3D scan model included the cartilage layer. Combining the two scans required three equivalent points on both models, because the cartilage layer was excluded from the CT scan, the articulating surface could not be used. Therefore reference points visible on both types' scans had to be inserted. Different types of metal screws and nails were examined in the CT scanner to evaluate the amount of scatter. Due to the scanning characteristics of Iodine, it was mixed with glue and added to the specimen. The Iodine/Glue mixture delivered the best results out of all the tested materials. Three panel pins covered with the iodine/glue mixture were hammered into the bones as reference markers (Figure 31). The pins were covered with a matt white paint for higher accuracy in the 3D scanner.

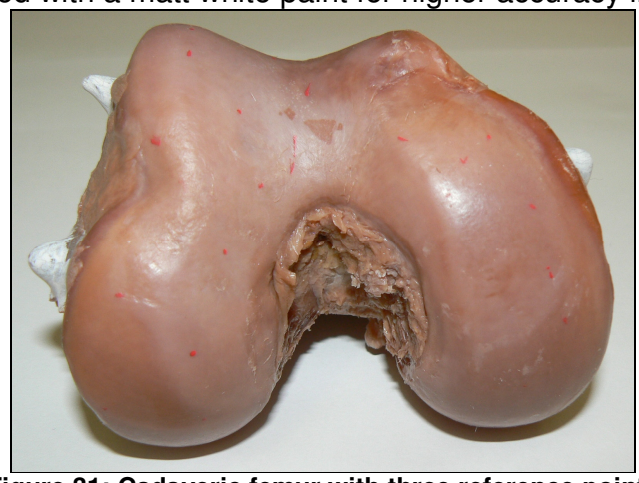

Figure 31: Cadaveric femur with three reference points

The two scans were overlaid using the three inserted reference points. The cartilage layer thickness was computed with another template created in MIMICS. A set of markers were placed on the CT scan model at specific areas and then a second set

was placed above the previous markers on the 3D scan model. The distance between the two points were measured as the cartilage thickness at that position. Fifteen positions around the articulating surface were allocated for measuring (Figure 32). The CT scan model is blue and the 3D scan model is red and transparent.

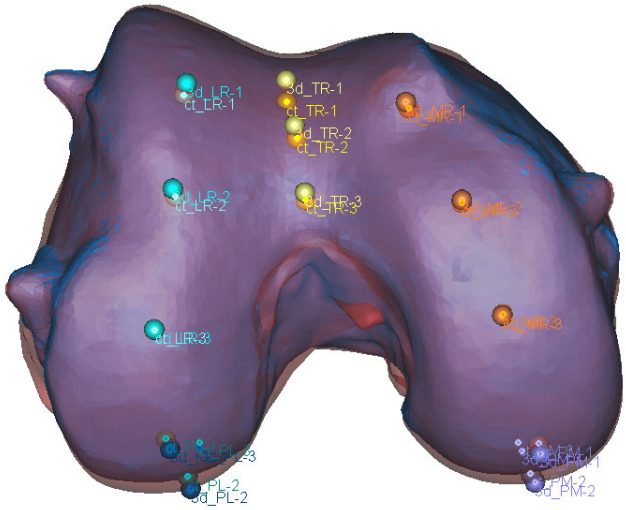

Figur **kness**

The cadaveric knee data are given in Appendix C.

3.4 Correlating Normal and Damaged Knees

The goal of a total knee replacement is to recreate the original surface of the femur. Thus to determine which size prosthesis to implant, the dimensions of the original distal femur is essential. It would have been excellent if CT scans of the patients were available before the knee was damaged; only the damaged knee dimensions were available before surgery. The healthy knee dimensions were estimated with correlation and interpolation with using cadaver knees and Self Organizing Maps (SOMs). The SOM, also known as a Kohonen map, is an unsupervised neural network. The SOM is a vector quantization method which places the vectors on a regular low-dimensional grid. The cells are arranged to various input values through unsupervised learning [80]. The array locations become ordered with similar cells grouped together from the input features. When mapping has been completed, an input matrix can be matched to the set of dimensions in the map. In the input matrix certain dimensions are left out and entered as a not-a-number (NaN) value. The input data is matched to the best matching unit (BMU) and delivers the remaining unknown dimensions which were entered as NaNs.

The 3D models created from the patients who underwent a total knee replacement had no cartilage layer and only CT scan data could be used to create the models. Twelve dimensions are used to describe the distal femur:

- Anterior Posterior (AP)
- Medial Lateral (ML)
- AP_{BOX}
- Lateral Condyle Radius (LCR)
- Medial Condyle Radius (MCR)
- Posterior Medial Radius (PMR)

- Posterior Lateral Radius (PLR)
- Trochlear Radius (TR)
- Trochlear Angle (TA)
- Sulcus Depth (SD)
- Resected Posterior Condyle (RPC)
- Sulcus Length (SL)

Only three out of the twelve dimensions were not measured from the cartilage layer edge and was therefore independent of the cartilage layer [17]. These unaffected dimensions were the ML, TA and SL. These three dimensions were used to determine the other dimensions in concurrence with the healthy cadaver database. Only cadaveric femurs with no visible damage were selected and dissected. Although the layer thickness was diminished due to the preservation, it was of good condition. The CT and 3D overlaid scans of the cadavers used in the previous paragraph was used as the healthy knees. The dimensions were measured with the same analysis template used on the damaged knees. The points were placed on the 3D scanner model when measuring around the articulating surface, while landmark points (l_p, m_p, m_s) were placed on the CT scan model. Thus the healthy knee dimensions were calculated with the cartilage layer thickness included. Using these overlapped models, two data sets were created. In the first data set, the AP, AP_{BOX} and RPC dimensions were measured in the same manner used on the damaged knees, with all of the cuts measured from the bone profile (CT scan). The total AP dimension was measured from most anterior point to most posterior point of the CT scan model, while the AP_{BOX} and RPC measurements were affected by the posterior and distal cuts respectively. These two cuts were taken directly from the bone surface. Thus no cartilage layer was included in these three measurements. Thus the three dimensions made on the damaged knee and in the first data set were comparable to each other. In the second data set, the three dimensions were measured from the cartilage layer (3D scan). The other nine dimensions were measured on the cartilage layer and were equal in both data sets. Thus the AP, AP_{BOX} and RPC dimensions were the only difference between the two data sets. The damaged knee generates six dimensions, of which three are true measurements (ML, TA, SL) and the other three were determined using no cartilage layer (AP, AP_{BOX}, RPC). Using self-organizing maps (SOMs), the six values were entered into the first data set to estimate the six unknown values. The AP, AP_{BOX} and RPC values were then removed and the remaining nine dimensions entered into the second data set to calculate the true values of the three removed dimensions (Figure 33). Thus the three values used with no cartilage thickness were only used to initiate the process and was phased out by the calculation procedure.

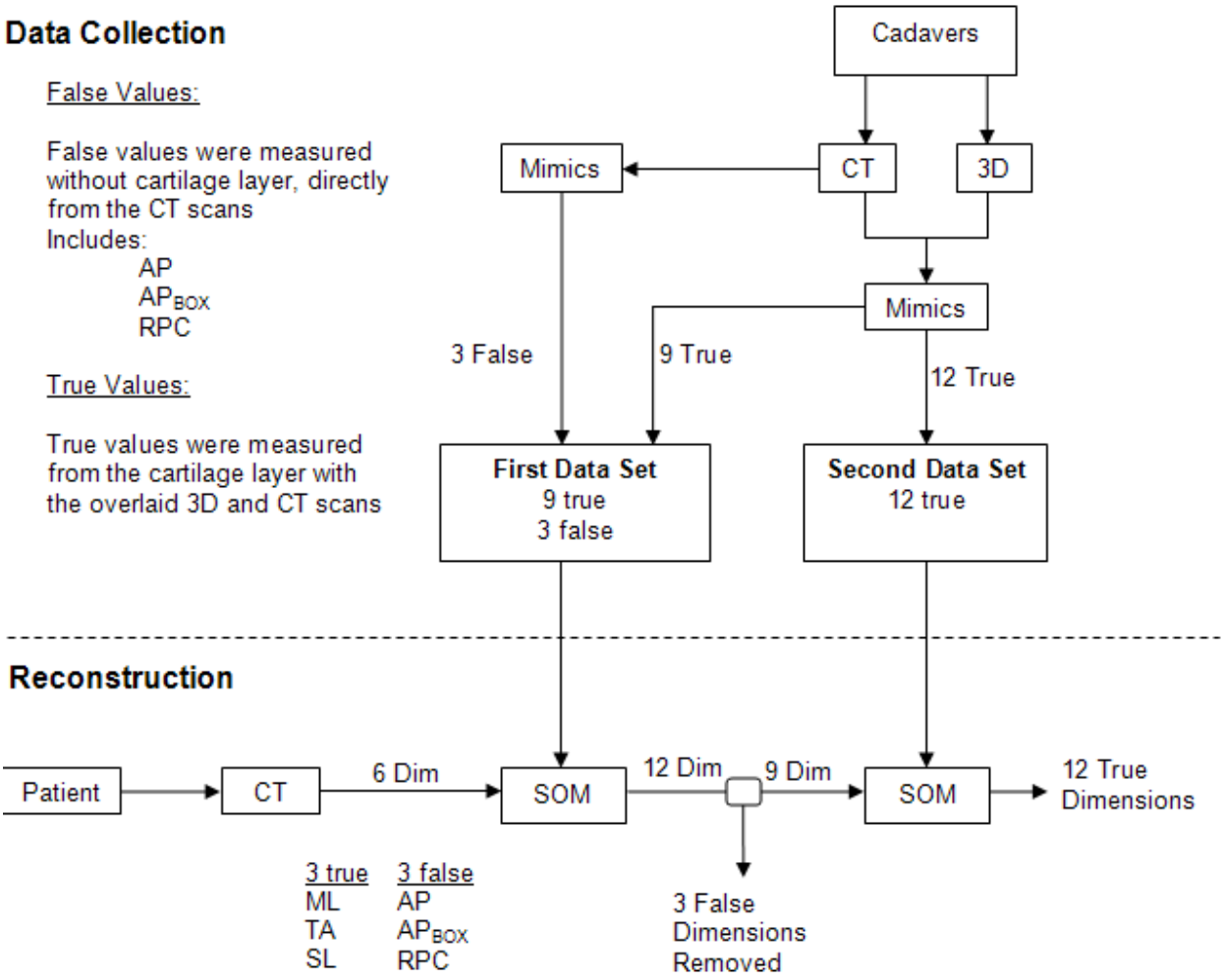

Figure 33: Estimation of healthy knee dimensions

The SOM of the AP, AP_{BOX} and RPC measured with no cartilage are shown below (Figure 34).

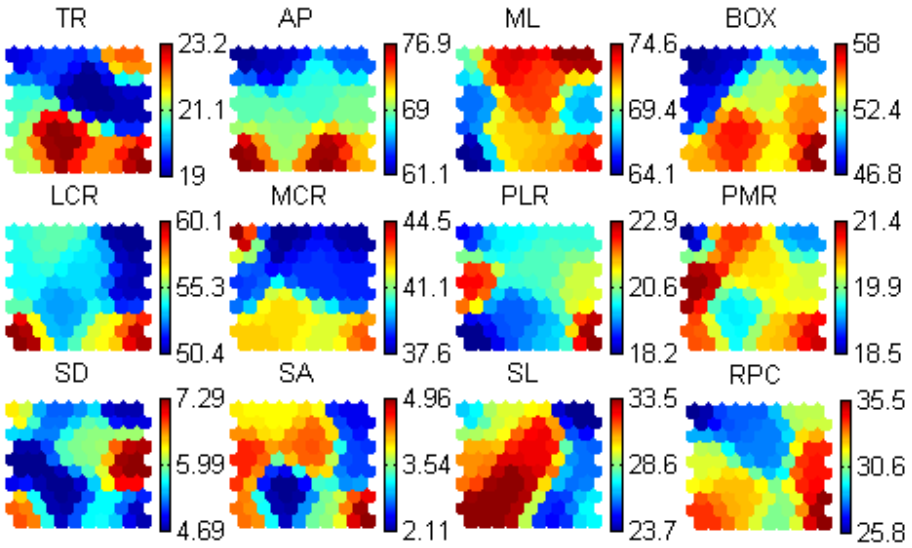

Figure 34: SOM with no cartilage

Only a limited number of data arrays were available due to the small number of specimens used. Thus the method would only work if the patient dimensions fell inside the specimen dimensions. The cadavers used were smaller than the patients and therefore the method was altered to make it dimensionless. Size was removed from the parameters by dividing all the parameters by one specific parameter. The ML dimension was used as the specific parameter, because it was accurately measured and was not affected by the cartilage layer. Thus the dimensions were compared to ratios between the dimensions and were not affected by the size of the femur. The problem of using a small cadaver database was also minimized by only calculating one unknown parameter at a time and substituting the calculated value in the original database to calculate the next. The method was repeated to calculate a new unknown dimension every iteration. This did not eradicate the problem completely; it only made the calculated parameters more accurate by using fewer unknowns in an iteration.
The database consisted of 35 CT scan knees (14 cadavers + 21 normal knees from CT scans). The dimensions of the CT knee database are displayed in Appendix C. The SOM method enabled faster calculation of dimensions and only six dimensions were required to determine the rest of the dimensions. This allowed for easier and faster use in practice before the surgery.

3.5 Digital Reconstruction of Knee Prosthesis

Two types of prostheses were evaluated in the project: a posterior retaining prosthesis (PRP) and a posterior sacrificing prosthesis (PSP). These were similar in function, the only difference being that the PRP retains the posterior cruciate ligament whereas the PSP the posterior cruciate ligament is sacrificed. The second design uses a stem below the trochlear groove to compensate for the posterior cruciate ligament. The medial and lateral posterior condyle radii were equal on both designs. The condyle radii were equal on the PRP and unequal on the PSP, with a larger lateral condyle. On both designs the

trochlear groove was tilted lateral relative to the prosthesis and the anterior cut was more than 90° to the distal cut.

3.5.1 Scanning

Computer aided design (CAD) models or 3D models of each commercial prosthesis size were required to determine the complete geometry of the standard sizes. However, CAD models could not be obtained from the manufacturers and each specific size was scanned with a 3D desktop laser scanner from NextEngine to create the CAD models (Figure 35).

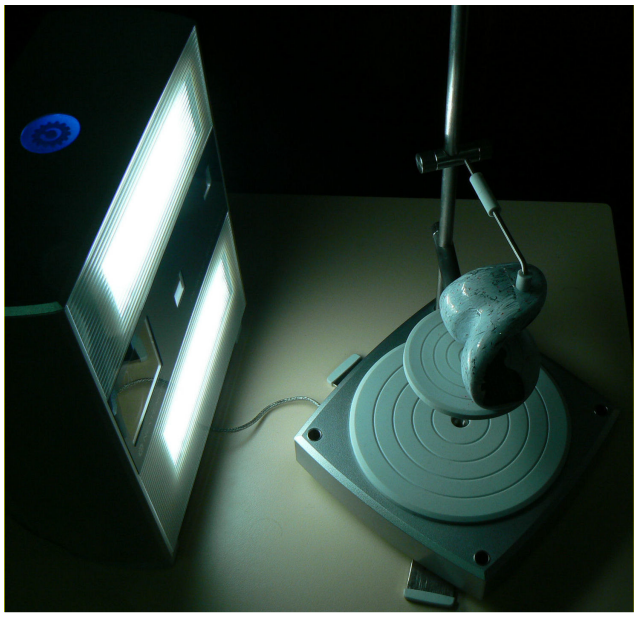

Figure 35: 3D scanner during scanning of prosthesis

The NextEngine scanner uses proprietary multistripe laser triangulation (MLT) technology [81]. Twin arrays of four 10 mW solid sate lasers with custom optics retrieve the 3D object (Figure 36). A dimensional accuracy of ± 0.005" can be achieved and an acquisition speed of 50 000 points per second could be processed by the scanner. The scanner capabilities were validated for flat and curved surfaces and the results are displayed in the second part of Appendix B.

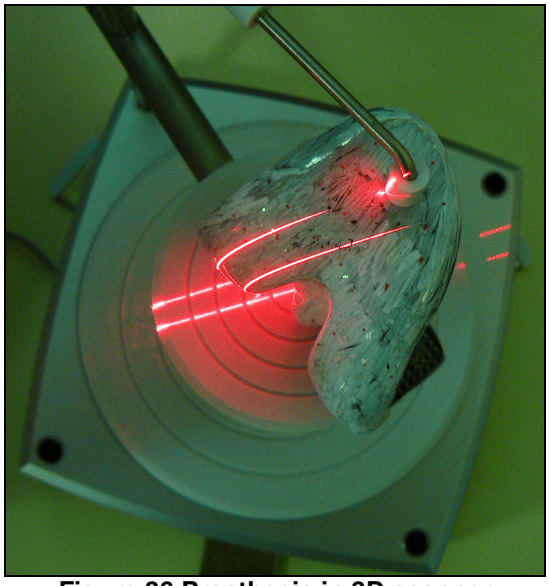

Figure 36 Prosthesis in 3D scanner

The scanner required a matt surface for correct and accurate functioning. This was not a problem with the cadavers, but the shiny surface of the metal prosthesis caused a loss of data points. The prostheses were painted white before scanning, to eliminate the problem. After the scanning was completed the model was imported into RapidWorks to clean up the scan data and fill small holes in the mesh (Figure 37). The completed 3D models were exported in STL format from RapidWorks.

Figure 37: Scanned prosthesis model after editing has been completed

3.5.2 Dimensions

Only the main dimensions of each prosthesis size were given in the prosthesis specifications (normally AP, AP_{BOX} and ML). These dimensions and the remaining dimensions had to be measured on the models constructed with the 3D scanner. The STL models were imported into MIMICS and an analysis template created to measure

all the necessary dimensions of the prosthesis. This template only measured the required parameters for the GOF method (Figure 38).

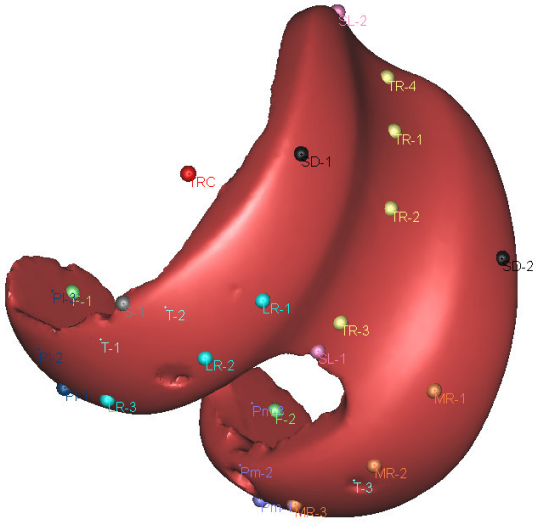

Figure 38: Prosthesis dimensions measurements

Because the distal cut on the femur was made perpendicular to the mechanical axis, the sagittal plane of the prosthesis was therefore equal to the mechanical axis of the femur. Thus the trochlear groove angle of the prosthesis was a deviation from the mechanical axis and not the anatomical axis. Therefore the trochlear angle measured from the prosthesis was subtracted from the patients' anatomical/mechanical axis angle to determine the trochlear angle of the prosthesis from the anatomical axis of the knee. The measured dimensions of all the prosthesis are displayed in Appendix D.

Chapter 4

4 Kinematic Simulation

4.1 Motivation

In the previous chapter the dimensions of the distal femur was determined. The kinematics of the femoral component plays no part in the size selection procedure. This delivered the following research question: Would a perfect duplicate of the distal femur recreate normal kinematics after surgery? This is due to the fact that when a ligament is sacrificed during surgery (usually the PCL) the natural geometry has to be altered to compensate for the loss of the ligament [47]. This change in geometry would decrease the geometric fit, although it might improve the kinematics of the component. If the ligaments were kept intact and unchanged, a perfect femoral duplicate would work. The alignment of the prosthetic components plays an important role in the knee kinematics. A femoral component can be perfectly customized according to the morphological dimensions of the distal femur and if it is not implanted with the correct alignment, the kinematics would be incorrect.

4.2 Procedure

The main aim of the simulations was to compare a healthy and prosthetic knee kinematics. In order to create two models which were only depended on the articulating shape required all the other factors to be held constant in both simulations.

The kinematic evaluation was performed by first simulating the normal healthy knee with all the ligaments and muscles intact. Measurements were made of certain parameters of the knee. The knee was then simulated with each of the sizes in the design range and the measurements recorded. The kinematics of the prosthesis simulation depends on the prosthesis shape, component alignment, ligament properties and attachment points. Thus by constraining certain factors and keeping it constant between the two simulations, the shape of the prosthesis can be compared to the normal femur shape. The simulations of the two different prostheses were compared to the simulations of the normal knee. A value was calculated for how well the prosthesis size replicates the normal knee kinematics called the kinematic GOF.

The ideal method would be to compare the simulation results with results gained from tests performed on “normal” cadaver knees.

4.3 LifeMOD

LifeMOD was added to the MSC ADAMS™ platform is used to simulate human motion. There are basically two major anthropometric databases used in LifeMOD, Generator of Body Data (GeBOD) and PeopleSize. These databases are based on surveys performed on human anthropometric dimensions. The two database sets were developed by different organizations. The LifeMOD biomechanics modeller can create a default standard kinematic knee joint. A more biofidelic representation of the force-based knee joint was created for the application. In this study patient geometry, tibio-femoral and patellofemoral contact forces were added to the model. The knee model was stabilized with ligament forces and driven using muscle forces.

4.3.1 Model Construction

The model consists of a single leg with a mass at the hip location to represent the mass of the upper body. The normal knee simulation used a 3D CT model generated in MIMICS. Therefore a full lower body was scanned and computer segmented. The other knees used in the measurements were scanned from the hip to just below the joint line. A full left leg was retrieved from the lower body to generate the entire femur and tibia (Figure 39).

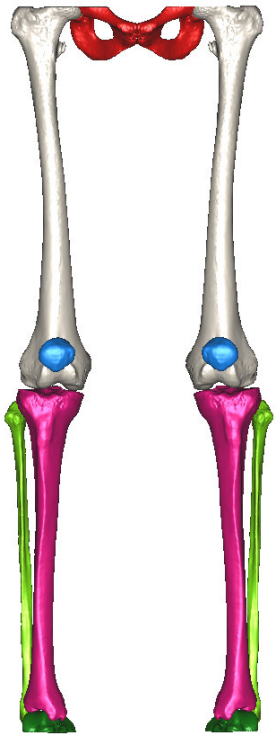

Figure 39: Lower body 3D model in Mimics

The femur, tibia and patella bone models were exported in ASCII STL file format from MIMICS.

4.3.2 Normal Knee

Firstly a full body model was created using the GeBOD database with specified length, weight and age of the patient. Segments were deleted to focus on the knee joint. All segments except the lower torso, left upper leg, left lower leg and left foot were not deleted (Figure 40). The mass of the pelvis was increased to compensate for the rest of the deleted body segments.

Figure 40: Default left leg model in LifeMOD

Simple kinematic Hybrid III joints with damping and stiffness forces, equal to the joints of a crash test dummy, were used for the ankle and hip joint. In the default body model there exists no segment for the Patella bone. An ellipsoid was created at the similar position as the patella part. The geometry of the model was a representation of the bones and was replaced with true imported models (Figure 41). The normal placement of the leg bones was equal to the positions in MIMICS. The models were all imported with the same rotation and translation to ensure that the relative distances between the bones were held constant. Thus the model created in LifeMOD would be an exact duplicate of the patient-specific model in MIMICS.

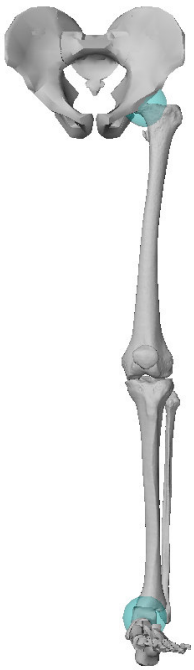

Figure 41: LifeMOD model with imported bone models

Ligaments were added to the model for joint stability. The ligaments were represented with point to point forces which generated a force between the two attachment points. The ACL, PCL and LCL were created with one ligament force while the MCL was divided into two ligaments. The patellar tendon was added between the patella and the tibia. The MPFL and LPFL were also included in the model. The ligaments were created by specifying the position and to which bone element it was connected too. These positions are the standard ligament attachment points specified in the literature [82]. Thus markers were generated at the correct positions to enhance the accuracy (Figure 42). These markers were then selected as the attachment points of the ligaments.

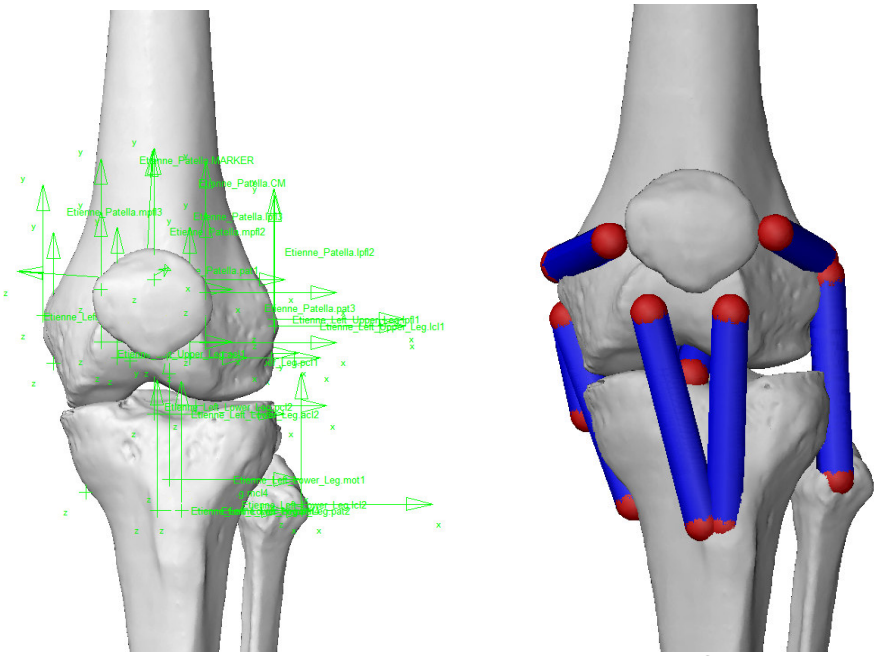

Figure 42: Knee ligaments a) Attachment position markers b) Soft tissue elements

After the ligaments were created, contact forces were generated between the shell models of each articulating component. Contacts were created for the tibio-femoral and patellofemoral joints. The next step was to insert the muscles elements of the knee model. A base set was automatically created of the basic muscle groups of the lower body. The muscle elements consisted of trainable and trained elements. The trainable elements were simple data collectors which record the contracting history of the muscle during a motion activity. The motion was created by external drivers called motion agents. The trained elements use the contraction data to induce the force on the skeleton to replicate the recorded motion. Since a new patella segment was created, the attachments of the muscles were repositioned to the patella segment. By default the Vastus Lateralis, Vastus Medialis and the Rectus Femoris muscles were attached to the lower leg in LifeMOD. A motion agent was placed on the lower leg segment. The motion agent added a displacement constraint along the anterior posterior axis of the knee and was free in the other five dof's. The displacement of the motion agent is controlled by the allocated spline path. The spline function controls the movement over a specific time interval. The lower leg had to move anterior, stop and return to the original position. Thus a spline was chosen to deliver the required displacement of the lower leg. The motion agent was driven by the following spline function (Figure 43).

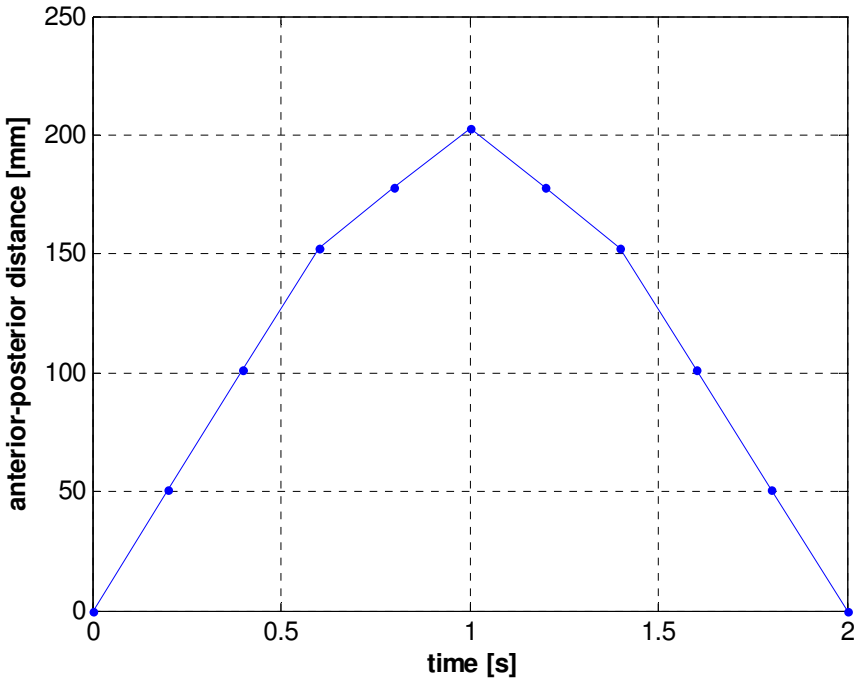

Figure 43: Input spline for motion agent

A fixed joint was placed on the foot and a vertical translation joint was placed on the lower torso to constrain their movement (Figure 44). An equilibrium analysis was performed to ensure that all the components were in contact. The motion agent was frozen to run the equilibrium analysis. The model posture was updated with the equilibrium results after the analysis.

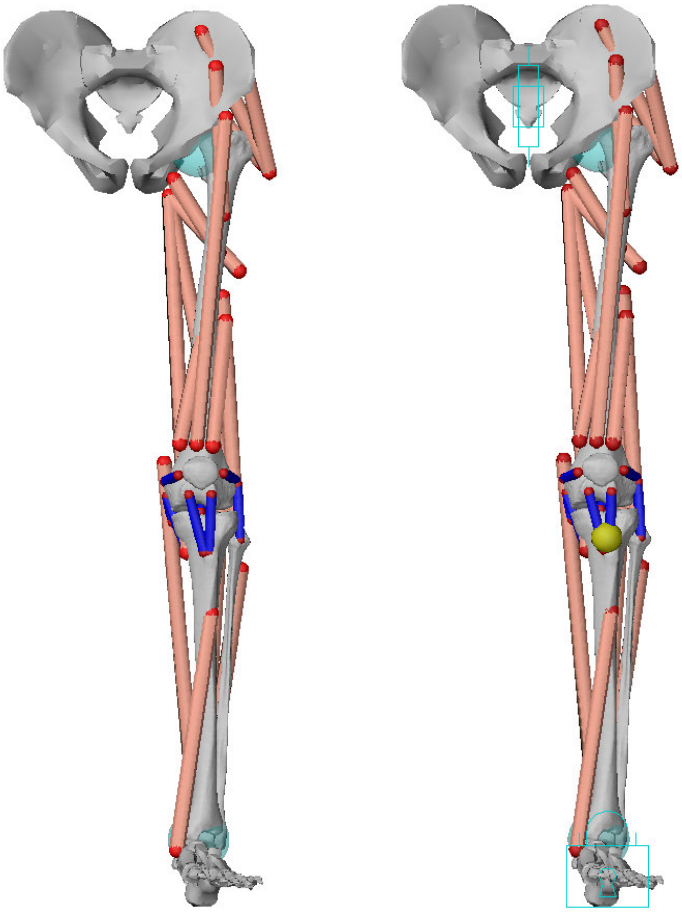

Figure 44: LifeMOD model a) Muscle elements added b) Motion agent added

The inverse-dynamic simulation was initiated, whereby the motion agent manipulated the model into a deep knee bend activity. During the analysis, the muscle contractions were recorded in the trainable muscle elements. The muscles were updated with trained elements from the recorded motion history. The motion agent was removed and the forward dynamic simulation activated. When the simulation was complete, the models were animated and the results presented. All the parameters required to create the simulation model are given in Appendix E.

4.3.3 Total Knee Replacement

The simulation of the knee replacement was created by importing prosthesis components into LifeMOD to replace the articulating surface. The CAD models were not of ideal quality due to the scanning, but the articulating surfaces were perfect and were used in the simulations. A prosthesis knee was created by using the normal knee simulation model before the equilibrium analysis and changed according to the type of prosthesis used. The tibio-femoral and femoral-patella contacts were removed and the prosthesis components imported into the model. The correct placement and rotational alignment of the components were ensured by importing the prosthesis models into MIMICS and implanting it at the correct position (Figure 45).

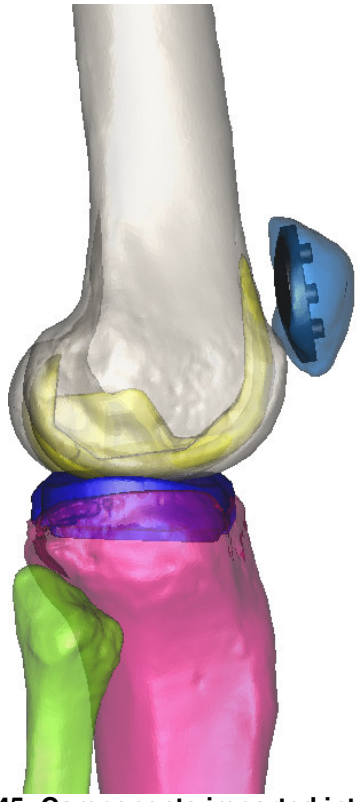

Figure 45: Components imported into Mimics

When the component alignment was satisfactory, the models were exported from MIMICS in *.stl format. Thus ensuring an equal relative centre to the bone structures in the model and were imported into LifeMOD with the same translation and rotation as the bone elements (Figure 46). Contacts were created between the femoral component and tibial insert as well as the patella and femoral components. The ACL was deleted and depending on the type of prosthesis used the PCL was also removed. When the model building was completed, the motion agent was frozen and the equilibrium analysis initiated. From this step onwards it was completed in the same manner as with the normal knee simulation.

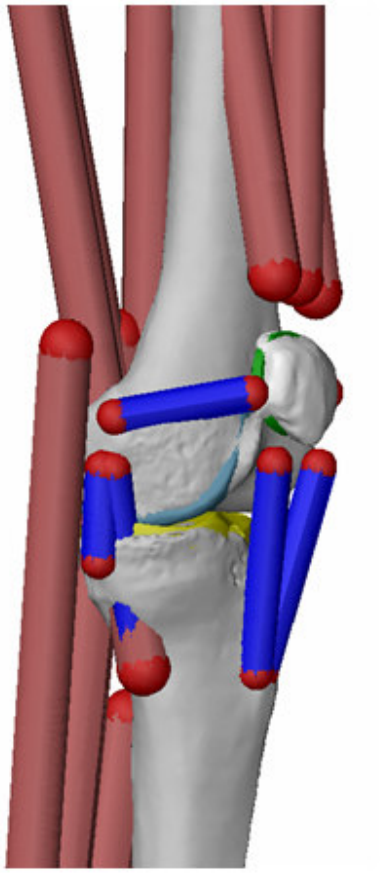

Figure 46: Knee replacement model in LifeMOD

4.4 Analysis

The results of the simulations were benchmarked against values in the literature for the AP displacement [83] (Table 1).

	Type	Disp. [mm]
Literature	PRP	5.8
	PSP	5.3
Simulations	Normal	4.5
	PRP	7.3
	PSP	5.1

Table 1: Benchmark values of AP Displacement

Although this gave a rough estimation of the kinematics of the knee joint, the results were not compared to other types of simulations or tests. The result of the replacement simulation was compared to a simulation model created in the same software and process. The only difference between the two simulations was the contact surfaces of the femur, tibia and patella. All the other factors were held constant in both cases and therefore the results of the simulations were only depended on the contact surface.

Thus the difference between the normal and TKA simulations could be used to determine how well the prosthesis shape delivered normal kinematics.

Different factors were investigated during the simulations to determine the difference. These factors included the displacements and rotations of the bones. Six standard measurements were created between the femur and tibia: the three translations and three rotations. These measurements were created by placing two markers on a single position with one marker connected to the femur and the other connected to the tibia. Thus at equilibrium the measurements were all zero and the software continuously measured the difference between the two bones during the simulation.

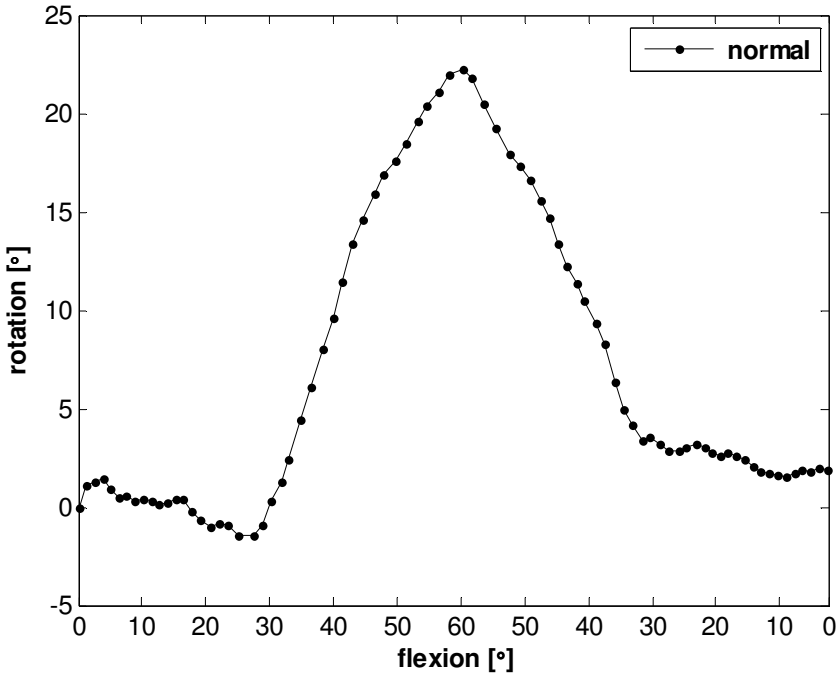

Figure 47: Simulation Results (+ External/ - Internal)

Seven simulations were completed in total. These included the normal knee, three posterior sacrificing prosthesis and three posterior retaining prosthesis simulations. The figures are continued in Appendix E.

4.5 Results

Although the simulation models were robust, the variable factors of the two models were held constant. The only factor that influenced the result was the shape of the articulating surface. The results obtained in the simulations were not accurate and could not be used for any calculations. It was only to illustrate the methodology of analyzing the kinematics of the knee joint using LifeMOD.
The normal knee simulation was natural, while the simulations of the prosthesis were unstable and the results were uneven. This is clearly visible on the figures and during the simulation. The method of comparing the two types of simulation can be used if the

simulations are improved. The different areas where the simulations should be improved will be listed in the recommendations section.

Chapter 5

5 Goodness-of-Fit

5.1 Introduction

Goodness-of-fit (GOF) is a statistical method typically used to determine how well a experiment fits a mathematical model. In this study, it was used to determine how well the prosthesis recreates the normal knee shape and kinematics. During surgery, when the components have been implanted, a similar test is performed to determine if the implanted size is adequate. The surgeon visually inspects the size of the component on the resected bone and the joint flexion is inspected to verify whether the components deliver good ligament stability. Although this is a simple method, this was the hypothesis of the GOF principle. Evaluating how the component matches overall resected dimensions and if it delivered normal kinematics as well as be performed preoperatively.

The GOF was calculated in two different domains: Geometric and Kinematic goodness-of-fit. The geometric goodness-of-fit (GGOF) was a procedure to determine how well the size of the prosthesis replaced the damaged knee surface. The kinematic goodness-of-fit (KGOF) tested the ligament stability and kinematics of the specific size for correct functioning.

5.2 Geometric Goodness-of-Fit (GGOF)

5.2.1 Goodness-of-fit

1) *Parameters*: The dimensions given in the prostheses specifications were used by the surgeon to determine preoperatively which size to implant. Normally these dimensions included the AP, ML and AP_{BOX} dimensions. The geometric goodness-of-fit (GGOF) used twelve dimensions listed below:

- Anterior Posterior (AP)
- Medial Lateral (ML)
- AP_{BOX}
- Lateral Condyle Radius (LCR)
- Medial Condyle Radius (MCR)
- Posterior Medial Radius (PMR)
- Posterior Lateral Radius (PLR)
- Trochlear Radius (TR)
- Trochlear Angle (TA)
- Sulcus Depth (SD)
- Resected Posterior Condyle (RPC)
- Sulcus Length (SL)

These parameters were selected to represent the most important dimensions the prosthesis should satisfy to ensure a good fit (Figure 48). Using more dimensions

ensured that the selected size would match the morphological dimensions of the femur with higher accuracy.

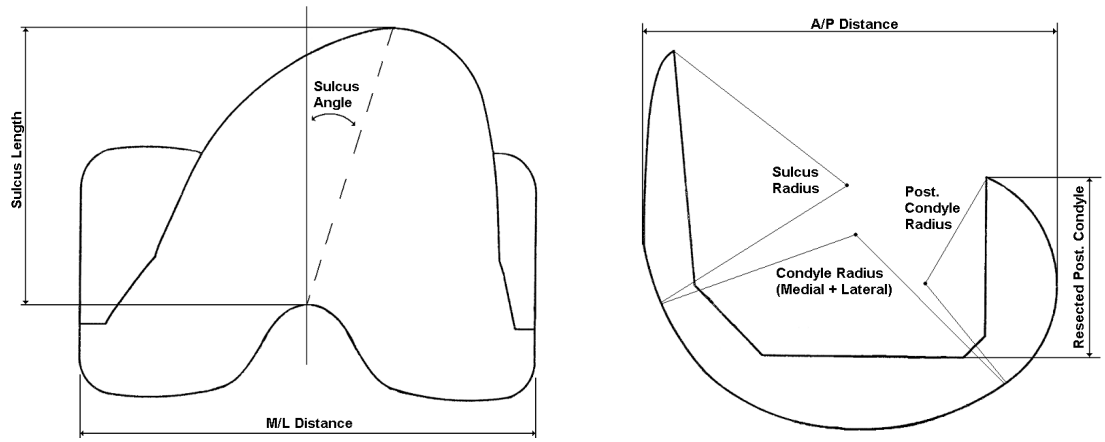

Figure 48: Dimensions

Although the sulcus depth is not displayed in the above figure, it is also one of the parameters.

2) *Equation*: The χ^2 test is a common method to determine how well a model fits experimental data. It was used to determine the difference between the morphological dimensions of the distal femur and the femoral prosthesis. The χ^2 value was determined with the following equation:

$$\chi^2 = \sum_{i=1}^{k} \frac{(Z_i - E_i)^2}{E_i} \qquad (1)$$

$$\overline{E} = |E_1 \quad E_2 \quad .... \quad E_k|$$
$$\overline{Z} = |Z_1 \quad Z_2 \quad .... \quad Z_k|$$

The value *k* is the number of parameters used in the equation (12 parameters). The vector $\overline{E}$ contains the selected morphological dimensions of the patient's femur (measured in MIMICS from CT scan data). The vector $\overline{Z}$ contains the dimensions of the prosthesis for a specific size (CAD models using the 3D scanner). There exists a $\overline{Z}$ vector for each size in the prosthesis range and a $\overline{E}$ vector for each patient.

3) *Weights*: Twelfth parameters were selected as the most important dimensions of the distal femur. Some of these parameters were deemed more important and weighting factors were added to the GOF calculation. A questionnaire was sent to several orthopaedic surgeons experienced in TKR. The surgeons were asked to rank the twelfth parameters from most to least important, based on their many years of experience with TKR. Only five surgeons replied to the questionnaire. The five surgeons all agreed that the AP_{BOX}, ML and AP were the three most important parameters, ranked in that order. There was greater variation around the other parameters, and an average rank list was determined. Due to the high importance of the three mentioned

parameters, more weight was allocated to these parameters. The points had to be unevenly divided between the different parameters. Different equations were evaluated to assign more weight to the first parameters and minimal deviation among the last parameters (Figure 49).

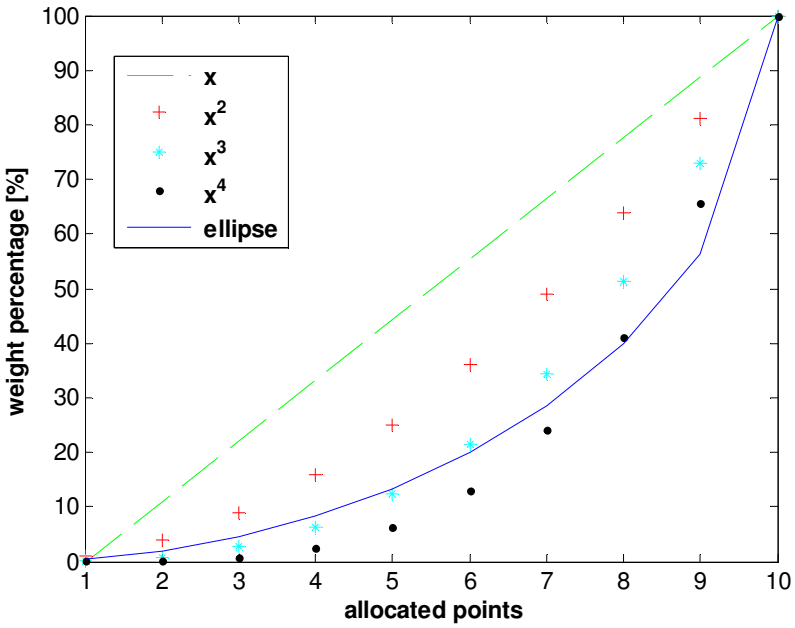

Figure 49: Weighted algorithm

An elliptic equation was used to calculate the weights of the parameters. The equation used the points out of ten allocated to each dimension and transformed it to a percentage value.

$$y = -100\left(\sqrt{1-\frac{x^2}{100}}\right)+100 \qquad (2)$$

The allocated points and percentage value of each dimension when calculated with the elliptical equation are displayed in Table 2.

Parameter	Points	Elliptic [%]
AP_{BOX}	10	100.00
ML	9	56.41
AP	8	40.00
Trochlear Radius	7	28.59
Condyle Radius	6	20.00
Post. Condyle Radius	5	13.40
Post. Condyle Length	4	8.35
Sulcus Depth	3	4.61
Sulcus Angle	2	2.02
Sulcus Length	1	0.50

Table 2: Weighted value for each dimension

The measured morphologic dimensions of 35 knees were compared to the values of the two commercial prosthetic designs: Posterior Retaining Prosthesis (PRP) and Posterior Sacrificing Prosthesis (PSP). It was found that the AP_{BOX}/AP ratio was generally higher in the real knees compared to the prostheses. The gradients of the mean values were similar for the two prosthesis types as well as the real knees (Figure 50). The similar gradient meant that the ratio of AP_{BOX}/AP of the prosthesis was equal to the measured population.

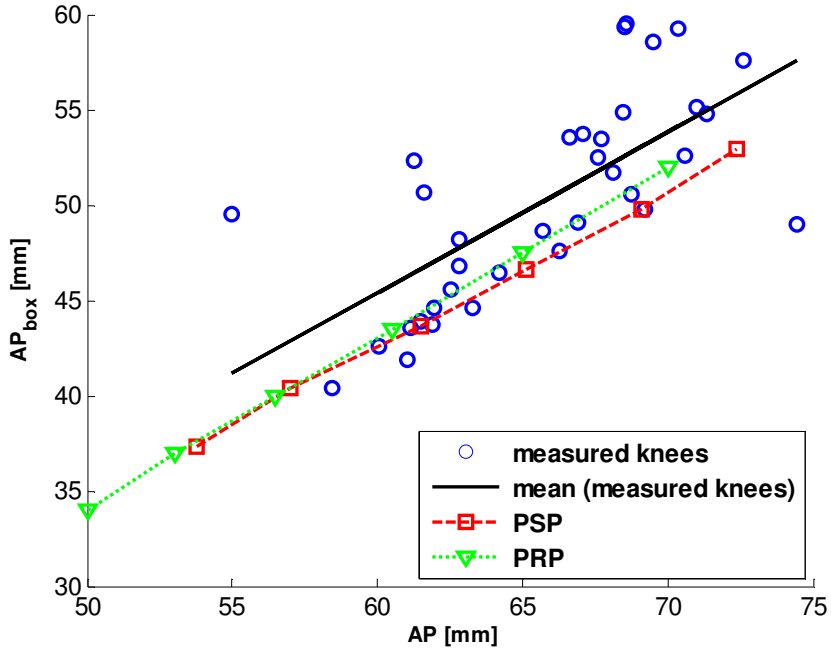

Figure 50: Difference between prosthesis and measured knees

Using the weighted χ^2 test, a GOF parameter for each size of the prosthesis commercial range was determined. The size with the highest GOF value was the prosthesis size satisfying the most dimensions of the distal femur (Figure 51). The figure displays which type and size prosthesis suits the patient best, based on all the morphological dimensions of the femur and geometry of the prosthesis.

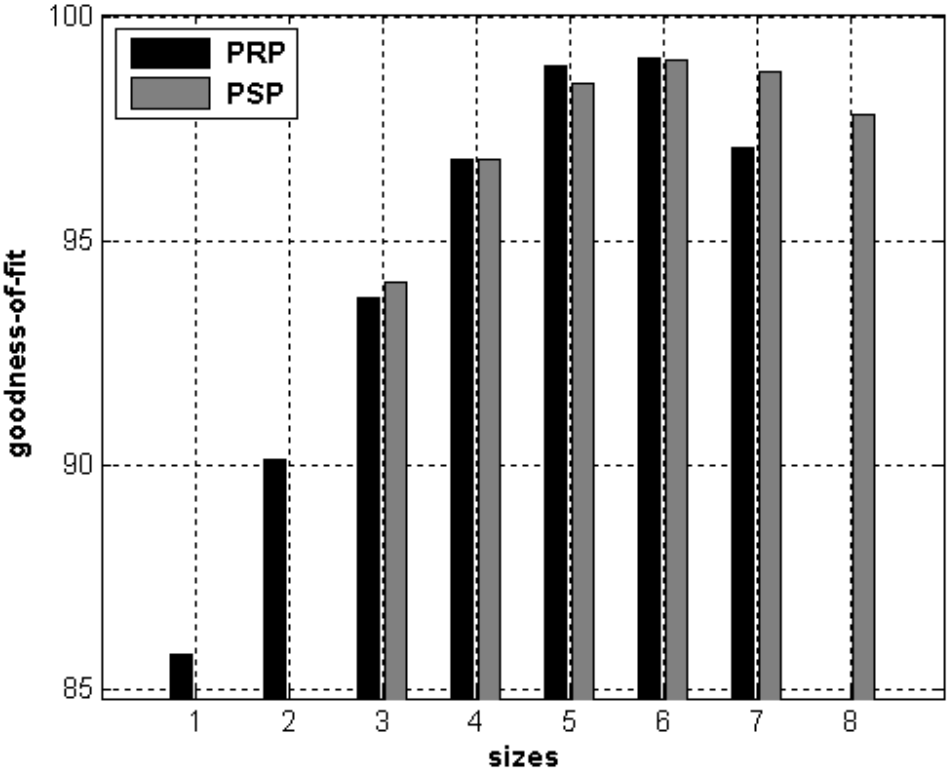

Figure 51: Goodness-of-fit example for patient #11

Naturally there is an asymmetry in the radii of the medial and lateral femoral condyles [17]. One of the prosthesis that was used, the two condyles was symmetrical and did not duplicate the natural asymmetry of the femoral condyles. This resulted in a GOF value that was always slightly less than 100%. The results of the GGOF method compared to the actual implanted size are displayed in Appendix E.

5.2.2 Volumetric Evaluation

Implantation

After the GOF was calculated for a specific patient, the two sizes with the highest GOF value was implanted into the 3D models to inspect the fit visually. The distal femur was cut according to the cutting planes given by the analysis template and the chosen prosthesis components placed at the correct position (Figure 52).

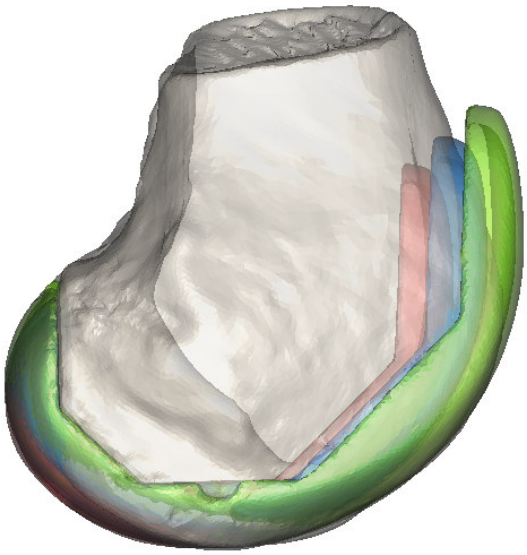

Figure 52: Different size components implanted on distal femur

The original shape of the femur was made visible to show where the component protrudes the bone surface (Figure 53). Thus a surgeon could implant and evaluate how well the prosthesis recreated the articulating surface before surgery.

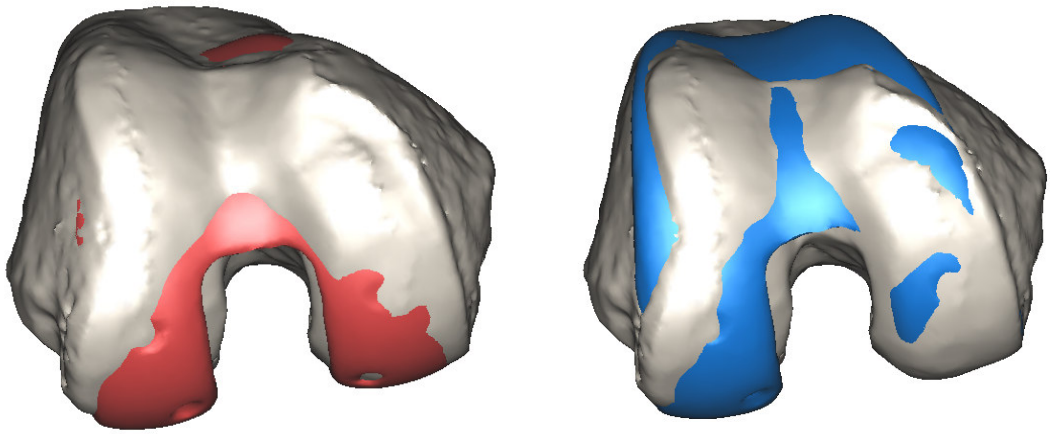

Figure 53: Evaluate difference between prosthesis and bone profile

Volumetric

The volumetric differences between the prosthesis model and the bone cut-offs were also calculated. The volume of each 3D model was available in MIMICS. The prosthesis model volume was always subtracted from the bone model. Thus a positive volumetric difference meant the size was smaller and a negative meant it was too large. This method only delivered an overall volume difference, which was not very accurate. The anterior section of the model could be larger and the posterior section smaller and the method would deliver a low difference value. The models were divided into six parts and the volume difference calculated for each section. First, the models were divided into a

medial and lateral half. Each half was then cut into an anterior, distal and posterior section (Figure 54). Thus each section could be subtracted from the bone model section and the six values added to give a better overall volumetric difference parameter.

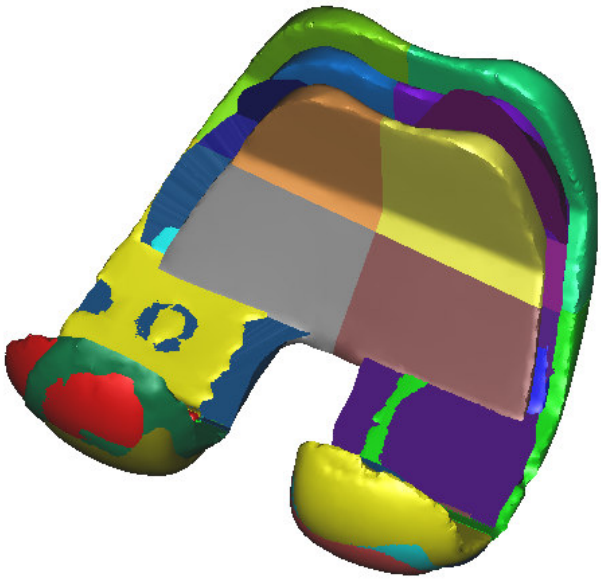

Figure 54: Volume difference measurement

The results of a volumetric test are displayed in the second half of Appendix F.

5.2.3 Case Study

One knee of which the GOF value was calculated was used in the case study. The femur and the prosthesis were printed using a 3D printer. The models were only evaluated on the geometric fit and no strength tests were performed. Thus the printed models were perfect for the application. The calculated femoral component was implanted onto the femur model. Only the best fitting sizes of the two design ranges were implanted to test the GGOF method. The normal implanting procedure was performed on the femur models using standard jigs. The prosthesis models were then implanted on the femur models to visually inspect the fit of the prosthesis. All the required parameters for the implantation were calculated with MIMICS. The size calculated with the GOF method was for both prosthesis types the best size to implant and thus illustrating that the geometric GOF method was accurate (Figure 55).

Figure 55: Case study models implanted on femur

5.3 Kinematic Goodness-of-Fit (KGOF)

5.3.1 Procedure

In the previous chapter, the normal knee and total knee replacement was simulated with equal properties. The goal of the prosthesis was to recreate the normal kinematics of a healthy knee. Thus the KGOF was determined by how good the prosthesis recreated the normal knee kinematics. The difference between the normal and TKA simulation was calculated over the entire simulation. The six measurements calculated in Chapter 4 was used to compare the two simulations.

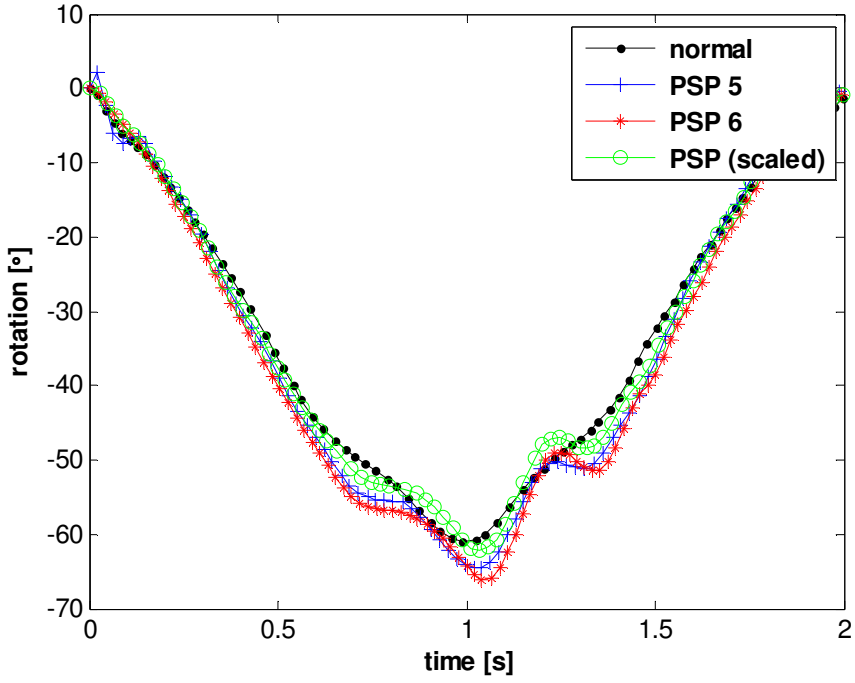

Figure 56: Simulation results (- Flexion/ + Extension)

5.3.2 Matlab Calculation

The two graphs were subtracted from each other and the average calculated for the overall difference. This average value gave an indication of the difference for a specific parameter. The overall deviation of the prosthesis to the normal kinematics was calculated with the absolute value between the two graphs. The KGOF was calculated for a prosthesis size by adding all the values of the six measurements. Adding the calculated values from the six measurements delivers an overall deviation of the prosthesis (Figure 57).

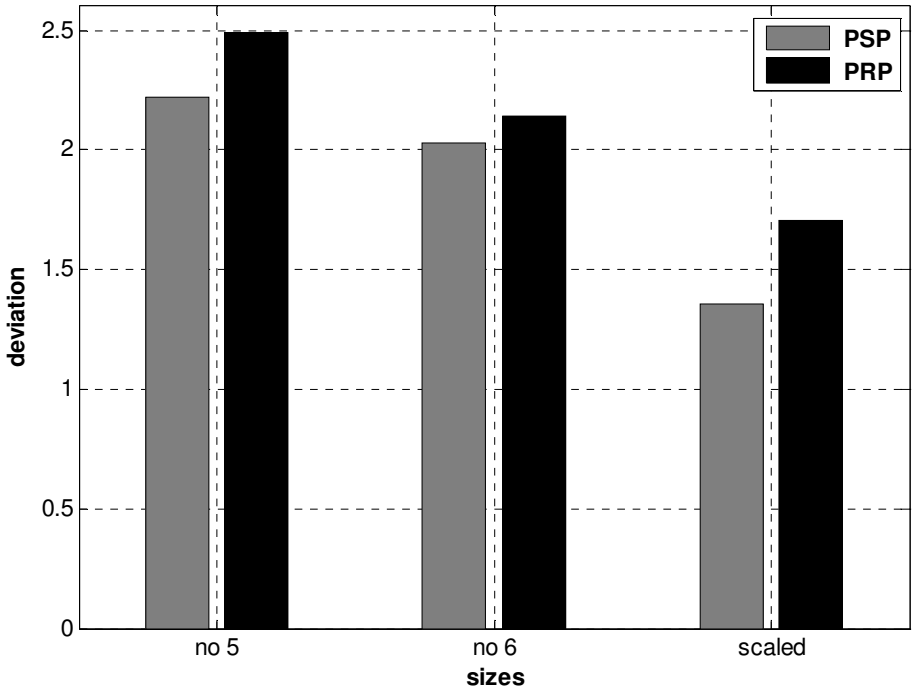

Figure 57: Overall kinematic deviation of one patient

5.4 Overall Goodness-of-Fit

An overall GOF parameter was calculated for a specific prosthesis size by incorporating the geometry and kinematics. The overall GOF was calculated by combining the results of the GGOF and KGOF. The importance of the two parameters relative to each other was unclear and thus each delivered 50% of the overall value. This method increased the accuracy of size selection for a specific patient and increased the efficiency of the implanted prosthesis.

5.5 Customization

5.5.1 Motivation

A specific size range was designed according to the average values measured from the population dimensions. The dimensional ratios were determined from the average population values. Thus a component could fit a patient perfect in a few dimensions, while other dimensions were incorrect. Ideal would be to create a customized prosthesis which incorporates patient-specific dimensions measured of the distal femur. Thus a patient would be examined and scanned and use the measured data to build a customized prosthesis. This delivered a prosthesis which perfectly replicates the articulating surface of the patient. The internal profile of the prosthesis could be held constant for the use of standard implantation methods and jigs. Two methods were given for customization of the prosthesis components. The first method used the original prosthesis design and only scales the model according to the femur size. This was perfect for a patient found to be in-between two sizes. The second method used the different dimension ratios of the prosthesis to create a new size. A developed program searched for specific ratios of the prosthesis found similar to the patient to create a new size. An outline of the customization procedure followed in the project is given below (Figure 58).

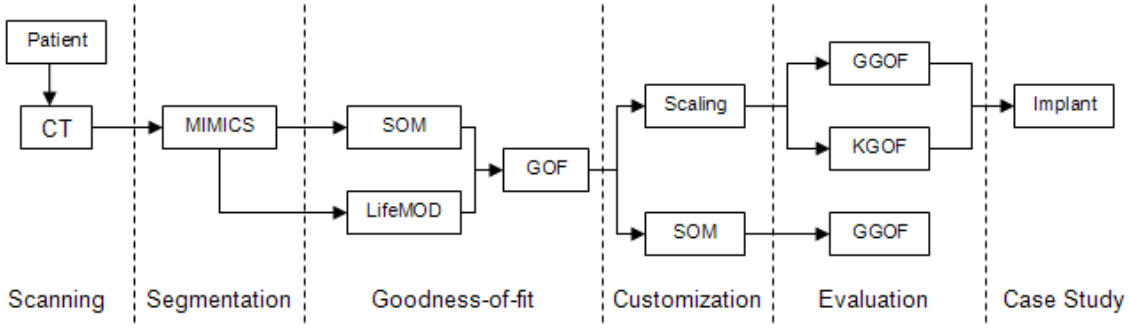

Figure 58: Customization process lay-out

5.5.2 Methods

Scaling

The final goal of this study was to create a customized prosthesis for a specific individual, the manufacturing of a customized femoral component that would fit a patient better than the available prostheses. The GOF principle was reversed to customize a femoral prosthesis for a patient. Altering the dimensions of the prosthesis until the component achieved the highest GOF. The normal GOF was performed to determine the best fitting prosthesis size. All the dimensions were divided by the AP_{BOX} value and therefore the dimensions of the GOF equation were in ratios of AP_{BOX}. Thus the GOF was depended upon the AP_{BOX} parameter only. A vector of AP_{BOX} values were entered

into the equation which calculated a vector of χ^2 values. The optimal AP_{BOX} value was found at the maximum point of the χ^2 vector (Figure 59). The prosthesis was scaled according to the AP_{BOX} value which delivered the best fit. The problem was that the available prosthesis size was scaled according to the size of the femur and the ratios of the prosthesis design were not altered during the process.

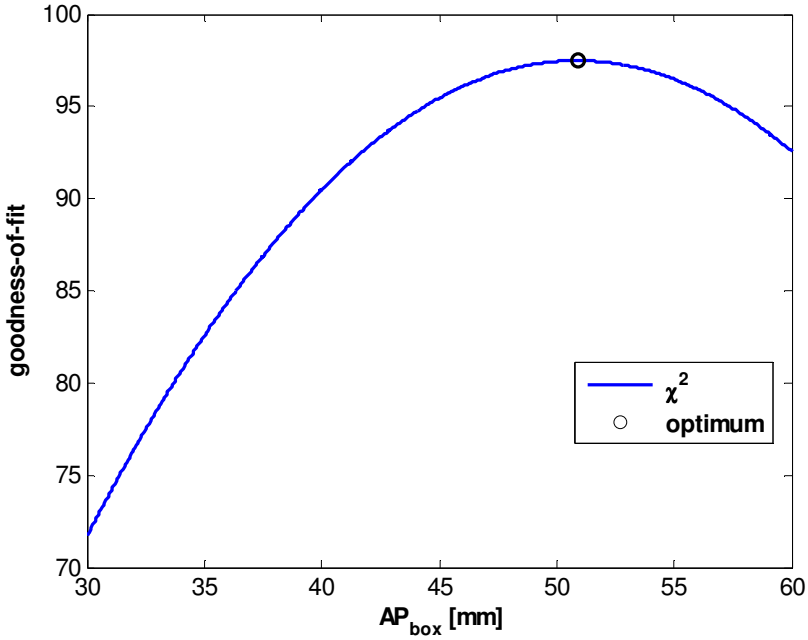

Figure 59: Component scaling method

SOM

The SOM customization method used the same procedure as the one used to determine the healthy knee dimensions in chapter 3. A database of the prosthesis dimensions was created and the dimensions of the femur were entered into the SOM. The customized prosthesis dimensions were calculated according to the ratios of the standard prosthesis dimensions. The SOM method was also made dimensionless, with the AP_{BOX} dimension used as the referencing parameter instead of the ML dimension. Thus the AP_{BOX} value was always one and was therefore always one in the maps (Figure 60).

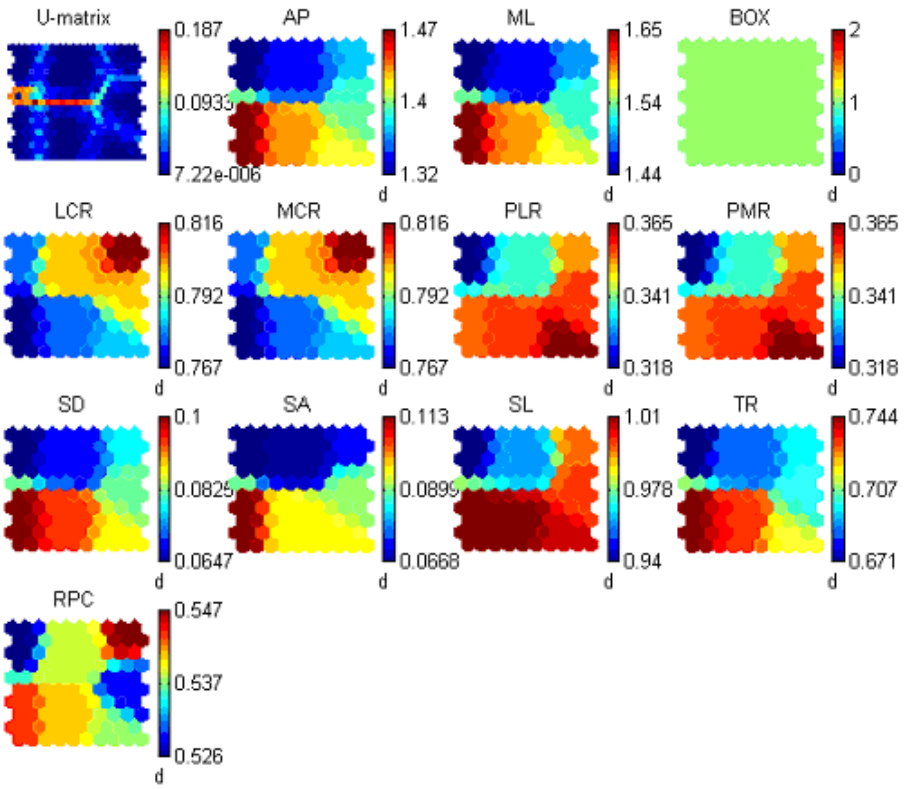

Figure 60: PRP customization map

This method was not that effective due to the small database used in the SOM. Unlike the SOM in chapter 3, this method used a fixed number in the database which could not be increased.

5.5.3 Results

GOF was performed on the new customized prosthesis size to ensure that it delivered a better fit.

Geometric Goodness-of-fit

After the scaled prosthesis dimensions was calculated, the GGOF was applied with the new calculated dimensions. The new GOF value was compared to the original GOF to ensure that the new dimensions were in fact better. The GOF of the scaling method was equal to the value calculated during the process. There was an increased GOF in 24 of the 35 patients tested. While the SOM customization process was unsuccessful, it determined dimensions that delivered a lower GOF values than the original prosthesis. This was due to the small data set of the prosthesis dimensions that was used. The results of the scaling method of the 35 knees are given in Appendix F.

Kinematic Goodness-of-fit

When the customized prosthesis was created it was imported into LifeMOD and the KGOF calculated. This KGOF was only performed for the scaled method. The scanned models were scaled to the calculated size using MIMICS. The dimensions of the

prosthesis were calculated with the SOM method, but no 3D models could be created. This proved that the kinematics of the knee joint was not increased by replicating the articulating surface.

Chapter 6

6 Conclusion and Recommendations

6.1 Conclusion

The main aim of the project was to develop a method of selecting a prosthesis size to use for a patient. This was determined preoperatively and used more dimensions for the selection criteria. Thus a better fitting component can be selected, increasing the alignment and ligament stability of the knee prosthesis. The method also enabled the surgeon to optimize the bone resections through accurate measurements of rotational angles on 3D models.

These 3D models of the knee joint were created through computer segmentation of the CT scan data. This segmentation process was performed with Materialise MIMICS. The software used templates of placed points to create required measurements. The measurements were made on the 3D models and all the techniques were validated. Other morphological dimensions can be measured and used to create a database of the population. The χ^2 GOF method used twelve morphological dimensions of the distal femur. This method would replace the dry cadaver bone measuring technique and use specimens of living people. Thus the population database would include specimens of all ages.

Two measurements (vulgus and rotational angle) of the GOF method made on the 3D models were more accurate. The standard method of using 2D CT scans to determine these two measurements was found to be limited and not patient specific. Using the 3D femur models in this project, these angles could accurately be determined and were patient specific. Thus this method could be used for the preoperative measurements and no changes are required for the implantation or size selection technique. This aids the surgeon to accurately align the components during surgery. The standard jigs will be used by setting the measured angles on the jigs. Thus a patient would come in for a regular preoperative check-up and CT scan. Then the 3D models created through computer segmentation and analyzed to determine the required angles for surgery.

The 3D models of the femur and tibia could be used to create customized prosthesis with an exact duplicate of the bone profiles. The only problem was that the CT scan models excluded the cartilage layer and therefore the CT scans alone could not be used to manufacture the prosthesis. Thus before the femoral component can be completely customized, the cartilage layer should be added to the models. The principle of applying a cartilage thickness to the measured data was a good theory. In reality the process was incomplete and delivered poor results. The database used was too small for any accurate calculations. The principle requires more specimens, races and genders to work properly.

The knee simulations were too robust to utilize and determine substantial results. Although the articulating shape was the only variable that was changed in the two

simulations, the parameters required for the creation of the simulation model consisting out of a large number of unknown values. The simulations created in the project were done to illustrate the necessity of kinematic simulations for size selection and to deliver a method of analyzing it.

The GGOF method was perfect for selecting the correct size. This was proven in the case study and volumetric test. The GGOF was performed on a patient and the calculated sizes were implanted. In both cases the allocated sizes was a perfect match to the distal femur. Thus the GGOF method could be used in practice to determine the size of the component.

6.2 Recommendations

Recommendations for further work are given for sections where the work should be enhanced or extra focus should be added. These were not performed for the project due to time constraints. The following aspects should be looked at:

- 3D computer segmentation
- Morphological dimensions
- Customization
- Simulations

6.2.1 3D Computer Segmentation

The quality of the 3D models affects all the results and therefore all the aspects of computer segmentation should be optimized. There was a large amount of different settings on the CT and MRI scanner. These settings were changed according to the region of interest in the images. A specific setting was used for the CT scanner to create perfect 3D models. The results were excellent except when using a segmentation process which was time-consuming for the damaged knees. Therefore it should be investigated whether other settings could be used when scanning damaged knees, to reduce the segmentation time and optimize the models.

On the MRI scan images there was a clear difference between the cartilage layer and the bone. When it was imported into MIMICS and segmented, the software could not distinguish between the two parts. Because the cartilage layer is of extreme importance, different settings for the MRI scanner should be tested.

6.2.2 Morphological Dimensions

The measuring technique of the morphological dimensions used was excellent, except that it was time consuming and was dependent on the user's judgment. An automated measuring technique would resolve these two problems. This can be either fully or partially automated, whereby the software could allocate all the points in the correct position or it could only identify the specific landmarks to start the process. This would improve the accuracy and reproducibility of the results and more femurs could be measured in a shorter time.

In this project the distal femur was the only bone which was evaluated. There are also certain dimensions and angles required for the patella and tibia. Although the femur dimensions were more important, the other two bones are part of the total knee replacement and should also be measured.

6.2.3 Customization

This project was a foundation for customization of the femoral component. Although the femoral component is a complex part, the customization of the component is hampered by the manufacturing possibilities. It would be easier to start with the customization of a partial knee replacement or the patella component. For the patella there exists a few factors which are required for the customization: the overall shape and size of the patella bone, the medial/lateral position of the ridge, and the sulcus wedge angle.

6.2.4 Simulations

The created simulations were simplified and very robust to ensure the functioning of the simulations. More detail should be devoted to the creation of the models in LifeMOD. Although it was established that it can be used to determine the kinematics of the knee, more time should be taken for the upgrading of the simulations. Firstly, the STL models consisted out of a large amount of triangles. The contacts between the models were determined between the triangles of the imported models and were too complex for the simulations and created unnatural motion of the models. These should be decimated before it is imported into LifeMOD. Secondly, the ligament attachment locations were general knee anatomy positions. It would be better if the patient's attachment points could be identified before the models are created. MRI scans could be used to identify these locations accurately. Lastly, the muscles in the simulations were elements that created a force between the two attachment points. In a real leg the muscles wrap around the bones and other muscles. This is applicable to the quadriceps muscles during flexion when it contacts and wraps over the distal femur. In the newer LifeMOD, muscles could be set to make contact with the bones and wrap around them. These alterations can easily be corrected in the simulations.

The following changes require more work to ensure that the results are satisfactory. In the normal knee simulations a rigid meniscus was added to the model. A general 3D model of the meniscus was made and imported into LifeMOD. The simulation would be more accurate if a patient-specific meniscus was used, either through computer segmentation of a MRI scan of the meniscus or using a cadaver meniscus scanned with the 3D scanner. The other problem was that the meniscus model was fixed to the tibia bone in the simulation, while during normal knee flexion/extension the meniscus translates and deforms [19, 20]. Thus the meniscus model should be able to translate during the simulation and change shape. A constraint should be added between the meniscus and the tibia, allowing the model to translate and rotate in any direction. The meniscus model should be made of a flexible body in the simulation model. All these changes would enhance the final result of the simulations.

No cartilage layer was present in the simulations. This had minimal effect on the characteristics of the femur, due to the bone profile. The unequal tibial cartilage profile altered the characteristics of the articulating shape of the tibial plateau. A method should be developed to add the cartilage layer to the articulating contact areas in the simulation model.

In the simulations a simple spline was used to drive the lower leg anterior and posterior to perform a knee bend. The other two directions were unconstrained and the leg was free to translate in those directions. The driving motion spline of the lower leg in the anterior/posterior direction should be determined with motion capturing methods for increased accuracy of the simulations. Then the driving splines of the other two unknown directions should be captured, thereby limiting the motion of the knee in the other directions and forcing it to move as a normal knee.

References

[1] Cluett, J, About.com: Orthopaedics, Total knee replacement, Oct 2006
Available at:http://orthopedics.about.com/cs/kneereplacement/a/kneereplacement.htm

[2] National Centre for Health Statistics, Rate of total knee replacements, Oct 2006
Available at: http://www.cdc.gov/mmwr/preview/mmwrhtm/mms407at.htm

[3] Zimmer, Gender solutions: Knee, Oct 2006\
Available at: http://www.genderknee.com

[4] Indicure, Medical Specialties, Orthopaedic Surgery, Total Knee Replacement, Oct 2006
Available at: http://www.indicure.com/knee_replacement.html

[5] American Academy of Orthopaedic Surgeons, Minimally invasive total knee replacement, Oct 2006
Available at: http://www.orthoinfo.aaos.org/fact/thr_report.cfm

[6] Scorpio, Single Axis Total Knee System, Catalogue, March 2006
Available at: http://www.scorpioknee.com

[7] Finsbury, Dual Bearing Knee, March 2006
Available at: http://www.finsbury.org

[8] DePuy, PFC Sigma Knee System, Technical Monograph, March 2006
Available at: http://www.mobilebearingknees.com

[9] Dupuis, R, Skalli, W, Lavaste, F, Morphological study of the knee for designing total knee prosthesis, *European Journal of Orthopaedic Surgery and Traumatology*, Vol. 11, pp. 225-229, 2001.

[10] Chin, K R, Dalury, D F, Scott, R D, Comparative measurements of male and female distal femurs during primary total knee arthroplasty.

[11] Victor, J, Cruciate deficiency in the replaced knee, *Total Knee Arthroplasty*, A guide to better performance, No 21.

[12] Steadman, J R, LeadingMD.com, empower your practice, March 2006
Available at: http://www.LeadingMD.com

[13] Lahey Clinic Foundation, March 2006
Available at: http://www.Lahey.org

[14] McMinn, R M H, Hutchings, R T, *A Colour Atlas of Human Anatomy*, Second Edition, pp. 304-311.

[15] Dye, S F, *The knees as orthopaedic rosetta stone*, Chronic ACL deficient knee, April 2006.
Available at: http://www.aclstudygroup.com/Powerpoint_pdf02/dye.pdf

[16] Meister, B R, Micheal, S P, Moyer, R A, Kelly, J D, Schneck, C D, Anatomy and kinematics of the lateral collateral ligament of the knee, *American Journal of Sports Medicine*, Vol 28, pp 869-878, 2000.

[17] Wu, J Z, Herzog, W, Ronsky, J, Modelling axi-symmetrical joint contact with biphasic cartilage layers – an asymphotic solution, *Journal of Biomechanics*, Vol 29, No 10, pp 1263-1281, 1996.

[18] Grassi, W, Filippucci, E, Busilacchi, P, Musculoskeletal ultrasound, *Best Practice & Research Clinical Rheumatology*, Vol 18, No 6, pp 813-826, 2004.

[19] Top view of meniscus, April 2006
Available at: http://www.medpics.findlaw.com/generateexhibit.php

[20] Vedi, V, Williams, A, Tennant, SJ, Spouse, E, Hunt, D M, Gedroyc, W M W, Meniscal Movement – An in-vivo study using dynamic MRI, *The Journal of Bone and Joint Surgery*, Vol 81-B, No 1, 1999.

[21] Griffin, F M, Math, K, Scuderi, G R, Insall, J N, Poilvache, P L, Anatomy of the epicondyles of the distal femur, MRI analysis of normal knees, *The Journal of Arthroplasty*, Vol. 15, No. 3, pp. 354-359, 2000.

[22] McCormack, D, *Mechanical axis deviation: Definitions*, measurements and consequences.

[23] Eckhoff, D G, Functional anatomy of the knee, *Total knee arthroplasty, A guide to better performance*, No 3, pp 18-24,2005.

[24] Derek, T, Cooke, M B, Scudamore, A, Greer, W, Operative techniques in sports medicine, *Axial alignment of the lower limb and its association with disorders of the knee*, Vol. 8, No 2 (April), 2000, pp 98 – 107

[25] Yoshino, N, Takai, S, Ohtsuki, Y, Hirasawa, Y, Computed tomography measurement of the surgical and clinical transepicondylar axis of the distal femur in osteoarthritic knees, *The Journal of Arthroplasty*, Vol. 16, No.4, 2001.

[26] Asano, T, Akagi, M, Nakamura, T, 2004, The functional flexion-extension axis of the knee corresponds to the surgical epicondyar axis, In vivo analysis using a biplanar image-matching technique, *The Journal of Arthroplasty*, Vol. 20, No. 8, pp 1060 – 1067

[27] Hollister, A M, Jatana, S, Singh, A K, Sullivan, W W, Lupichuk, A G, *Scorpio® Clinical History Booklet*, The axes of rotation of the knee, Clinical History 2

[28] Freeman, M A R, Pinskerova, V, The movement of the normal tibio-femoral joint, *Journal of Biomechanics*, No 38, pp 197-208, 2005.

[29] Johal, P, Williams, A, Wrags, P, Hurt, D, Gedroyc, W, Tibio-femoral movement in the living knee, A study of weight bearing and non-weight bearing knee kinematics using interventional MRI, *Journal of Biomechanics*, No 38, pp 269-276, 2005.

[30] Luo, C F, Koshino, T, Takeuchi, R, Saito, T, Reliability of the transepicondylar line as a parameter of femoral axial alignment, *Journal of Orthopaedic Science*, Vol. 6, pp. 373-377, 2001.

[31] Müller, W, Form, function and ligament reconstruction, *The Knee*, pp 1-146, 1982.

[32] Smith, P N, Refshauge, K M, Scarvell, J M, *Development of knee concepts of knee kinematics*, Arch phys med rehalib, Vol 84, pp 1895 – 1902, 2003.

[33] Elias, S G, Freeman, M A R, Gokcay, E I, *Scorpio® Clinical History Booklet*, A correlative study of the geometry and anatomy of the distal femur, Clinical History 1.

[34] Siu, D, Rudon, J, Wevers, H W, Griffiths, P, Femoral Articular shape and geometry, A three dimensional computerized analysis of the knee, *Journal of Arthroplasty*, Vol 11, No 2, pp 166-173, 1996.

[35] Nuňo, N, Ahmed, A M, Three-dimensional morphometry of the femoral condyles, *Clinical Biomechanics*, Vol 18, pp. 924-932, 2003.

[36] Eckhoff, D G, Bach, J M, Spitzer, V M, Reinig, K D, Bagur, M M, Balbini, T H, Flannery, N M P, Three-dimensional mechanics, Kinematics, and morphology of the knee viewed in virtual reality, *The Journal of Bone and Joint Surgery*, Vol 87-A, suppl. 2, pp. 71-80, 2005.

[37] Hungerford, D S, Hungerford, M W, Alignment of the normal knee, Relationship to total knee replacement, *Total Knee Arthroplasty, A guide to better performance*, No 4, pp 25-31, 2005.

[38] Baré, J V, Gill, H S, Beard, D J, Murray, D W, A convex lateral tibial plateau for knee replacement, *The Knee*, Vol 13, pp 122-126, 2006.

[39] Hehne, H J, Biomechanics of the patellofemoral joint and its clinical relevance, *Clinical Orthopeadics*, No 258, pp 73-85, 1990.

[40] Stiehl, J B, A clinical overview of patellofemoral joint and application to total knee arthroplasty, *Journal of Biomechanics*, No 38, pp 209-214, 2005.

[41] Luyten, F P, Westhovens, R, Taelman, V, Arthritis of the knee: Diagnosis and management, *Total Knee Arthroplasty, A guide to better performance*, No 1, pp 3-13, 2005.

[42] Lotke, P A, Ecker, M L, Influence of positioning of prosthesis in total knee replacement. *The Journal of Bone and Joint Surgery*, Vol 59-A, No 1, pp 77-79, 1977.

[43] Shakespeare, D, Kinzel, V, Ledger, M, Achieving ligament stability and correct rotational alignment of the femur in knee arthroplasty, A study using the medial pivot knee, *The Knee*, Vol 12, pp 419-423, 2005.

[44] Rauh, M A, Mihalko, W M, Krackow, K A, Optimizing alignment, *Total Knee Arthroplasty, A guide to better performance*, No 25, pp165-169, 2005.

[45] Siston, R A, Patel, J J, Goodman, S B, Delp, S L, Giori, N J, The variability of femoral rotation alignment in total knee arthroplasty, *The Journal of Bone and Joint Surgery*, Vol 87-A, No 10, pp 2276-2280, 2005.

[46] Katz, M A, Beck, T A, Silber, J S, Seldes, R M, Lotk, P A, Determining femoral rotation alignment in total knee arthroplasty, Reliability of techniques, *The Journal of Arthroplasty*, Vol 16, No 3, pp 301-305, 2001.

[47] Victor, J, Computer assisted surgery: Coronal and sagittal alignment, *Total Knee Arthroplasty, A guide to get better performance*, No 39, pp. 247-253, 2005.

[48] Incavo, S J, Coughlin, K M, Beynnon, B D, Femoral component sizing in total knee arthroplasty – Size matched resection versus flexion space balancing, *The Journal of Arthroplasty*, Vol. 19, No. 4, 2004.

[49] Erasmus, S, Biomechanics and bone cuts in TKA, Presentation.

[50] Boldt, J G, Stielh, J B, Munzinger, U, Beverland, D, Keblish, P A, Femoral component rotation in mobile-bearing total knee arthroplasty, *The Knee*, Vol 13, pp 284-289, 2006.

[51] Kawamura, H, Bourne, R B, Factors affecting range of flexion after total knee arthroplasty, *Journal of Orthopaedic Science*, Vol 6, pp 248-252, 2001.

[52] Villa, T, Migliavacca, F, Gastaldi, D, Colombo, M, Contro, R, Pietrabissa, R, Computer assisted design and evaluation of the knee prosthesis, Summer bioengineering conference, June 25-29, 2003.

[53] Kinzel, V, Ledger, M, Shakespeare, D, Can the epicondylar axis be defined accurately in total knee arthroplasty? *The Knee*, Vol 12, pp 293-296, 2005.

[54] Matsumoto, T, Tsumura, N, Kurosaka, M, Muratsu, H, Kuroda, R, Ishimoto, K, Tsujimoto, K, Shiba, R, Yoshiya, S, *Prosthetic alignment and sizing in computer-assisted total knee arthroplasty*, International orthopaedics, No. 28, pp. 282-285, 2004.

[55] Enderle, J D, Blanchard, S M, Bronzino, J D, *Introduction to biomedical engineering*, Second edition, Elsevier Academic Press, 2005.

[56] McPherson, A, Kärrholm, J, Pinskerova, V, Sosna, A, Martelli, S, Imaging knee position using MRI, RSA/CT and 3D digitization, *Journal of Biomechanics*, No 38, pp 263-268, 2005.

[57] Blaha, J D, Mancinelli, C A, Simons, W H, Using the transepicondylar axis to define the sagittal morphology of the distal part of the femur, *The Journal of Bone and Joint Surgery*, Vol. 84-A, suppl. 2, pp. 48-55, 2002.

[58] Yip, D K H, Zhu, Y H, Chiu, K Y, Ng, T P, Distal rotational alignement of the Chinese femur and its relevance in total knee arthroplasty, *The Journal of Arthroplasty*, Vol 19, No 5, pp 613-619. 2004.

[59] Hitt, K, Shurman, J R, Greene, K, McCarthy, J, Moskal, J, Hoeman, T, Mont, M A, Anthropometric measurements of the human knee: Correlation to the sizing of current knee arthroplasty systems, *The Journal of Bone and Joint Surgery*, Vol 85-A, suppl. 4, pp. 115-122, 2003.

[60] Ho, W P, Cheng, C K, Liau, J J, Morphometrical measurements of resected surface of femurs in Chinese knees: Correlation to the sizing of current femoral implants, *The Knee*, vol. 13, pp. 12-14, 2006.

[61] Guy, P, Krettek, C, Mannss, J, Whitall K P, Schandelmaier, P, Tscherne, H, *CT-based analysis of the geometry of the distal femur, Injury*, Vol. 29, suppl. 3, pp. 3-21, 1998.

[62] Ireland, M L, Ballantyne, B T, Little, K, McClay, I S, A radiographic analysis of the relationship between size and shape of the intercondylar notch and anterior cruciate ligament injury, *Knee Surgery, Sports Traumatology, Arthroscopy*, Vol 9, pp 200-205, 2001.

[63] Takahasti, T, Yamanaka, N, Komatsu, M, Ogawa, Y, Yoshida, S, Yamamoto, H, A new computer-assisted method for measuring the tibio-femoral angle in patients with osteoarthritis of the knee, Osteoarthritis Research Society International, *OsteoArthritis and Cartilage*, Vol 12, pp 256-259, 2004.

[64] Rooney, N, FitzPatrick, D P, Ishibashi, H, Lawlor, G, FitzPatrick, C, Lee, J, Ethnic variation in distal femoral geometry: Knee prosthesis design, *Bioengineering In Ireland Conference*, Jan 27-28, 2006.

[65] Kordelle, J, Millis, M, Jolesz, F A, Kikinis, R, Richolt, J A, *Three-dimensional analysis of the proximal femur in patients with slipped capital femoral epiphysis based on computed tomography*.

[66] Lee, I S, Choi, J-A, Kim, T K, Han, I, Lee, J W, Kang, H S, Reliability analysis of 16-MDCT in preoperative evaluation of total knee arthroplasty and comparison with intraoperative measurements, *AJR* 186, pp 1778-1782, 2006.

[67] Halloran, J P, Patrella, A J, Rullkoeter, P J, Explicit finite element modeling of total knee replacement mechanics, *Journal of Biomechanics*, No 38, pp 323-331, 2005.

[68] Bei, Y, *Dynamic simulations of knee joint contact during human movement*, 2003.

[69] Fregly, B J, Sawyer, W G, Harman, M K, Banks, S A, Computational wear prediction of total knee replacement from in vivo kinematics, *Journal of Biomechanics*, No 38, pp 305-314, 2005.

[70] Dietrich, M, Kedzior, Z, Skalski, K, *Designing and manufacturing of customized human bone endoprosthesis*.

[71] Seedhom, B B, Chelule, K L, Berry, E, Computer assisted surgery: Radiation free, expedited design of disposable patient specific templates for total knee replacement, *Engineering and Physical Sciences Research Council*, December, 2006.

[72] OtisMed, Custon Fit Total Knee Replacement, OtisKnee™, Sep 2007
Available at: http://www.otismed.com/index.html

[73] Harrysson, O L A, Hosni, Y A, Nayfeh, J F, Custom-designed orthopedic implants evaluated using finite element analysis of patient-specific computed tomography data: femoral-component case study, *BMC Musculoskeletal Disorders*, Vol 8, No 91, 2007.

[74] Werner, A, Lechniak, Z, Skalski, K, Kedzior, K, Design and manufacturing of anatomical hip joint endoprosthesis using CAD/CAM systems, *Journal of Materials Processing Technology*, No 107, pp 181-186, 2000.

[75] Evans, B, Cohen, C, Mitchel, J, Heppenstal, R, Ducheyne, P, Cuchler, I, *Relationships between canal fill and interfacial displacement for an in vivo loading porous ingrowth of femoral prosthesis*, Trans Orthopeadic Research Society, No 15, pp 201, 1990.

[76] Huo, M H, Salvati, E A, Lieberman, J R, Burstein, A H, Wilson, P D, Custom designed femoral prosthesis in total hip arthroplasty done with sement fro severe dysplasia of the hip, *The Journal of Bone and Joint Surgery* 75A, No 10,pp 1497-1504, 1993.

[77] Medical Technology Business Europe, Siemens CT scanner, Oct 2006
Available at: http://www.mtbeurope.info/news/2005/503026.htm

[78] Battiato, S, Bosco, C, Farinella, G M, Impoco, G, *3D CT segmentation for clinical evaluation of knee prosthesis operations,* Eurographics Italian Chapter Meeting, 2006.

[79] Viceconti, M, Zannoni, C, Pierotti, L, TRI2SOLID: an application of reverse engineering methods to the creation of CAD models of bone segments, *Computer Methods and Programs in Biomechanics*, Vol 56, pp 211-220, 1998.

[80] Karayiannis, N B, Venetsanopolous, A N, *Artificial neural networks: Learning algorithms*, Performance evaluation and applications, Kluwer Academic Publishers, Norwell, 1993.

[81] NextEngine™, 3D Desktop Scanner, May 2007
Available at: http://www.nextengine.com

[82] LaPrade, R F, Engebretsen, A H, Ly, T V, Johansen, S, Wentorf, F A, Engebretsen, L, The anatomy of the medial part of the knee, *The Journal of Bone and Joint Surgery*, Vol 89-A, No 9, 2007

[83] Ishii, Y, Matsuda, Y, Ishii, R, Sakata, S, Omari, G, Sagittal laxity in vivo after total knee arthroplasty, *Archives of Orthopaedic and Trauma Surgery*, Vol 125, No 4, 2005.

Appendix

Appendix A: Unhealthy Knee Data

Name	AP	ML	Box	SA	SL	RPC	LCR	MCR	PLR	PMR	SD	TR
Patient 1	58.42	62.80	40.37	2.10	31.78	27.91	41.97	38.79	20.82	20.03	5.65	27.14
Patient 2	67.74	66.36	52.01	5.05	35.88	30.40	47.21	37.54	19.98	20.06	5.50	23.50
Patient 3	61.60	62.72	45.77	3.70	31.35	25.40	43.44	39.44	19.45	18.39	7.44	36.26
Patient 4	61.25	76.88	52.34	1.30	36.06	28.25	44.25	43.87	16.27	20.10	7.39	33.61
Patient 5	71.32	73.20	54.39	3.76	30.17	30.86	52.85	46.12	20.84	19.22	6.39	21.89
Patient 6	71.00	75.04	54.37	3.02	38.77	31.72	51.81	44.70	21.47	19.54	6.78	27.48
Patient 7	69.49	74.97	54.02	3.38	35.46	31.70	45.35	44.01	20.07	21.75	7.70	39.76
Patient 8	68.50	71.13	56.67	3.12	34.47	28.35	45.00	46.11	19.45	17.02	8.99	39.24
Patient 9	70.58	74.72	51.55	2.85	35.90	29.66	46.45	43.24	22.56	20.70	5.94	25.86
Patient 10	64.22	64.22	46.40	2.35	33.64	25.51	44.11	46.33	18.75	18.59	6.23	23.84
Patient 11	68.75	71.67	49.98	3.58	35.58	31.44	46.59	45.68	18.53	20.96	7.40	30.61
Patient 12	61.91	63.16	42.21	3.07	33.19	26.53	48.77	39.38	18.16	17.78	4.52	18.91
Patient 13	54.99	60.89	45.63	1.07	30.17	23.68	48.20	37.55	17.75	17.15	5.50	31.02
Patient 14	61.05	61.64	41.81	2.47	27.35	27.34	51.06	47.83	18.16	18.70	6.85	23.34
Patient 15	62.83	75.34	46.77	4.93	32.65	26.26	45.51	43.38	19.09	17.29	9.02	21.01
Patient 16	67.10	64.78	55.46	2.81	38.24	31.95	50.84	44.14	19.94	20.01	5.58	37.16
Patient 17	61.14	64.54	43.08	4.09	32.79	27.21	44.48	45.72	17.98	17.28	7.08	34.69
Patient 18	61.48	62.55	42.60	4.91	30.15	28.47	51.09	38.91	20.20	20.26	6.10	29.08
Patient 19	72.09	75.06	57.05	2.56	32.78	31.52	50.42	37.16	21.81	21.42	7.11	24.64
Patient 20	71.23	72.26	49.03	5.83	37.69	30.79	44.92	44.82	21.82	20.95	4.27	18.98
Patient 21	66.29	71.88	47.60	6.72	35.69	28.16	47.28	42.52	20.82	18.52	7.61	21.47
Patient 22	69.23	72.73	51.30	2.43	34.74	36.38	41.70	42.75	22.83	19.32	8.02	23.87
Patient 23	66.92	74.81	48.71	3.69	34.33	27.92	41.54	43.14	20.60	18.05	7.60	25.74
Patient 24	63.28	66.94	42.80	3.34	30.04	27.63	50.05	36.49	21.33	17.90	5.64	33.29
Patient 25	62.79	66.08	44.22	2.08	27.32	23.03	46.86	41.62	18.42	17.99	7.48	17.50
Patient 26	68.83	73.97	55.85	4.98	31.35	29.99	46.74	47.94	20.81	21.75	7.35	29.61
Patient 27	70.38	75.86	59.27	3.90	41.97	31.33	50.87	47.24	22.09	19.54	7.12	31.64
Patient 28	65.67	68.96	47.81	3.32	28.77	30.25	46.71	43.65	20.62	18.99	5.91	23.84
Patient 29	67.59	68.71	52.47	3.62	26.89	30.67	49.59	38.22	19.60	22.37	5.39	27.08
Patient 30	68.11	75.51	51.68	3.92	29.62	32.17	48.57	46.82	19.16	19.58	7.34	33.12
Patient 31	66.63	63.42	52.98	5.35	27.20	29.50	48.72	43.93	19.79	19.23	7.09	24.68
Patient 32	61.96	64.53	44.28	4.05	27.95	29.35	47.83	42.02	19.78	18.80	4.30	21.73
Patient 33	60.06	62.76	41.52	4.50	24.39	25.69	53.31	43.35	18.66	17.68	7.16	21.04
Patient 34	68.45	72.16	54.42	1.82	32.49	32.70	46.08	44.67	18.82	19.57	8.44	32.80
Patient 35	62.51	65.36	45.57	3.80	31.21	27.83	45.53	38.16	18.73	18.54	4.94	19.82

Table 3: Unhealthy knee dimensions

Appendix B: Segmentations and Measurements

Filters

The dimensional measurements of the distal femur had to be accurate. The 3D models had to be of actual size and surface texture, therefore the CT scan had to be clear and accurate. A smooth surface texture of the 3D models was required to deliver an accurate interpretation of the bone profile, for accurate placement of landmark markers. The required time for segmentation had to be minimized, to shorten the data acquisition period. Filters were added to the scan data after the patient was removed from the scanning table. There were two types of filters: the first filter was a grainy type, while the second filter smoothed the recorded data (Figure 61).

Figure 61: CT scan data of right knee a) Grainy filter b) Smooth filter

The grainy filter is called the U90 filter. This filter was used when the images were printed for presentation reasons. It delivered high quality detail and contrast between the different elements in the scan data images. The smooth filter is called the B10 filter. When this filter was applied, it was difficult to interpret and distinguish between different elements in 2D. Applying a threshold to the two filter types gave a better understanding of why the smooth filter was used for the creation of 3D models from the scan data. The grainy filter selected voxels of the bone as well as small speckles throughout the entire scan, while the smooth filter captured the voxels of the bone structures (Figure 62).

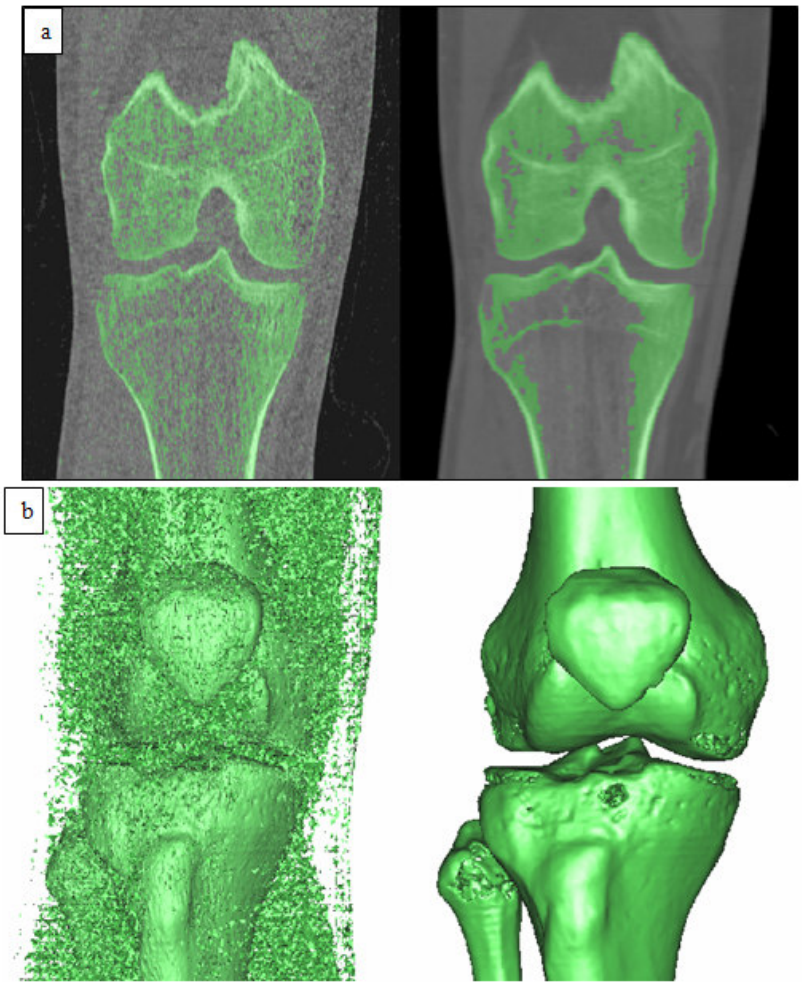

Figure 62: a) 2D threshold interval selected for both filter b) 3D models of both filters

The voxels selected outside of the bone profile, made close proximity bones conjoint to each other. Thus the bones had to be separated manually, which was time consuming and the 3D models were inaccurate.
After the editing of the scans was completed, the surface texture of the 3D models was different. The U90 filter had a very rough surface texture and any specific landmarks were difficult to identify, while the 3D models of the B10 filter had a smooth surface texture with an exact bone profile (Figure 63).

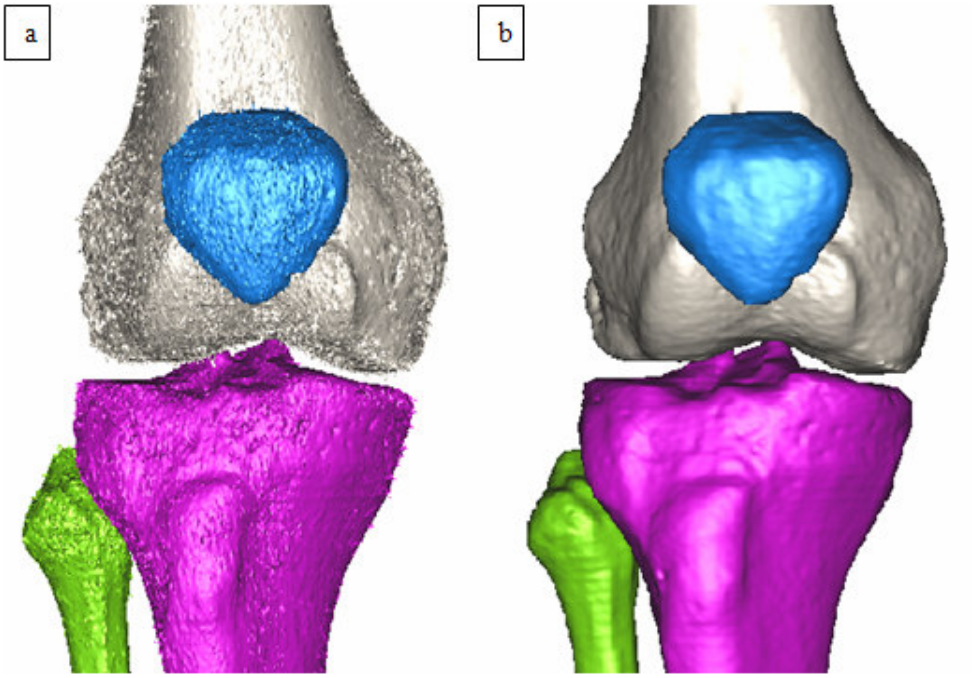

Figure 63: 3D models after region growing

Knee Analysis

The measuring of the morphological dimensions was done when computer segmentation of the knee models was completed. The measuring procedure was initiated through different cuts required for specific measurements. In order to create a basis of measurements which were measured in an equal manner to the preoperative planning, different planes were required. The transverse plane was made by viewing the model from the front and cutting horizontally into the screen on the femur shaft. This process was repeated a small distance above the first cut, creating a circular disc. In the frontal view, a vertical cut was made in the disc to create a flat surface for the sagittal plane. The model was turned and viewed from the left side. Again a vertical cut was made in the disc, creating a flat surface for the frontal plane. All the unwanted off-cuts were deleted. In the simulation module, the anthropometric analysis was selected with the knee template. Using this template, only the points need to be indicated at the specific landmarks. The procedure was completed by placing the points in alphabetical order, but it will be explained in order of plane construction. First, the three reference planes were created. Points T-1, T-2 and T-3 were placed in a triangle on the bottom of the circular disc to create the transverse plane. F-1 and F-2 were placed on the back surface and S-1 placed on the side of the part for the frontal and sagittal plane (Figure 64).

Figure 64: Reference cuts

Again a part was cut from the femur to create the anatomical axis of the femur. A 100mm piece was cut from the shaft of the femur, approximately 100mm proximal from the most distal part of the femur. This shaft cut-out is coloured brown as in the figure below. Points A-1 and A-2 were then placed at the centres of the two ends of the cut-out to create the anatomical axis of the femur (Figure 65).

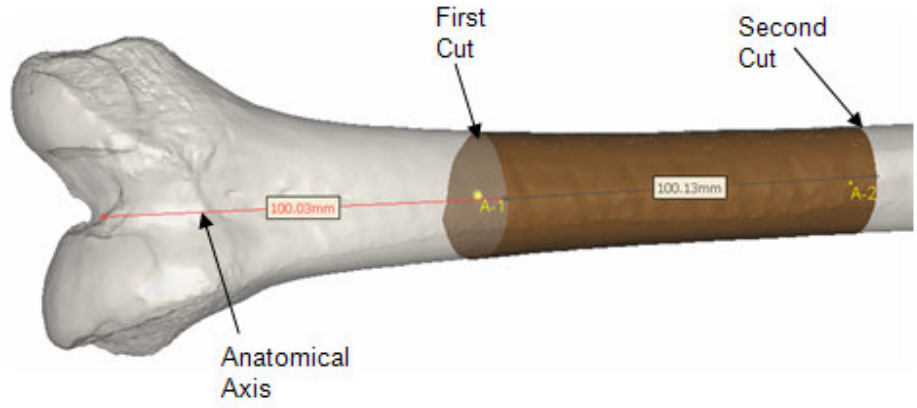

Figure 65: Anatomical axis generation

The mechanical axis was created with two points. M-1 was placed on the arch between the two condyles and M-2 was placed in the centre of the hip sphere. The placement of the points E-1 and E-2 for the posterior condylar axis was done using different views to determine the most posterior points of the two condyles. The two epicondylar axes were created with three points placed on the specific landmarks. Point l_p was placed on the highest point of the lateral epicondyle and the point *mp* was placed on the highest point

of the medial epicondyle. These two points created the clinical epicondylar axis. Point m_s were placed on the medial sulcus, located posterior to the medial prominence. The m_s and l_p points created the surgical epicondylar axis (Figure 66).

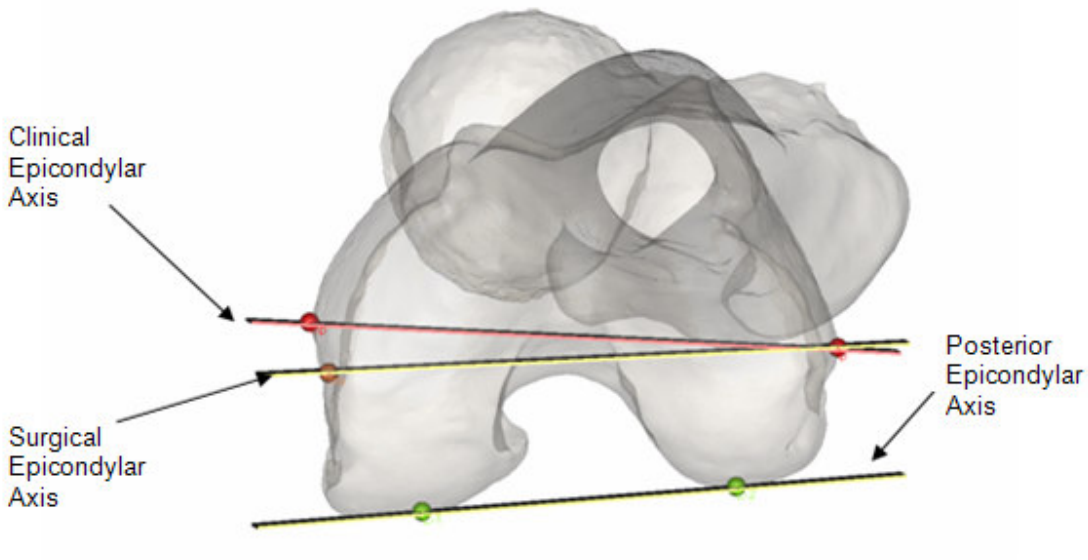

Figure 66: Epicondylar axis of the knee

These points determined the main axes of the femur. The next step was too indicate the positions of the points used to create the cutting planes. First, the most distal point was allocated with the point B. This gives a reference marker to measure the cut-off distance. The point Cut-1 was placed on the medial condyle proximal to the point B. This point should be adjusted proximal/distal until the distal cut measurement was at the correct length. The same procedure was followed with point Cut-2 for the posterior cut. This point should be adjusted in the anterior/posterior direction. The anterior cut was created through the placement of two planes. The first was to determine the anterior face of the femur shaft, achieved by placing points D-1 and D-2 on the anterior face of the shaft. Point W-1 was placed where this plane intersects the anterior part of the femur. W-2 was placed distally and posterior to point W-1 until the cutting angle was correct.

The AP dimension was measured from the point L_{ac} to the posterior epicondylar axis and L_{ac} was placed at the most anterior point of the lateral condyle. The ML dimension was measured by placing the two points $Z_{ml\text{-}1}$ and $Z_{ml\text{-}2}$ on either side of the distal cut. The point Z_p is placed next to the Cut-2 point to measure the RPC dimension. The trochlear groove angle was measured by placing point G-1 at the most distal point and G-2 at the most proximal point in the groove. Point SL was placed at the most proximal point of the sulcus.

Condyle Radii

The LR, MR, Pl and Pm points were used to measure the condyle radii. No planes or measurements were linked to these points; only the exported coordinates were used.

The three LR points created the lateral condyle radius. Point LR-2 was placed on the lateral condyle at the most distal point of the condyle. LR-1 was placed anterior and LR-3 was placed posterior in a straight line to point LR-2. The same procedure was followed for the placement of MR points on the medial condyle. The Pl points were placed on the posterior lateral condyle in the same manner, except that Pl-2 was placed on the most posterior point of the condyle. Point Pl-1 was placed distal and Pm-2 is placed proximal in a straight line to point Pl-2. The same procedure was followed for the placement of Pm points on the posterior medial condyle (Figure 67).

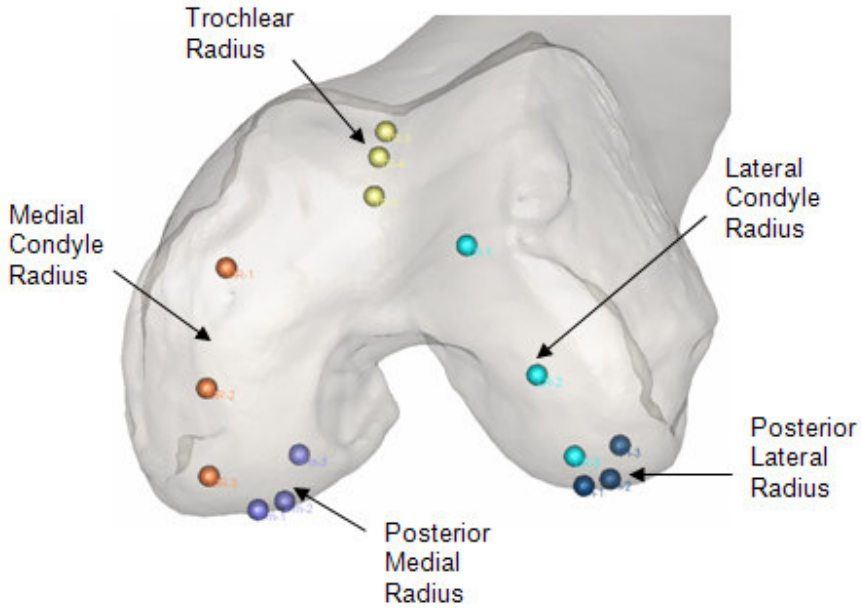

Figure 67: Condyle radii point placement

Extra Measurements

These measurements include all the dimensions that was only done to illustrate what can be measured and to measure dimensions of the population. The first extra measurement was the calculation of the femoral version. This was the angle of the proximal femur neck relative to the posterior epicondylar axis. The femur was viewed from the side and two cuts were made through the femur neck. The points H-1 and H-2 was placed at the centre of each cut in the same manner as with the anatomical axis. Points SA-1 and SA-2 were placed medial and lateral to the point TR-4 on the highest points of the groove ridges. These two points also calculated the groove wedge angle. The notch width was measured by placing points N-1 and N-2 on either side of the notch. The TT/TG was measured by placing the point P on the tibial tubercle and a distance was measured to the point G-1. A point M_{ac} was placed on the most anterior point of the medial condyle creating a plane with point L_{ac}. The trochlear version was calculated as the angle between this plane and the posterior epicondylar axis.

Validation

All measuring techniques and objects used to determine any parameters were validated.

Measurements

Most of the measurements made in the study were performed using MIMICS. Thus the measurement results were validated by measuring a model with known values. The model consisted of five distances ranging from 10 mm to 50 mm (Figure 68). The five different distances were measured and delivered exact results. Thus any distance measurements made with MIMICS was perfect.

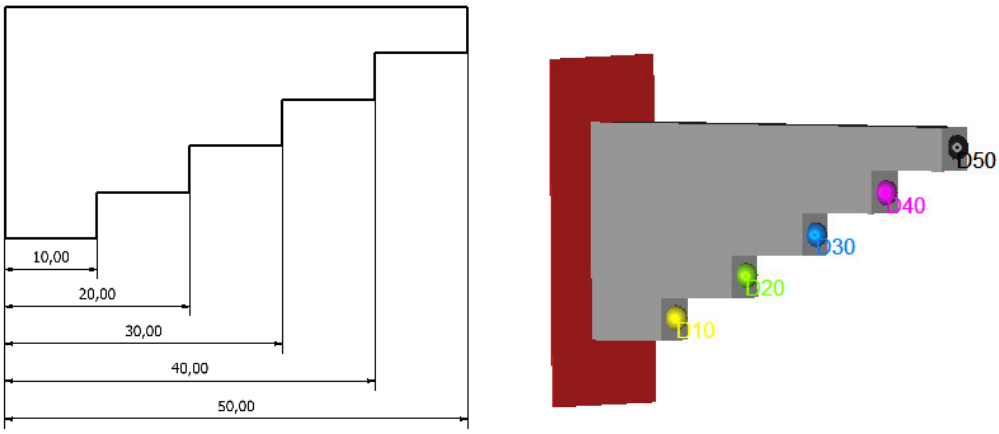

Figure 68: MIMICS validation of measurement results

Radius

The radius measurement was validated to ensure that the radius calculation program delivered the actual value of the curvature. A test was the set up where the radius was measured on four circular discs with known diameters. The model was created in CAD and exported as STL to MIMICS. The diameters of the four discs were 10 mm, 20mm, 30mm and 40mm. In the knee analysis only small parts of the circumference were available for measuring. Therefore the points were spaced at different angles to illustrate that the measuring technique was not depended on the length of the available curvature (Figure 69).

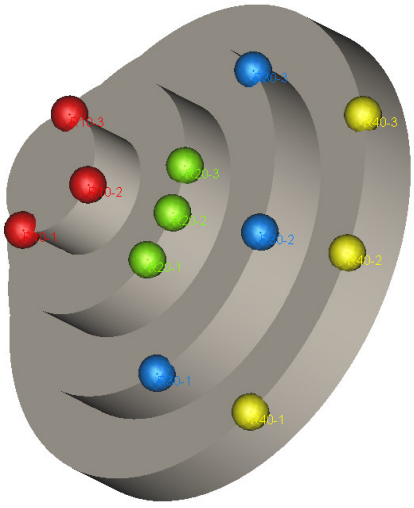

Figure 69: Radius validation model with four discs

The differences between the measured and actual values are displayed below (Table 4).

	Diameter [mm]	Measured [mm]	Error [%]
Red	10	9.9472	0.5281
Green	20	19.8588	0.7059
Blue	30	29.9856	0.0481
Yellow	40	40.0133	0.0332

Table 4: Radius Validation Results

Overall the radius calculation method delivered 99.3% accuracy. The method delivered good results and was therefore suitable for the knee analysis.

Angle

The angle measuring method was validated by using a model with a known angle. The necessary planes were created and the positions of the four points were calculated from the planes (Figure 70). The model was given a 10° angle and the program delivered a 9.999° angle. Overall the angle calculation method delivered 99.9% accuracy. Thus the method of measuring the trochlear angle was accurate and could be used in the analysis.

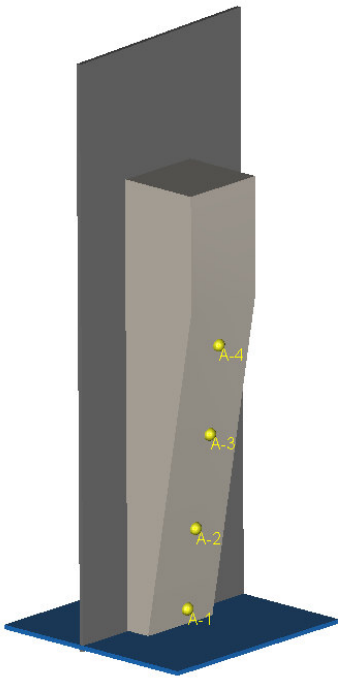

Figure 70: Angle validation model in MIMICS

Scanners

All the measurements were performed on CT or 3D scanner models. Thus the accuracy of the 3D models created from the scanner was evaluated. The accuracy of the scanner was tested by scanning a block and a ball with both scanners. The models were

imported and measured in MIMICS. The block tested the distance accuracy, while the ball tested the accuracy of a model with rounded surfaces. The physical pieces were measured with an electronic vernier caliper and micrometer.

3D scanner

The two models were scanned with the NextEngine 3D scanner to test the accuracy of the scanner using flat and round surfaces (Figure 71).

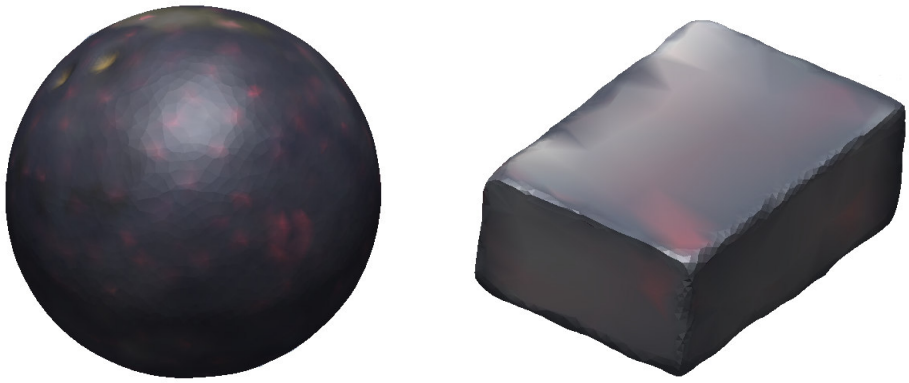

Figure 71: Models of ball and block scanned with NextEngine scanner

CT scanner

The two physical pieces were CT scanned and imported into MIMICS (Figure 72). The material type was not important, because there was no other material in the scanning field. Thus a threshold interval could be selected which included the entire model.

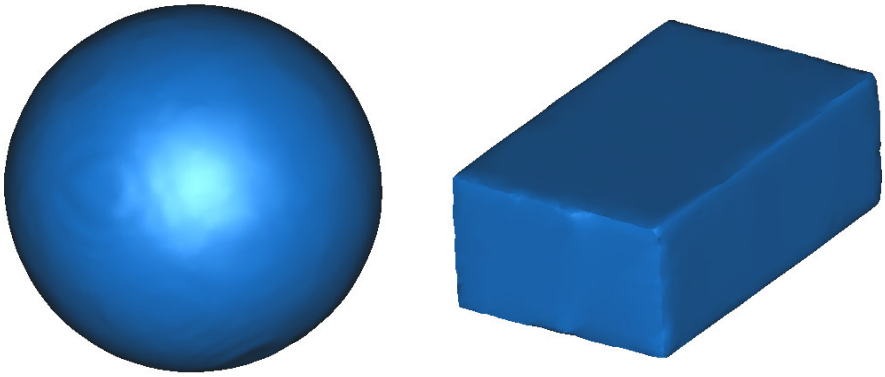

Figure 72: CT scan models of ball and block

Measurement

After the two models were scanned using the two different scanners, two templates were created to measure the two specific models. The ball radius was measured in three directions and the height, length and width of the block was measured (Figure 73). The models were measured before it was scanned in the allocated dimensions and compared to the MIMICS measurements.

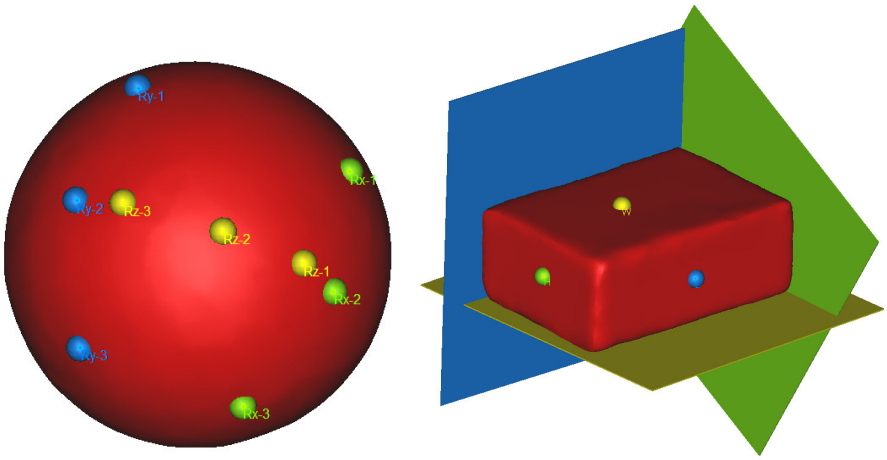

Figure 73: Ball and block imported into MIMICS and measured

These measurements used the radius calculation method which calculated smaller values and therefore the radius accuracy was first applied to the measured values. The measurements of the three diameters were compared to the true values of the diameters (Table 5).

	True	3D	CT
Rx	39.5	39.6245	39.22
Ry	39.5	39.6807	39.27
Rz	39.5	39.6274	39.17

Table 5: Ball overall dimensions

The 3D scanner delivered 99.63% (100.37) accuracy; while the CT scanner had an accuracy of 99.26%.The MIMICS measurements were compared to the true values of the three dimensions of the block model (Table 6).

	True	3D	CT
Height	40.78	40.84	40.69
Length	26.33	26.41	26.27
Width	15.19	15.26	15.13

Table 6: Block overall dimensions

The 3D scanner delivered 99.69% accuracy, while the CT scanner had an accuracy of 99.71%. Both scanner delivered high accuracy and therefore the models could be used for the analysis. From the measured results, it was clear that the model created by the 3D scan was larger and the CT scan model was smaller than the true model.

Reproducibility

The measuring analysis was validated to analyze the reproducibility of the point's placement procedure. The reproducibility of the measurements was analyzed in 20 consecutive measurements of the same 3D knee model. Only seven measurements were made for each test (Table 7).

Parameter	Mean [mm]	Std. Dev. [mm]	Std. Error [mm]
AMA	6.41	0.28	0.06
Femoral Version	19.79	4.5	1.00
Notch Width	17.47	0.91	0.20
Post/Clinical Epicondylar	4.44	0.76	0.17
Post/Surgical Epicondylar	1.40	0.68	0.15
TT\TG	8.58	1.30	0.29
Trochlear Version	10.59	2.40	0.53

Table 7: Reproducibility test results

Measurements placed on precise landmarks were found to more repeatable compared to measurements which were depended upon the opinion of the user performing the analysis

Appendix C: Knee Studies

The two models was overlaid, the 30 points were placed on the models to measure the cartilage thickness in 15 specific points. All the dimensions in the table were measured in millimetres.

Cadaver	LR-1	LR-2	LR-3	MR-1	MR-2	MR-3	PL-1	PL-2	PL-3	PM-1	PM-2	PM-3	TR-1	TR-2	TR-3
103	1.66	1.34	1.47	2.00	1.82	1.56	2.17	2.44	2.30	1.85	2.06	1.85	3.15	3.08	2.06
104	1.17	0.46	1.91	0.83	0.59	1.43	2.23	2.28	2.00	1.72	1.60	1.54	2.71	2.63	1.07
105	1.16	1.19	2.14	0.39	0.6	1.61	2.17	1.65	0.97	1.69	1.35	1.27	1.99	1.76	0.90
108A	1.84	0.8	1.66	1.61	0.94	1.69	2.58	2.15	1.91	1.66	1.97	1.82	3.11	3.01	1.48
109	2.05	0.98	1.84	1.01	1.19	1.12	2.80	1.37	1.21	1.24	0.88	1.07	2.22	3.74	2.70
109A	2.77	2.49	2.38	1.35	1.75	2.36	2.90	1.52	1.52	2.68	2.34	2.35	3.61	3.98	2.19
204	1.48	1.70	1.25	1.35	0.92	1.70	2.08	1.69	1.19	1.66	1.67	2.47	2.93	2.47	1.75
205A	1.92	1.40	1.07	1.00	0.26	0.88	2.16	1.71	1.54	1.33	1.05	1.89	3.55	2.87	1.57
210	1.05	0.82	0.97	0.50	0.84	2.24	1.85	1.78	1.54	2.30	1.25	0.66	2.33	3.11	0.84
DL13	1.64	1.61	2.43	0.96	0.59	1.21	2.47	1.26	0.66	1.93	1.59	1.97	1.52	2.00	1.47
DL10A	0.94	0.87	0.95	1.11	0.74	0.83	2.09	1.85	2.20	0.78	1.00	2.35	1.86	1.77	0.96
DL11	2.73	2.05	1.31	1.66	0.85	1.47	0.86	1.08	1.57	1.38	1.69	2.59	2.76	2.12	1.85
DL14	1.23	0.85	0.17	1.47	0.88	0.67	0.70	0.48	1.85	0.46	0.35	0.81	3.69	2.48	0.92
DL15	1.78	2.00	2.81	1.48	1.26	1.91	2.66	1.68	1.29	1.89	1.45	0.58	2.48	2.76	2.48
NDL_13A	2.80	2.26	1.85	1.70	1.29	2.11	2.32	2.67	2.08	2.34	2.41	2.21	2.55	2.51	2.05
NDL_14A	3.46	2.23	2.54	1.13	0.41	1.37	2.81	2.39	2.87	1.88	2.50	2.87	2.66	4.10	2.34
NDL_15A	1.63	1.41	1.41	1.20	0.79	1.75	1.54	1.73	2.86	1.70	2.37	2.62	3.35	3.62	2.47
NDL_16A	1.16	2.22	1.82	1.16	1.24	2.12	2.70	2.85	2.82	2.02	2.10	2.28	2.44	1.45	1.42

Table 8: Cartilage thickness of cadavers

Name	AP	ML	Box	SA	SL	RPC	LCR	MCR	PLR	PMR	SD	TR
Fem 103	66.71	67.19	51.77	4.10	25.81	30.96	50.86	46.82	20.93	20.16	5.94	23.84
Fem 104	62.27	66.41	42.62	4.55	30.89	30.85	49.63	45.67	22.34	21.39	4.70	20.86
Fem 105	72.53	64.09	52.59	4.32	33.44	32.23	46.62	42.36	19.24	20.84	6.77	21.29
Fem 108A	66.64	73.55	53.83	4.98	27.34	33.44	48.93	43.20	22.94	21.19	4.78	23.22
Fem 109	64.79	72.83	50.28	4.39	32.52	26.33	53.69	44.70	20.3	20.39	6.00	24.53
Fem 109A	66.04	71.69	49.03	3.55	24.83	26.83	56.29	41.63	19.67	20.49	5.69	22.12
Fem 204	61.28	74.66	44.62	3.32	23.66	28.99	50.41	43.93	20.19	19.22	4.79	22.33
Fem 205A	65.32	71.31	52.53	3.69	33.46	30.78	53.00	42.23	19.21	19.51	4.68	23.24
Fem 210	58.17	73.87	45.58	3.91	29.37	27.12	54.91	42.75	19.94	20.93	5.23	22.87
DL13	58.28	68.92	43.29	3.94	26.81	23.42	54.28	44.63	18.80	18.45	6.41	24.68
DL10A	65.81	69.18	46.28	4.17	29.13	25.15	59.93	42.78	19.72	19.37	4.70	20.07
DL11	72.86	78.33	55.17	5.20	33.87	33.21	56.90	37.61	22.59	22.41	4.99	22.77
DL14	69.95	68.24	53.09	3.48	39.39	33.45	59.21	43.72	22.59	22.95	6.40	23.73
DL15	62.20	66.21	44.62	3.95	36.41	23.88	55.58	42.19	20.69	20.48	3.75	22.44
NDL_13A	57.07	68.91	40.73	3.89	24.35	23.64	48.19	36.29	20.11	19.06	2.82	19.53
NDL_14A	69.91	71.02	46.03	3.91	34.78	29.21	61.97	41.75	20.93	19.27	5.37	23.08
NDL_15A	65.56	76.74	44.10	4.35	36.01	25.06	60.71	40.15	21.60	19.41	4.92	23.05
NDL_16A	61.38	69.21	45.65	3.02	31.62	26.30	59.16	41.13	20.90	20.17	3.71	23.53

Table 9: Cadaveric dimensions without cartilage

Name	AP	ML	Box	SA	SL	RPC	LCR	MCR	PLR	PMR	SD	TR
Fem 103	68.87	67.19	54.25	4.10	25.81	33.63	50.86	46.82	20.93	20.16	5.94	23.84
Fem 104	68.35	66.41	46.91	4.55	30.89	31.41	49.63	45.67	22.34	21.39	4.70	20.86
Fem 105	76.89	64.09	53.66	4.32	33.44	33.39	46.62	42.36	19.24	20.84	6.77	21.29
Fem 108A	71.91	73.55	57.03	4.98	27.34	35.20	48.93	43.20	22.94	21.19	4.78	23.22
Fem 109	67.76	72.83	51.92	4.39	32.52	27.54	53.69	44.70	20.3	20.39	6.00	24.53
Fem 109A	76.82	71.69	52.64	3.55	24.83	29.43	56.29	41.63	19.67	20.49	5.69	22.12
Fem 204	64.17	74.66	48.45	3.32	23.66	30.27	50.41	43.93	20.19	19.22	4.79	22.33
Fem 205A	68.98	71.31	55.55	3.69	33.46	32.11	53.00	42.23	19.21	19.51	4.68	23.24
Fem 210	62.03	73.87	46.34	3.91	29.37	27.62	54.91	42.75	19.94	20.93	5.23	22.87
DL13	61.05	68.92	45.74	3.94	26.81	24.95	54.28	44.63	18.80	18.45	6.41	24.68
DL10A	68.63	69.18	46.94	4.17	29.13	28.27	59.93	42.78	19.72	19.37	4.70	20.07
DL11	75.16	78.33	56.11	5.20	33.87	35.85	56.90	37.61	22.59	22.41	4.99	22.77
DL14	71.43	68.24	53.61	3.48	39.39	34.68	59.21	43.72	22.59	22.95	6.40	23.73
DL15	62.59	66.21	45.08	3.95	36.41	25.80	55.58	42.19	20.69	20.48	3.75	22.44
NDL_13A	60.02	68.91	43.18	3.89	24.35	26.44	48.19	36.29	20.11	19.06	2.82	19.53
NDL_14A	73.24	71.02	51.33	3.91	34.78	31.49	61.97	41.75	20.93	19.27	5.37	23.08
NDL_15A	70.69	76.74	47.98	4.35	36.01	28.56	60.71	40.15	21.60	19.41	4.92	23.05
NDL_16A	65.74	69.21	47.10	3.02	31.62	29.52	59.16	41.13	20.90	20.17	3.71	23.53

Table 10: Cadaveric dimensions with cartilage

Normal knee dimensions

Name	AP	ML	Box	SA	SL	RPC	LCR	MCR	PLR	PMR	SD	TR
Cadaver 1	64.5	62.77	49.98	1.61	20.88	30.41	50.76	40.67	18.93	18.10	7.95	23.94
Cadaver 2	59.34	62.63	43.63	3.84	26.31	30.66	44.32	39.03	18.74	20.78	6.15	25.75
Cadaver 3	65.46	67.96	54.11	4.29	26.71	30.25	47.52	39.33	18.45	19.9	8.47	20.45
Cadaver 4	66.04	71.53	52.55	4.63	22.78	29.04	46.89	43.88	19.24	18.83	5.27	24.77
Cadaver 5	64.24	64.21	47.29	3.13	28.79	27.00	50.97	41.02	19.13	19.07	6.09	22.64
Cadaver 6	64.55	65.65	49.35	3.60	24.9	27.41	54.48	40.55	17.30	18.46	7.11	24.32
Cadaver 7	64.82	61.01	50.99	4.28	27.01	29.51	52.16	44.08	18.37	18.35	4.66	27.82
Cadaver 8	59.89	58.66	44.76	3.38	23.17	29.22	46.15	34.48	19.52	17.17	4.39	22.37
Cadaver 9	55.51	69.14	42.75	2.19	23.88	26.62	46.56	34.11	16.45	16.98	7.16	31.62
Cadaver 10	65.81	69.18	46.28	4.17	29.13	25.15	57.93	42.78	19.72	19.37	4.7	20.07
Cadaver 11	72.86	78.33	55.17	5.20	33.87	33.21	56.9	37.61	22.59	22.41	4.99	22.77
Cadaver 12	69.95	68.24	53.09	3.48	39.39	33.45	57.21	43.72	22.59	22.95	6.4	23.73
Cadaver 13	62.20	66.21	44.62	3.95	36.41	23.88	55.58	42.19	20.69	20.48	3.75	22.44
Cadaver 14	58.28	68.92	43.29	3.94	26.81	23.42	54.28	44.63	18.80	18.45	6.41	24.68
Cadaver 15	60.02	68.91	43.18	3.89	24.35	26.44	48.19	36.29	20.11	19.06	2.82	19.53
Cadaver 16	73.24	71.02	51.33	3.91	34.78	31.49	51.97	41.75	20.93	19.27	5.37	23.08
Cadaver 17	70.69	76.74	47.98	4.35	36.01	28.56	50.71	40.15	21.6	19.41	4.92	23.05
Cadaver 18	65.74	69.21	47.10	3.02	31.62	29.52	57.16	41.13	20.9	20.17	3.71	23.53
Normal 1	65.43	74.95	49.41	3.80	33.11	30.68	52.55	40.67	19.63	20.83	6.15	23.45
Normal 2	76.20	73.08	58.01	2.01	30.5	33.37	47.20	40.63	22.57	20.79	4.98	24.56
Normal 3	64.49	72.3	53.94	4.66	28.65	32.02	49.44	41.50	19.28	20.83	4.77	21.94
Normal 4	65.71	68.67	40.69	4.38	29.28	28.45	55.77	40.30	23.55	19.51	5.98	21.29
Normal 5	73.69	68.01	58.97	3.58	22.14	33.99	56.84	38.43	20.04	19.42	4.99	26.90
Normal 6	69.59	68.57	55.49	4.62	34.67	29.51	55.81	40.12	18.52	18.73	7.59	21.52
Normal 7	63.92	67.23	41.71	2.01	29.33	24.54	50.78	44.41	19.91	18.55	6.13	24.33
Normal 8	67.70	63.13	50.40	4.47	30.21	28.45	55.36	43.9	19.31	19.00	6.73	27.72
Normal 9	62.81	63.17	40.88	3.35	33.46	22.88	53.79	41.28	18.43	17.39	8.39	21.32
Normal 10	66.25	66.73	53.58	1.88	25.11	30.83	47.92	43.88	19.18	20.65	5.63	26.56
Normal 11	67.95	64.21	46.74	4.52	28.9	26.47	56.12	43.01	17.86	18.33	6.46	19.92
Normal 12	56.07	56.78	38.94	2.43	24.26	21.8	54.16	38.13	15.24	16.07	6.51	22.13
Normal 13	64.15	69.78	47.65	4.10	27.79	28.55	50.86	43.89	20.5	19.04	8.28	23.47
Normal 14	64.30	69.22	47.73	1.35	22.2	25.26	58.42	40.34	18.11	17.24	6.89	25.18
Normal 15	65.54	69.78	43.6	1.72	29.78	29.54	50.12	41.36	18.88	18.12	6.55	18.85
Normal 16	61.99	67.34	38.19	2.38	33.88	28.85	49.94	33.78	20.76	18.22	5.61	24.41
Normal 17	67.23	76.73	49.79	2.02	32.78	31.36	48.12	41.79	20.67	20.04	6.24	20.36

Table 11: Normal knee dimensions

Appendix D: Prosthesis Dimensions

The first table contains the data of the PRP. This prosthesis design range has seven available sizes.

PRP	1	2	3	4	5	6	7
AP_{BOX}	34.0	37.0	40.0	43.5	47.5	52.0	57.0
ML	56.0	59.0	62.5	66.5	71.0	76.0	82.0
AP	50.0	53.0	56.5	60.5	65.0	70.0	75.5
TR	25.3	27.1	28.6	30.5	33.1	35.7	38.6
CR	26.1	28.7	31.3	34.8	38.8	41.7	44.3
PCR	12.1	13.2	14.6	15.5	16.7	17.5	18.1
RPC	18.5	20.0	21.5	23.0	26.0	28.0	30.0
SD	3.40	3.50	3.50	3.60	3.70	3.60	3.70
SA	3.80	3.60	3.80	3.90	3.39	3.54	3.80
SL	34.5	37.5	40.4	43.5	47.35	50.0	53.6

Table 12: PRP dimensions of size range

The second table contains the dimensions of the PSP. There are more than six sizes available in the design range, but only six where used in the project. The other sizes are not used that often and are only used in special cases.

PSP	3	4	5	6	7	8
AP_{BOX}	37.2	40.3	43.5	45.6	48.2	49.5
ML	64.0	67.0	70.0	73.0	76.0	78.0
AP	56.0	59.0	62.0	65.0	68.0	71.0
TR	22.4	26.7	29.7	34.0	37.0	39.6
LCR	45.7	47.9	49.6	52.9	55.8	59.5
MCR	41.7	43.3	45.2	46.0	47.6	49.1
PCR	16.7	17.9	19.1	20.5	21.5	22.7
RPC	22.6	24.8	25.8	28.8	29.9	32.1
SD	2.4	2.20	2.40	3.40	3.30	3.70
SA	2.8	3.10	2.80	3.00	2.90	2.90
SL	43.2	44.7	47.1	48.5	50.5	52.5

Table 13: PSP dimensions of size range

Appendix E: LifeMOD Data

The LifeMOD model was created with patient specific coordinates.

Import Coordinates:

Rot:	-0.24	-.903	0.191
Trans:	178.098	96.111	181.9229

Contact Properties:

Contact	Stiffness	Exponent	Damping	Depth	Static	Dynamic
Tibio-femoral	1e7	1	1e5	0.001	0.03	0.01
Patellofemoral	1e9	2	1e5	0.001	0.03	0.01

Table 14: Contact Properties

Ligament Attachment Points

Point	X	Y	Z
LCL1	0.1314290	-0.470261	-0.0111300
LCL2	0.1375900	-0.529998	-0.0127373
MCL1	0.0440999	-0.476422	-0.0223808
MCL2	0.0499933	-0.508568	-0.0213093
MCL3	0.0440999	-0.476422	-0.0185739
MCL4	0.0553524	-0.525439	-0.0125521
ACL1	-0.1055960	-0.476559	-0.0212271
ACL2	-0.1038050	-0.497261	0.0121579
PCL1	-0.0833599	-0.476960	-0.0180143
PCL2	-0.1010740	-0.504533	-0.0348196
Pat1	0.0813667	-0.471484	0.0382722
Pat2	0.0895048	-0.559400	0.0245420
Pat3	0.1040090	-0.471484	0.0382722
Pat4	0.0969645	-0.559400	0.0245420
MPFL1	-0.0544395	-0.457679	-0.0043601
MPFL2	-0.0996036	-0.445715	0.0422744
MPFL3	-0.0972928	-0.461259	0.0418543
LPFL1	-0.1430870	-0.458318	-0.0161238
LPFL2	-0.1361550	-0.445715	0.0332416
LPFL3	-0.1388860	-0.463360	0.0326114
Mot1	0.0950965	-0.529534	0.0214111

Table 15: Ligament attachment point coordinates

Ligament Properties:

Ligamnet	Stiffness	Damping	Preload
LCL	1e7	1e5	3

MCL1	5e3	1e5	3
MCL2	5e4	1e5	3
ACL	1e7	1e5	3
PCL	1e7	1e5	3
PT	1e5	1e5	0
PFL	100	1000	0

Table 16: Ligament Properties

Joint Properties:

Joint	X	Y	Z
Hip	1000	100	1000
Ankle	1000	100	1000

Table 17: Joint Properties

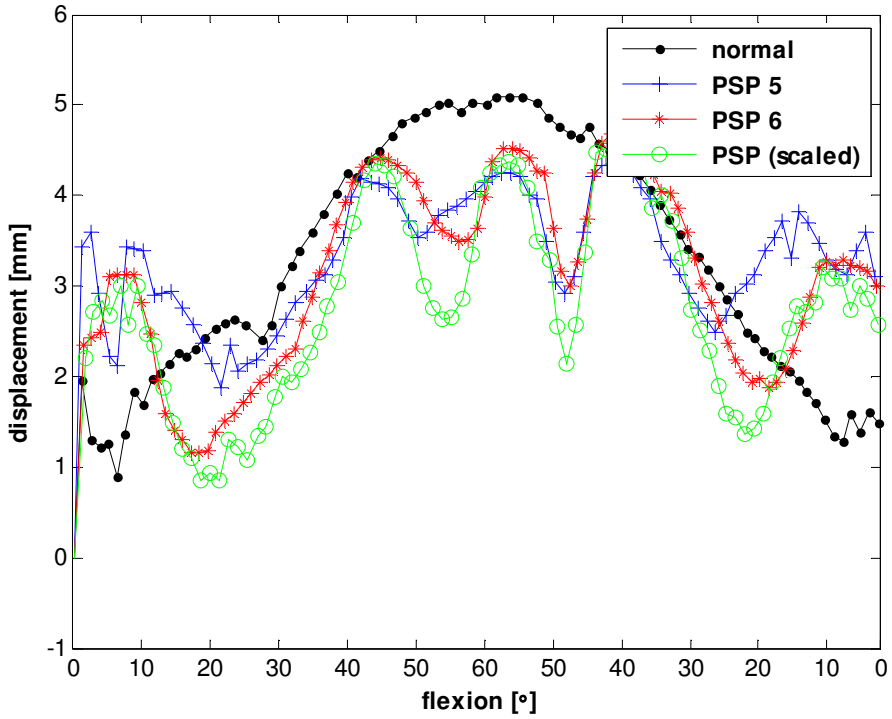

Figure 74: Medial/Lateral displacement of PSP (+ Medial/ - Lateral)

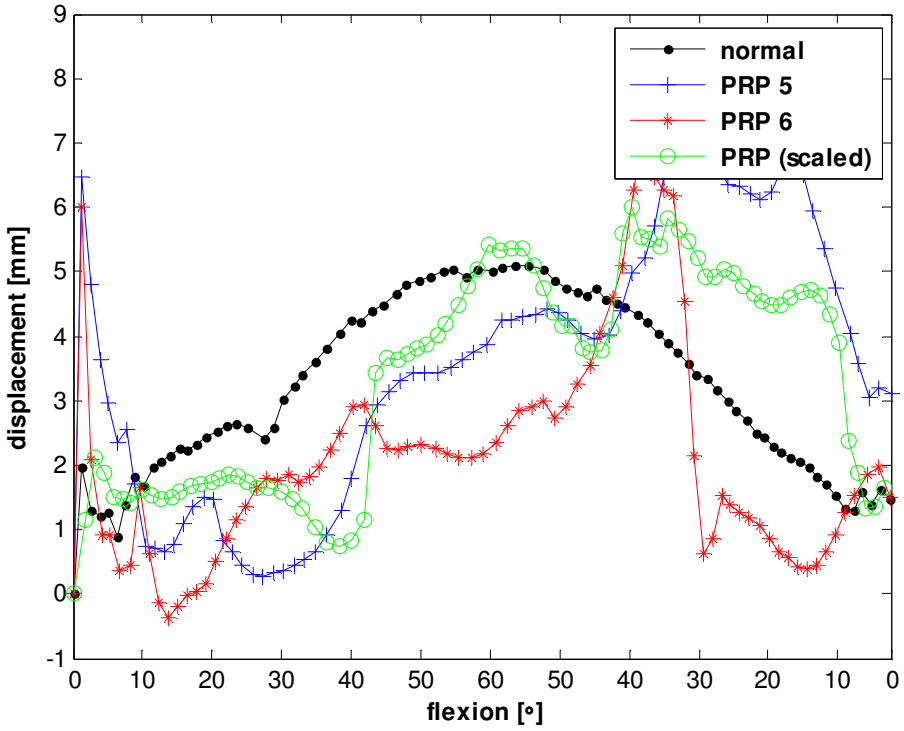

Figure 75: Medial/Lateral displacement of PRP (+ Medial/ - Lateral)

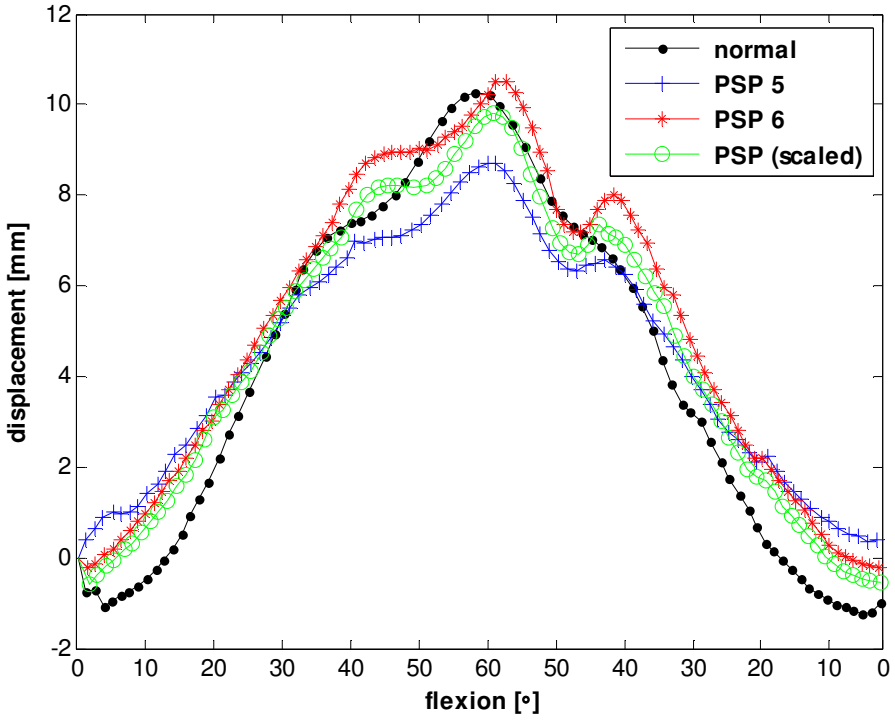

Figure 76: Proximal/Distal displacement of PSP (+ Proximal/ - Distal)

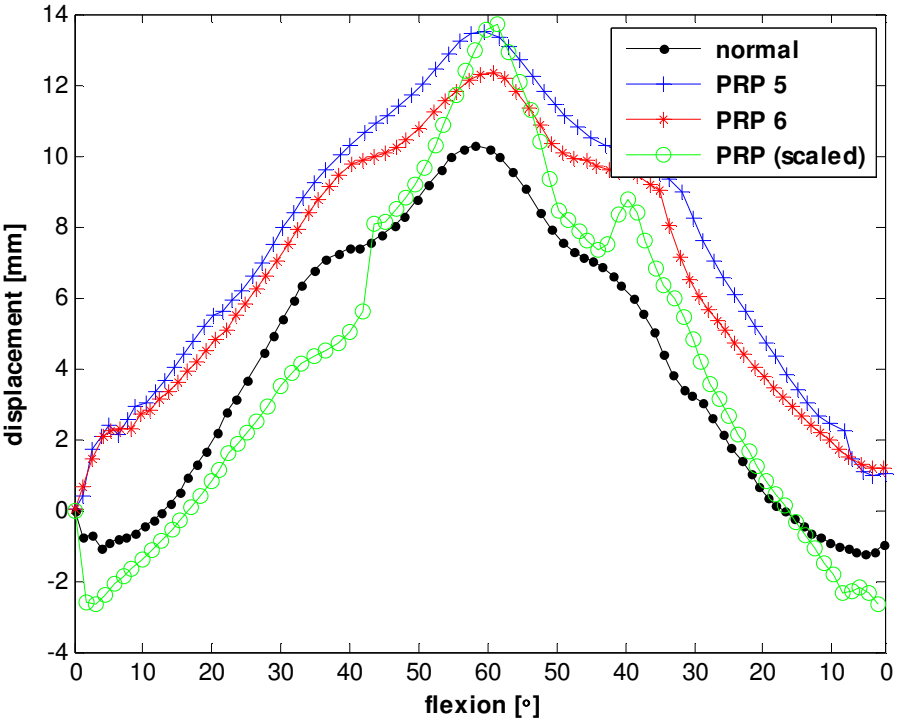

Figure 77: Proximal/Distal displacement of PRP (+ Proximal/ - Distal)

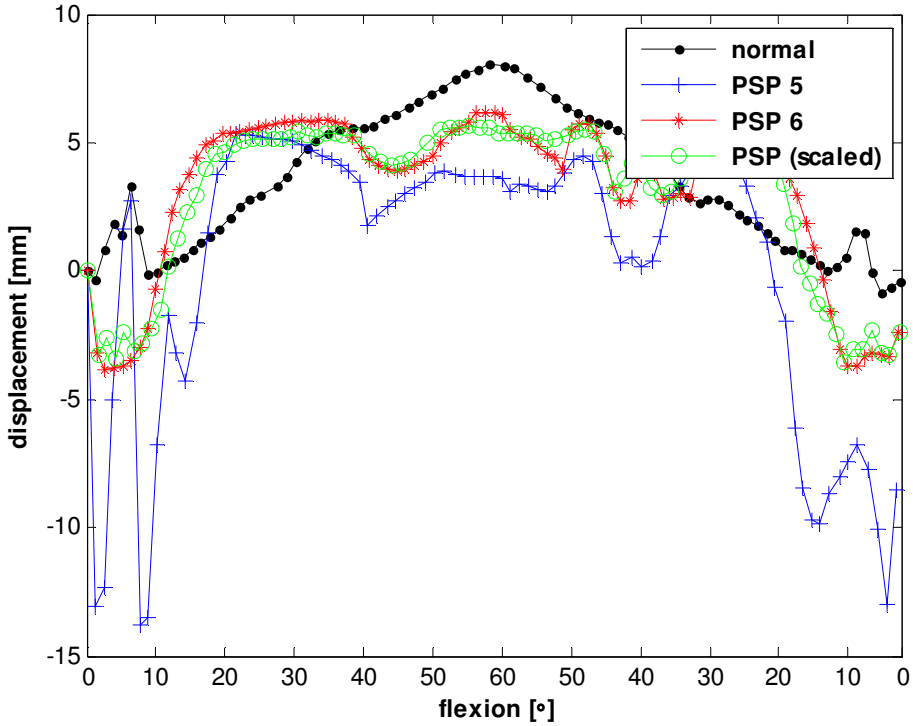

Figure 78: Anterior/Posterior displacement of PSP (+ Anterior/ - Posterior)

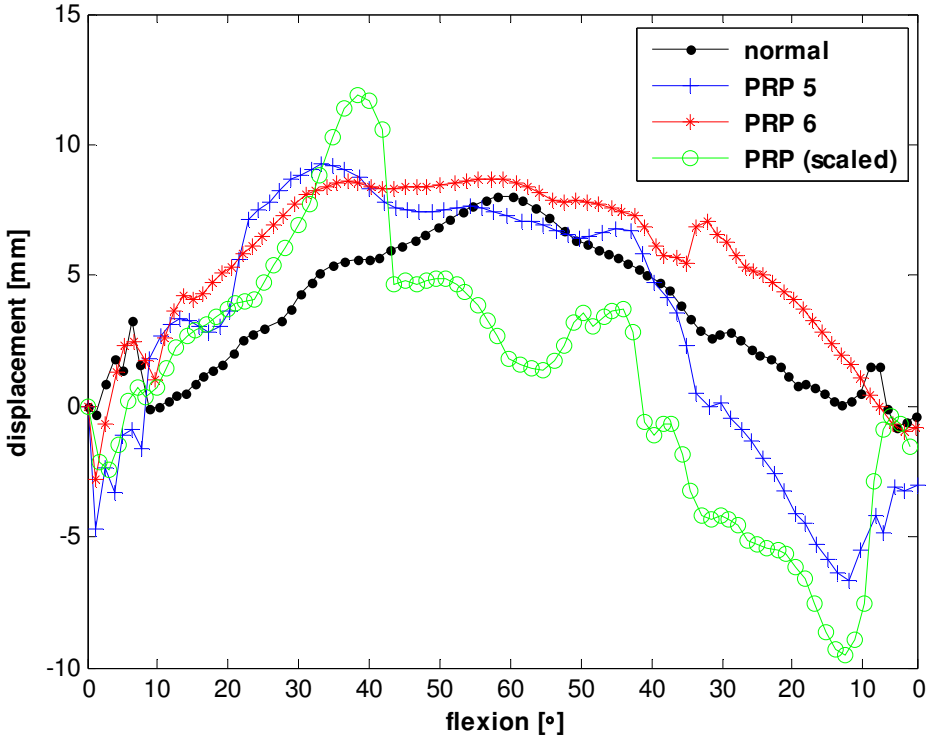

Figure 79: Anterior/Posterior displacement of PRP (+ Anterior/ - Posterior)

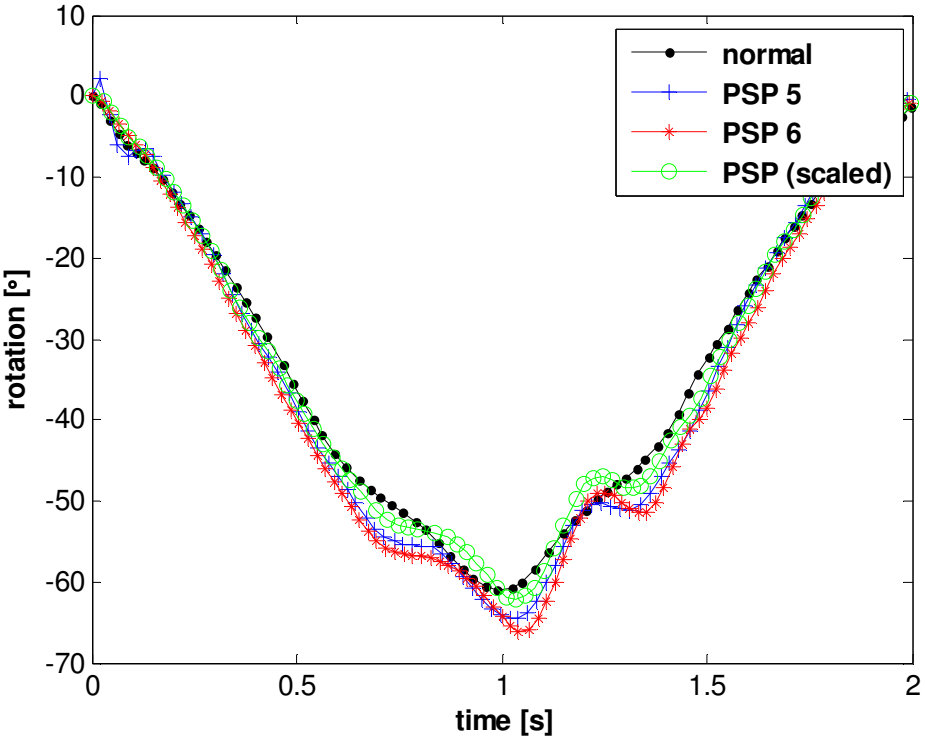

Figure 80: Flexion/Extension of PSP (- Flexion/ + Extension)

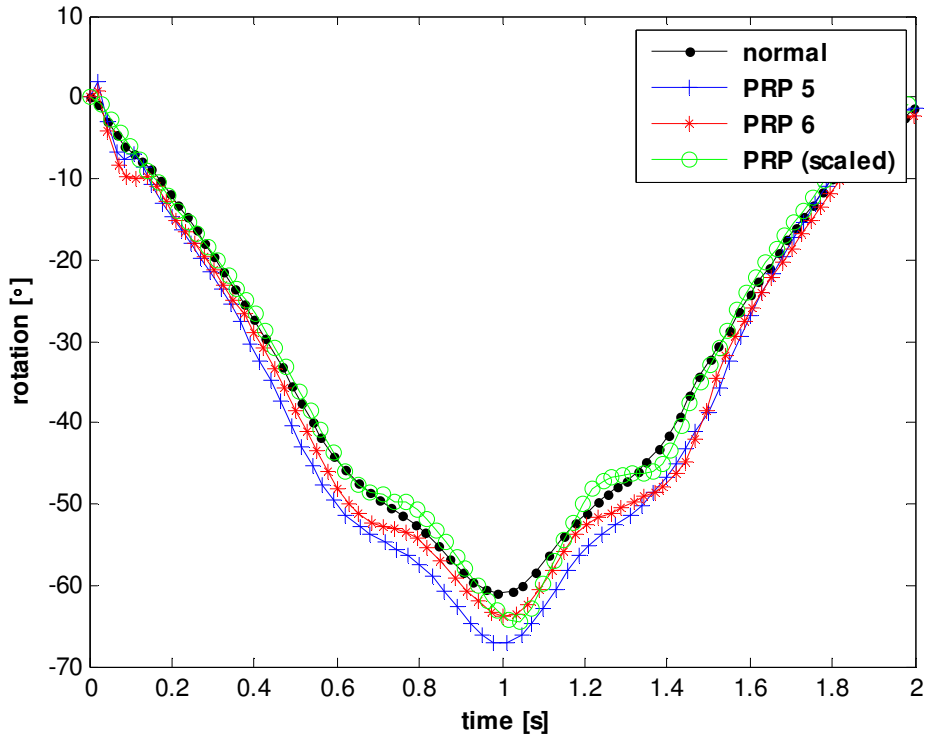

Figure 81: Flexion/Extension of PRP (- Flexion/ + Extension)

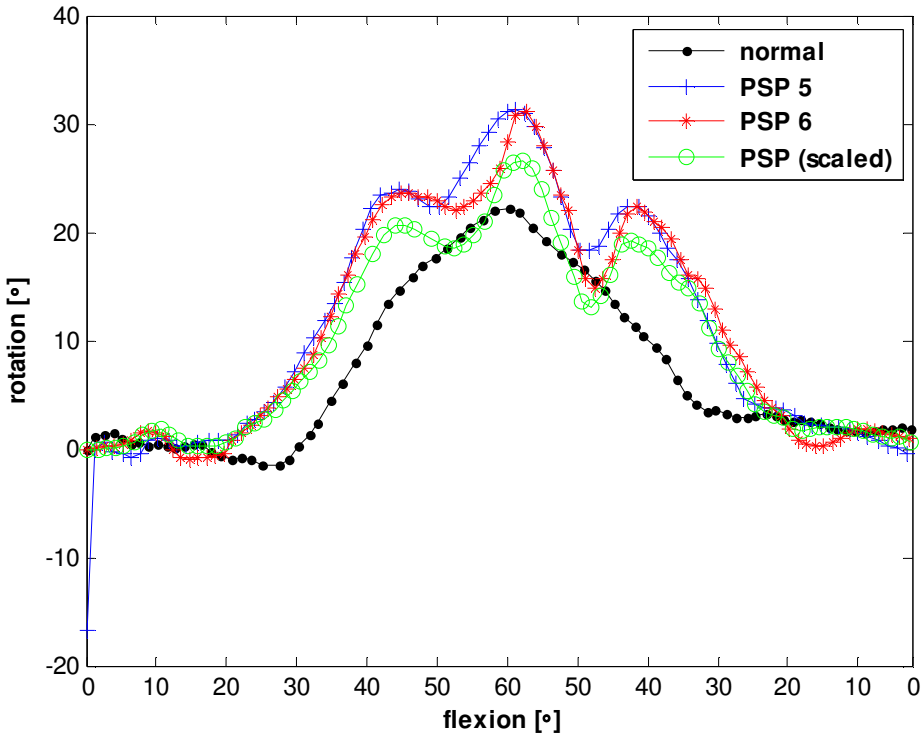

Figure 82: Internal/External rotation of PSP (+ External/ - Internal)

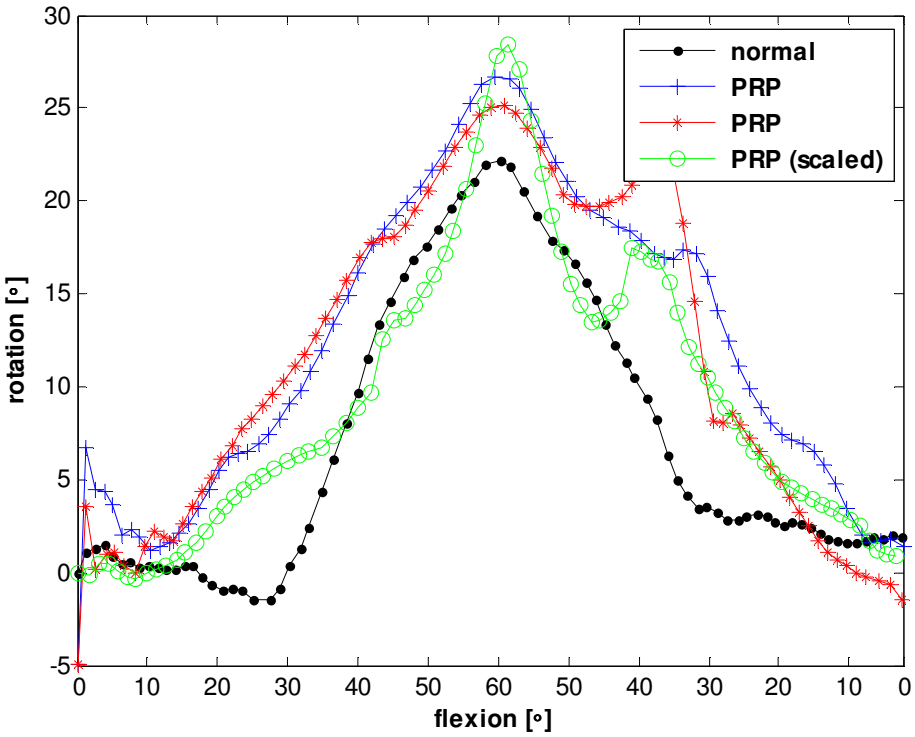

Figure 83: Internal/External rotation of PRP (+ External/ - Internal)

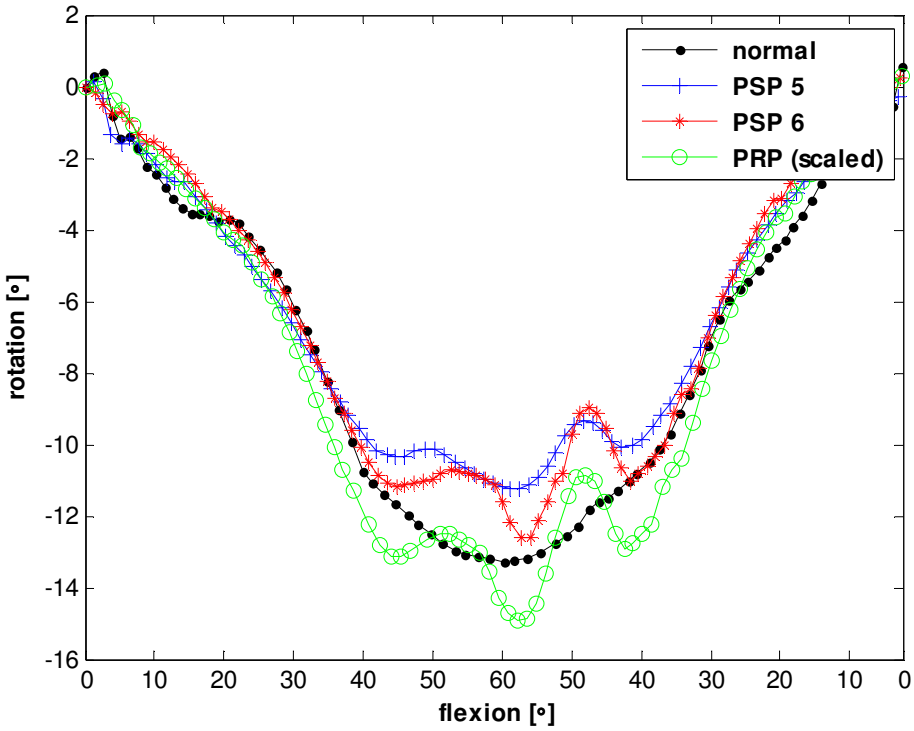

Figure 84: Abduction/Adduction of PSP (- Abduction / + Adduction)

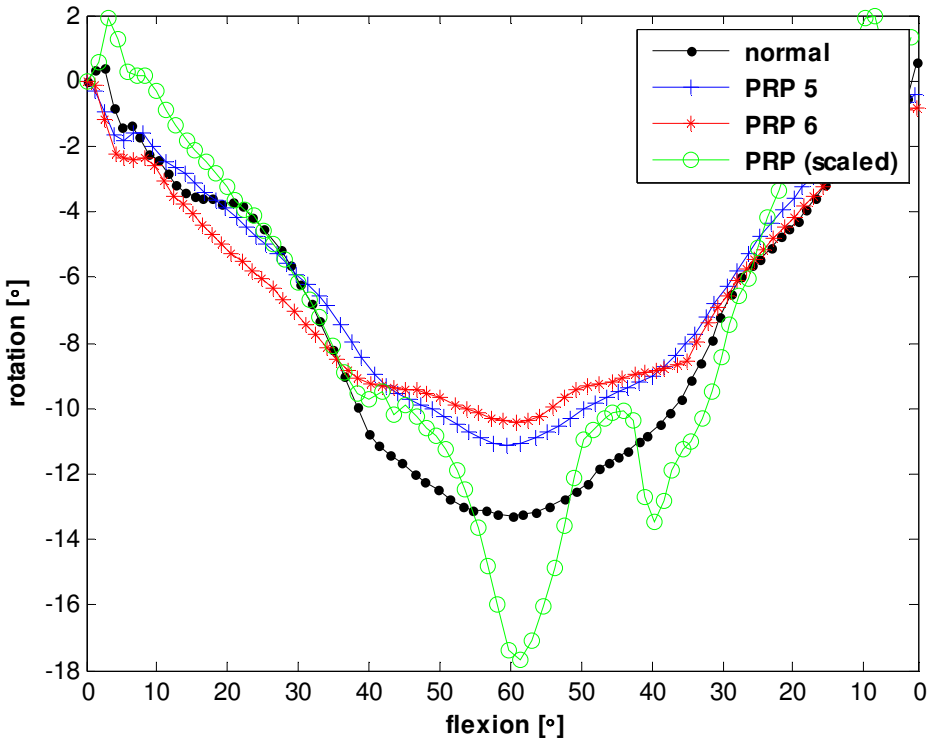

Figure 85: Abduction/Adduction of PRP (- Abduction / + Adduction)

Appendix F: Goodness-of-Fit

The results of the GOF calculations compared the actual prosthesis sizes which were implanted.

Name	GOF	Calculated		Implanted	
		Type	Size	Type	Size
Patient 1	99.32	PSP	4	PSP	2
Patient 2	95.26	PRP	5	PSP	3
Patient 3	97.90	PRP	5	PRP	3
Patient 4	96.63	PRP	6	PSP	5
Patient 5	96.38	PRP	6	PSP	5
Patient 6	95.64	PRP	6	PSP	3
Patient 7	99.42	PRP	6	PRP	5
Patient 8	98.97	PRP	6	PRP	5
Patient 9	98.51	PRP	6	PSP	5
Patient 10	98.8	PSP	5	PSP	3
Patient 11	99.06	PRP	6	PSP	5
Patient 12	98.78	PSP	3	N/A	N/A
Patient 13	98.36	PSP	4	PRP	3
Patient 14	99.13	PSP	4	PSP	1
Patient 15	97.69	PSP	5	PRP	5
Patient 16	98.07	PRP	6	PSP	5
Patient 17	99.18	PSP	5	PSP	5
Patient 18	99.15	PSP	4	PSP	3
Patient 19	97.32	PRP	6	PSP	6
Patient 20	96.85	PSP	5	PSP	5
Patient 21	98.25	PSP	5	PSP	4
Patient 22	97.76	PRP	5	PSP	4
Patient 23	98.77	PRP	5	PSP	5
Patient 24	99.19	PSP	5	PSP	3
Patient 25	97.91	PSP	3	PRP	3
Patient 26	98.70	PRP	6	PRP	6
Patient 27	98.47	PRP	7	PSP	6
Patient 28	98.83	PSP	5	PRP	4
Patient 29	98.17	PRP	5	PSP	2
Patient 30	99.31	PRP	6	PSP	4
Patient 31	97.17	PRP	5	PSP	4
Patient 32	98.99	PSP	4	PRP	3
Patient 33	98.49	PSP	3	PSP	3
Patient 34	99.29	PRP	6	PSP	5
Patient 35	98.26	PSP	4	PSP	3

Volumetric Difference

Size 5

Total	6010	
Anterior	2745	-330
Distal	1189	2627
Posterior	-1967	1343

Size 6

Total	221	
Anterior	822	-1626
Distal	405	1630
Posterior	-2442	1030

Size 7

Total	-7583	
Anterior	-1761	-1626
Distal	-457	453
Posterior	-2811	521

Appendix G: Customization

The results of the customization when scaling method was applied.

Name	Original [%]	Scaling	
		GOF [%]	Scaled
Patient 1	99.32	99.61	0.8689
Patient 2	95.26	97.53	1.0032
Patient 3	97.90	99.08	0.9579
Patient 4	96.63	99.26	0.9827
Patient 5	96.38	96.20	0.9846
Patient 6	95.64	98.52	1.0144
Patient 7	99.42	99.52	1.0279
Patient 8	98.97	99.04	1.0212
Patient 9	98.51	98.56	0.9827
Patient 10	98.8	98.26	0.8797
Patient 11	99.06	99.19	0.9712
Patient 12	98.78	98.48	0.9215
Patient 13	98.36	99.02	0.8898
Patient 14	99.13	98.77	0.8887
Patient 15	97.69	96.59	0.9004
Patient 16	98.07	98.10	0.9854
Patient 17	99.18	99.56	0.8786
Patient 18	99.15	99.51	0.9062
Patient 19	97.32	97.34	1.0115
Patient 20	96.85	95.40	0.9212
Patient 21	98.25	97.27	0.9108
Patient 22	97.76	97.95	1.0358
Patient 23	98.77	98.83	1.0221
Patient 24	99.19	99.61	0.8869
Patient 25	97.91	97.61	0.9399
Patient 26	98.70	98.75	1.0173
Patient 27	98.47	98.56	0.9781
Patient 28	98.83	98.21	0.9118
Patient 29	98.17	98.32	1.0337
Patient 30	99.31	99.35	1.0038
Patient 31	97.17	97.18	1.0053
Patient 32	98.99	98.52	0.9040
Patient 33	98.49	98.50	0.9261
Patient 34	99.29	99.29	1.0038
Patient 35	98.26	97.60	0.8974